Faculty V - Mechanical Engineering and Transport Systems
Institute of Land and Sea Transport Systems
Department of Dynamics of Maritime System

Bachelor Thesis

Floating Offshore Wind Turbines – Required Technological Innovations

Author: Florian Dach

Matriculation number: 381371

Submission Date: 03. December 2020

Supervisors: Prof. Dr.-Ing. Andres Cura Hochbaum (TU Berlin)

Dr.-Ing. Walter Kühnlein (Terra Blue)

Dipl.-Ing. Laura Grüter (TU Berlin)

Eidesstattliche Erklärung

Hiermit erkläre ich, dass ich die vorliegende Arbeit selbstständig und eigenhändig sowie ohne unerlaubte fremde Hilfe und ausschließlich unter der Verwendung der aufgeführten Quellen und Hilfsmittel angefertigt habe.

Berlin, den 03. Dezember 2020

X 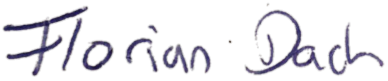

Florian Dach

Abstract

Floating offshore wind turbines find a growing application in the renewable energy sector. As they are a fairly new technology, this thesis will examine in a literature review if there are technological innovations that can enable the commercialisation of the floating offshore wind technology. Therefore, after a short introduction into the topic, the components of a floating offshore wind turbine are investigated in detail. Furthermore, the different project stages during the lifecycle are reviewed and different use cases for the technology will be examined.

Substructures are a large cost factor of floating offshore wind turbines. To have a better understanding of the wave loads a floating substructure is facing in the offshore environment, a subsequent part will determine these wave loads on an exemplary substructure by using the Morison equation as well as determine the corresponding response amplitude operators.

Keywords: Floating Offshore Wind Turbine, Technological innovations, Renewable Energy, Wave Loads, Morison Equation, Response Amplitude Operator (RAO)

Kurzfassung

Schwimmende Offshore-Windanlagen finden zunehmende Anwendung in dem Bereich der Erneuerbaren Energien. Da diese Form der Anlagen relativ neu ist, wird in dieser Arbeit untersucht, ob es technologische Innovationen gibt, die die Kommerzialisierung der Technologie ermöglichen können. Dafür werden nach einer kurzen Einführung die unterschiedlichen Komponenten einer schwimmenden Offshore-Windanlage im Detail untersucht. Anschließend werden die verschiedenen erforderlichen Projektphasen, die während der Lebenszeit einer Anlage durchgangen werden, betrachtet, sowie neue Anwendungsfälle für die Technologie.

Die schwimmenden Fundamente der Windenergieanlage haben einen großen Anteil an den Anschaffungskosten. Um besser zu verstehen, welche Kräfte auf diese Fundamente wirken, werden die Wellenkräfte auf ein beispielhaftes schwimmendes Fundament mit Hilfe der Morison Gleichung untersucht. Darauf aufbauend werden anschließend die resultierenden Übertragungsfunktionen ermittelt.

Schlüsselwörter: Schwimmende Offshore-Windanlage, Technologische Innovationen, Erneuerbare Energien, Wellenkräfte, Morison Gleichung, Übertragungsfunktion

Table of Contents

Eidesstattliche Erklärung i
Abstract ii
Kurzfassung ii
Table of Contents iii
List of Figures v
List of Tables vi
Abbreviations vii
1 Introduction 1
1.1 Technology 2
1.2 Ongoing projects & Market outlook 5
1.3 Cost of floating wind 10
2 General 12
3 Nacelle components 12
3.1 Generator 12
3.2 Drive Train 13
3.3 Convertor 14
3.4 Gearbox 16
3.5 Controller 16
3.6 Monitoring 17
4 Rotor 18
4.1 Rotor components 18
4.2 Modelling & Testing 20
4.3 Turbine configuration 20
5 Substructure 24
5.1 Substructure design 24
5.2 Substructure materials 25
6 Cables & electrics 27
6.1 Dynamic cables 27
6.2 Substations 31
6.3 Monitoring 32
6.4 Electrical grid 32
7 Moorings 34
7.1 Mooring design 34
7.2 Anchors 37

7.3 Monitoring 38
8 Wind park development 39
8.1 Planning process 39
8.2 Environmental impact 41
9 Installation and infrastructure 42
9.1 Turbine assembly 42
9.2 Cable installation 44
9.3 Mooring installation 45
9.4 Offshore operation 46
10 Operation & Maintenance 47
10.1 Operational strategies 47
10.2 Maintenance strategies 47
10.3 Crew transport & Access 49
10.4 Automated O&M 50
10.5 Monitoring 51
10.6 Decommissioning 52
11 Use cases 53
12 Wave loads and motions acting on a FOWT 56
12.1 Definition of the floater 56
12.2 Hydrodynamic Model 58
12.3 Calculation of wave forces 60
12.4 Determination of RAOs 68
12.5 Wave loads for different drafts 75
13 Conclusion 79
Bibliography I
Appendix A VI
Appendix B VII
Appendix C IX
Appendix D X
Appendix E XI

List of Figures

Figure 1: Different offshore wind turbine foundations (Monopile, jacket, TLP, spar-buoy, semi-submersible) (Hannon et al. 2019, p. 17) 2
Figure 2: Stability concepts of the different floater types (Hannon et al. 2019, p. 18) 3
Figure 3: Technology Readiness Levels (Friends of Floating Offshore Wind 2018, p. 18) 4
Figure 4: TRL of different floater types (Proskovics 2018, p. 4) 4
Figure 5: 2MW Floatgen demonstrator on a barge platform (Ideol) 5
Figure 6: Hywind Scotland project with spar-buoys (Renewables Now) 6
Figure 7: WindFloat Atlantic project with semi-submersibles (Larson 2020) 6
Figure 8: Demonstration, pilot, pre-commercial and commercial floating offshore wind projects (Global Wind Energy Council 2020, p. 88) 7
Figure 9: Water depth in northern and western Europe (Friends of Floating Offshore Wind 2018, p. 7) 7
Figure 10: Deployment ambitions of FOWT with different deployment scenarios (Carbon Trust 2020, p. 18) 8
Figure 11: Capacity growth of offshore wind turbines (Global Wind Energy Council 2020, p. 83) 9
Figure 12: CAPEX breakdown of a FOWT in 2018 (National Renewable Energy Laboratory 2019, p. 24) 10
Figure 13: LCOE reduction with different policies (ETIP Wind 2020, p. 4) 11
Figure 14: LCOE estimations of different organisations (U. S. Department of Energy - Office of Energy Efficiency & Renewable Energy 2018, p. 64) 11
Figure 15: Comparison of the motion response of a conventional wind turbine controller and the bespoke Hywind controller (Proskovics 2018, p. 5) 17
Figure 16: Floating vertical turbine prototype by SeaTwirl (SeaTwirl 2015) 21
Figure 17: PivotBuoy concept with a downwind turbine (Ferraro 2020) 22
Figure 18: Prototype of an onshore multi rotor turbine by Vestas (van der Laan et al. 2019, p. 253) 23
Figure 19: Prototype of an energy kite on a floating platform by Makani (Garcia 2019) 23
Figure 20: Elements of a static HV subsea cable with one core and three cores (Weerheim 2018, p. 21) 27
Figure 21: Cross-section of a dynamic subsea cable (Jensen et al. 2015, p. 139) 28
Figure 22: Profile of a metallic corrugated tubular sheathing (Weerheim 2018, p. 45) 28
Figure 23: Different hanging configurations of a dynamic cable (Weerheim 2018, p. 35) 30
Figure 24: Mid-water cable configuration for floating wind turbines (Weerheim 2018, p. 36) 30
Figure 25: Catenary and taut mooring configuration (Corewind 2020, p. 10) 34
Figure 26: Total mooring system cost with increasing water depth (Carbon Trust 2018, p. 42) 34
Figure 27: different anchor types (Corewind 2020, p. 24) 37
Figure 28: Layout of the Horns Dev 2 wind farm (Baring-Gould 2014, p. 6) 39
Figure 29: Layout for a floating offshore wind farm (Schepers et al. 2015, p. 115) 40
Figure 30: Different installation methods for floater designs (Carbon Trust 2018, p. 53) 42
Figure 31: Objects condition in different maintenance types (Corewind 2020, p. 42) 48
Figure 32: Different solutions for hydrogen production (Global Wind Energy Council 2020, p. 93) ... 54
Figure 33: Complete OC5 DeepCwind Floating Wind System (Robertson et al. 2016, p. 4) 56
Figure 34: Description of the floater (Robertson et al. 2016, p. 23) 56
Figure 35: Different wave heading angles facing the floater 57
Figure 36: Vertical added mass coefficients of the different cylinders (Clauss et al. 1992, p. 281) 62
Figure 37: Comparison of the absolute values of the normalized horizontal and vertical forces with columns and caissons for $\beta = 0°$ 65
Figure 38: Horizontal forces on a semisubmersible with four legs (Clauss et al. 1992, p. 273) 66

Figure 39: Normalized real and imaginary parts of the horizontal force with base columns for β = 0° 66
Figure 40: Heave exciting forces of a caisson-type semi-submersible with n columns (Clauss et al. 1992, p. 284) 67
Figure 41: Normalized horizontal and vertical wave forces on the floater for different wave heading angles 67
Figure 42: Degrees of freedom of a buoy (Pecher and Kofoed 2017, p. 140) 68
Figure 43: Absolute value and phase of surge RAO 71
Figure 44: Absolute value and phase of sway RAO 72
Figure 45: Absolute value and phase of heave RAO 72
Figure 46: Sway RAO of a four-legged semisubmersible (Clauss et al. 1992, p. 274) 73
Figure 47: Comparison of RAOs for surge and heave motion for different models of the OC5 semisubmersible (Robertson et al. 2017, p. 52) 74
Figure 48: Comparison of RAOs at a wave height of 9.4 m and a period of 14.3 m (Robertson et al. 2017, p. 48) 74
Figure 49: Comparison of the absolute values of the normalized horizontal force with different drafts for β=90° 75
Figure 50: Comparison of the absolute values of the normalized vertical force with different drafts for β=0° 76
Figure 51: Comparison of the absolute values of the surge RAO with different drafts for β=0° 77
Figure 52: Comparison of the absolute values of the sway RAO with different drafts for β =90° 77
Figure 53: Comparison of the absolute values of the sway RAO with different drafts for β =0° 78

List of Tables

Table 1: Structural and hydrodynamic properties of the system (Robertson et al. 2016, p. 17) 57
Table 2: Distances between the origin and the different columns 60
Table 3: Added mass coefficients 69
Table 4: Three-dimensional added mass coefficients 69
Table 5: Equation of motion for the different transitional DOFs 69
Table 6: Absolute values and phases for sway and heave motion 71
Table 7: Parameters for a 20% larger draft 75
Table 8: Parameters for a draft decrease of 20% 75

Abbreviations

AC	alternating current
AEP	annual energy production
AHV	anchor handling vessel
BC	base column
BCS	base caisson
CAPEX	capital expenditure
CLV	cable laying vessel
CM	condition monitoring
CTV	crew transfer vessel
DC	direct current
DOF	degree of freedom
DP	dynamic positioning
DSS	distributed strain sensing
DTS	distributed temperature measurement system
EERA DTOC	The European Energy Research Alliance Design Tools for Offshore Wind Farm Cluster
FCR	fixed charged rate
FOWT	floating offshore wind turbine
HLV	heavy lift vessel
HV	high voltage
HVDC	high voltage direct current
kW	kilowatt
LCOE	levelized cost of energy
LiDAR	Light Detection And Ranging
MC	main column
MOCO	motion compensation
MV	medium voltage
MVDC	medium voltage direct current
MW	megawatt
MWh	megawatt-hours
NREL	National Renewable Energy Laboratory
OC	offset column
OC5	Offshore Code Comparison Collaboration, Continued, with Correlation
OPEX	operational expenditure
O&G	oil & gas
O&M	operation & maintenance
PDM	partial discharge monitoring
PtX	Power-to-X
RAO	Response amplitude operator
ROV	remotely operated vehicle
SPAR	Single point anchorage
TLP	tension leg platform
TRL	Technology Readiness Level
UC	upper column

1 Introduction

In 2019 62.6% of the total electricity generated in the U.S. sourced from fossil fuels, precisely either natural gas (38.4%), coal (23.4%), petroleum (0.4%) or other gases (0.3%) (U.S. Energy Information Administration 2020b). According to the IPCC report in 2014, the consumption of fossil fuels for electricity and heat production contributes 25% of all greenhouse gas emissions, mainly carbon dioxide, whereby this sector is the single largest contributor of greenhouse gas emissions globally (IPCC 2014, p. 8).

However, in April of 2016 175 countries signed the Paris agreement and thereby agreed "[to hold] the increase in the global average temperature well below 2°C above pre-industrial levels and [to pursue] efforts to limit the temperature increase to 1.5°C above pre-industrial levels" (United Nations 2015, p. 3). If these goals are fulfilled, the risks and impacts of climate change would significantly reduce.

To achieve the 1.5°C goal, the electricity and heat sector must drastically reduce its greenhouse gas emissions. As an alternative to fossil fuels, renewable energies can be used as they don't emit greenhouse gases during electricity production. Renewable energies include wind energy, hydropower, solar energy, biomass and geothermal energy. However, this thesis will only focus on wind energy, more precisely offshore wind energy.

Installing wind turbines offshore has several advantages as higher wind speeds occur at lower altitudes due to no disturbance of the surface boundary layer and larger wind parks can be realised due to increased space offshore. Water depth has been a limiting factor of offshore wind until floating offshore wind turbines (FOWTs) were recently introduced to the market. In this technology, in contrast to bottom-fixed offshore wind turbines, the turbine is installed on a floating substructure, commonly called floater, whereby FOWTs are economically feasible to be deployed in water depth potentially up to 900 m (Hannon et al. 2019, p. 46).

In this thesis, at first, the technology and market potential of FOWTs will be introduced. Afterwards, the innovations to improve the technology to commercial readiness will be examined. In the final part, the wave-induced loads and motions on an exemplary FOWT will be determined.

1.1 Technology

Most offshore wind turbines are currently installed on bottom-fixed foundations which majorly are monopiles or jackets. Monopiles are especially suitable for water depths up to 35 m and are rarely installed above 50 m, while jackets have only been installed in water depths up to 56 m (Hannon et al. 2019, p. 17). However, these depths only present a small proportion of the global offshore wind resources as 80% of its potential lies in water depths above 60 m. Additionally, wind speeds are in those deeper waters higher and more reliable as they are usually further from shore (Global Wind Energy Council 2020, p. 85).

Floating offshore wind turbines can utilise this potential, as they also can be installed at very great depths. The floater is the main distinction feature to the bottom-fixed solutions. Generally, it can be divided into three different types of floaters: the semi-submersible, the spar-buoy and the tension leg platform (TLP), which can be seen in figure 1 next to the bottom-fixed monopile and the jacket.

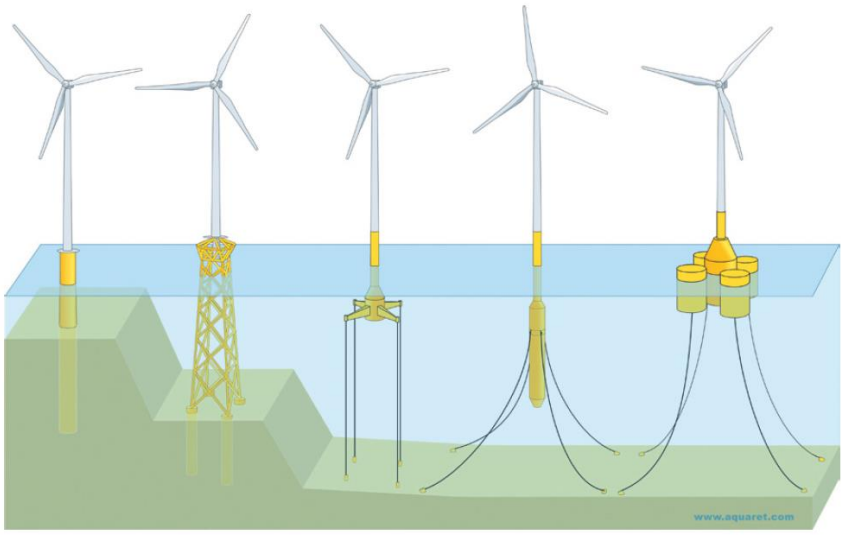

Figure 1: Different offshore wind turbine foundations (Monopile, jacket, TLP, spar-buoy, semi-submersible) (Hannon et al. 2019, p. 17)

The different floater designs have different methods to maintain the stability of the FOWT:

The semi-submersible consists of spread large columns with pontoons and bracings that stabilises the turbine through an increased buoyancy force of the submerged leeward section of the floater, whereby a restoring moment is created that counters the inclining moment (Hannon et al. 2019, p. 18). The large buoyancy force can be achieved by having a large waterplane area and sufficiently spread columns, whereby no large draft is required to maintain stability. That results in an installed draft of 15 m – 25 m and the applicability of semi-submersibles for water depth as shallow as 40 m (ETIP Wind 2020, p. 2). The anchoring of the semi-submersible has no large requirements and no specialised vessels are required for installation and transport, however, as the semi-submersible is a large, complex structure, the manufacturing of the structure will be more expensive (Hannon et al. 2019, p. 18).

One substructure type that is very similar to semi-submersibles and is usually considered as one subcategory of them is the barge foundation. In contrast to the semi-submersible, the barge doesn't use a sufficiently spread but rather large waterplane area, which is created through a hull structure made from steel or concrete. The barge has an even shallower installed draft of 10 m to 15 m and thereby is already applicable at sites with a water depth of 30 m (ETIP Wind 2020, p. 3).

Single point anchorage (spar) buoys have a small waterplane area as they only consist of one large cylinder. This cylinder stabilises the turbine by being ballasted with water or solid ballast, which creates a large vertical distance between the centre of gravity and the centre of buoyancy. When aerodynamic thrust inclines the spar-buoy, the gravitational force and the buoyancy force counteract the inclining moment, resulting in large platform stability. In contrast to semi-submersibles, which are very susceptible to motions inclined by large waves due to their large waterplane area, spar-buoys have minimal heave motions (Hannon et al. 2019, p. 19). As the cylinder has to be very large to ensure platform stability, the installed draft ranges from 70 m to 90 m, which also complicates the assembly of the turbine. Spar-buoys are suitable for deep waters with a water depth starting at 100 m (ETIP Wind 2020, p. 2).

Tension-leg platforms have a large submerged volume, which results in a high buoyancy force. This force is restrained by the moorings of the platform, which are either cables, tendons or solid rods. If the wind inclines the TLP, the increased tension in the windward leg creates a restoring moment that counteracts the inclining moment. Thereby, TLP has very high stability and little motions. However, the anchors of the tension legs have very high seabed requirements to ensure the required tension. Additionally, most of the TLP designs cannot float by themselves due to their high buoyancy force, which results in a more complex installation process (Hannon et al. 2019, p. 20). With their draft of 25 – 30 m, they can be installed at water depth starting at 50 m (ETIP Wind 2020, p. 3). Yet, they are also suitable for very deep waters as their mooring cost only increase linearly in contrast to the catenary moorings of the spar-buoy and the semi-submersible (Hannon et al. 2019, p. 20).

A summary of the different floater stability concepts can be seen in figure 2.

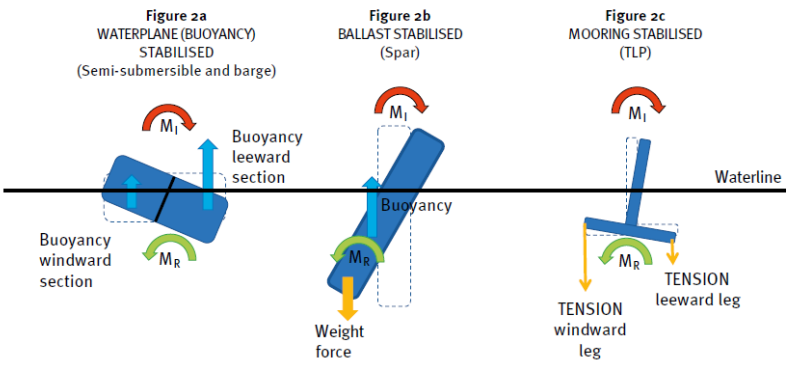

Figure 2: Stability concepts of the different floater types (Hannon et al. 2019, p. 18)

Besides the floater, crucial components of the FOWT are the mooring lines, the dynamic cables, the floating substation and the turbine, which consists of a rotor and a nacelle. The different components will be further examined in chapters 3 to 7.

Floating offshore wind technology is still in development an not yet completely developed for a large scale commercial development. Therefore, it is essential for investors and developers to assess the stage of development of the technology to plan the next project stages. Here, the Technology Readiness Level (TRL) of a technology can be a good indicator for the commercial readiness of the technology. To run through the different stages of TRL, compare figure 3, a lot of research and investments are required to reach the demonstration of the full range of expected conditions at TRL 9 (Offshore Renewable Energy Catapult 2015, p. 5). Floating offshore wind technology improved significantly in recent years through the deployment of several demonstration projects. The TRL of the different floater types can be seen in figure 4, an assessment of the TRL of specific floater concepts including planned upcoming projects is displayed in Appendix A. Previously, semi-submersibles and spar-buoys have already been successfully deployed in the oil & gas sector, which helped the fast progress of the technology. TLPs have already been tested in 2008 as one of the first foundations. Still, there is a lot of uncertainty regarding the technology and its cost, whereby little to no TRL progression was seen in recent years (Hannon et al. 2019, p. 20). However, this will change with the deployment of the Provence Grand Large project in 2022.

TRL 1	2	3	4	5	6	7	8	9
Basic Priciples Observed	Technology Concept Formulated	Experi-mental Proof of Concept	Technology Validation in Lab	Technical Validation in Relevant Environment	Demon-stration in Relevant Environment	Demon-stration in Operational Environment	Pilot Project	Commercial Deployment

Figure 3: Technology Readiness Levels (Friends of Floating Offshore Wind 2018, p. 18)

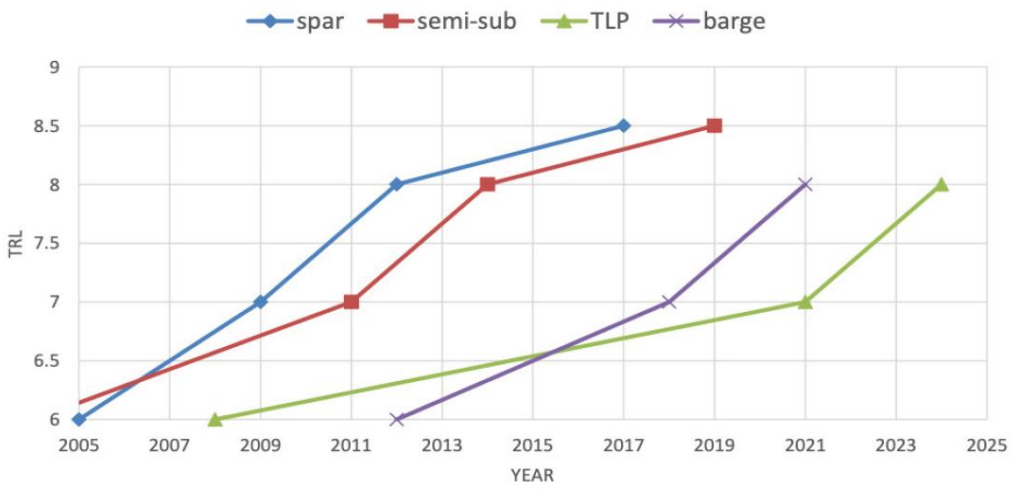

Figure 4: TRL of different floater types (Proskovics 2018, p. 4)

1.2 Ongoing projects & Market outlook

Even when technology reaches TRL 9, after the initial deployment, there still could be a large commercial uncertainty and remaining risk, which is not attractive for investors. Therefore, developers need to create a virtuous circle that proves the potential for cost competitiveness and thereby attracting more investors for the next larger project. The learnings of the next project will then lead to further cost reduction and the next large-scale deployment. This virtuosos circle then continues until the technology achieves commercial readiness (Offshore Renewable Energy Catapult 2015, p. 6).

If this is applied to floating wind, the different projects can be separated into four stages: the demonstration project, the pilot project, the pre-commercial project and the commercial-scale project (Carbon Trust 2020, p. 11).

Demonstration projects usually consist of a single, multi-MW unit which provides new learnings for de-risking the technology ahead of a large-scale deployment. Those projects have relatively high project cost for a single turbine as the new concept has to be tested. For example, the 2 MW Floatgen demonstrator project by Ideol, which can be seen in figure 5, had a total budget of €36 million (Greennovate Europe). Other examples of demonstration projects are the Hywind demonstrator or the Fukushima FORWARD project.

Figure 5: 2MW Floatgen demonstrator on a barge platform (Ideol)

After the demonstration projects are completed, pilot projects with a small array of turbines can be deployed. Those projects help to process towards commercialisation and improve the understanding of the behaviour of multiple floaters. Compared to the demonstration projects, those projects already deliver significant cost reduction, for example, the Hywind Scotland project with five 6 MW turbines, which can be seen in figure 6, proclaimed to achieved a 60%-70% cost reduction by having project cost of NOK2 billion (€186.5 million) (Equinor). Other recent pilot projects are the WindFloat Atlantic project by Principle Power with three 8.4 MW turbines that is displayed in figure 7 and the 48 MW Kincardine Offshore Windfarm project, that is expected to be commissioned late 2020.

Figure 6: Hywind Scotland project with spar-buoys (Renewables Now)

Figure 7: WindFloat Atlantic project with semi-submersibles (Larson 2020)

Pre-commercial scale projects will be a stepping stone between the pilot projects and commercial projects as capacity increases. In those projects, 50 MW – 200 MW wind farms will test the supply chains as several units will have to be manufactured and installed at once. The costs are again expected to reduce relatively significantly, e.g. the 88 MW Hywind Tampen project, which is the only current pre-commercial scale project with a final investment decision, has a total cost of NOK5 billion (€466.6 million). Equinor is aiming to reduce the project cost by 40% compared with Hywind Scotland (Reuters Events 2019).

The cost will then be brought down additionally when the commercial-scale projects (> 200 MW) will improve the efficiencies of all processes as well as being large assets for investors. Broad industry collaboration is required to enable those projects, which are generally expected to be significantly larger than the 200 MW.

The large-scale deployment of FOWT also could have 'hidden' benefits. For example, it would provide a greater transmission utilisation which results in reduced transmission expenditure. Additionally, grid frequency would be less variable as the aggregate wind output is more consistent, therefore balancing cost decreases, and the uncertainty regarding the overall long-term wind output would be reduced which results in lower financing (Global Wind Energy Council 2020, p. 82).

At the end of 2020, 15 floating offshore wind projects with a total capacity of 135.8 MW are expected to be installed and operational. Until 2025, the installation of FOWT is expected to ramp up with several pre-commercial projects that will demonstrate the technological improvements in recent years. At the end of the decade, floating offshore wind technology is expected to enter its commercial phase with several projects with potentially up to 2 GW of capacity (Global Wind Energy Council 2020, p. 87).

Generally, it can be said that projects in Europe will be the 'test-bed' for most of the early-stage projects before deployment is seen in the U.S. or in Asia. However, as the technology is soon entering the pre-commercial phase, those projects outside of Europe are already on the rise (Quest Floating Wind Energy 2020, p. 2). A selection of operational, planned and announced can be seen in figure 8. A broader overview is provided in Appendix B.

Operational Projects (Demonstration and trial phase)	Projects under Construction or plan to be built by 2025 (Pre-commercial phase)	Projects announced in developing partnerships or auctions and to be operational by 2030 (Commercial phase)
Hywind Demo, Norway (2.3 MW)- 2009	EolMed project, France (24.8 MW)- 2021	JERA, ademe and Ideol project (2000 MW)- Japan
WindFloat 1 Prototype, Portugal (2 MW)- 2011	Provence Grand Large floating, France (25.2 MW)- 2021	Equinor & KNOC floating projects (800MW)-South Korea
Kabashima Floating, Japan (2 MW)- 2013	DemoSATH, Spain (2 MW)- 2021	Ulsan 1GW floating (1000 MW)- South Korea
Fukushima FORWARD, Japan (2 MW)- 2013	Hywind Tampen, Norway (88 MW)- 2022	Equinor floating project (300 MW)- Greece
Fukushima FORWARD, Japan (7 MW)- 2016	Atlantic Marine Energy Test Site, Ireland (30MW)- 2022	FLAGSHIP Iberdrola (10 MW)- Norway
Hywind Scotland, UK (30 MW)- 2017	Les Éoliennes Flottantes du Golfe du Lion, France (30 MW)- 2023	Erebus demonstration (TOTAL) project (96 MW)- UK
Floatgen, France (2 MW)- 2017	Groix Belle Ile wind farm, France (28.5 MW)- 2023	Parque Eólico Gofio (50 MW)- Spain
Fukushima FORWARD, Japan (5 MW)- 2017	CTG first floating tender, China (10 MW)- 2022	Industry proposed floating projects (1000 MW)- Norway
Kincardine, UK (2 MW testing)- 2018	Aqua Ventus, USA (12 MW)- 2023	Celtic Sea Floating (1000 MW)- The UK
Hibikinada KitaKyushu Demo, Japan (3 MW)- 2019	Goto (GCS) Floating, Japan (21MW)- 2023	French floating auctions (750MW)- France
PLOCAN's Test Site, Spain (0.2 MW)- 2019	Celtic Sea Folating, UK (32MW)- 2024	
WindFloat Atlantic, Portugal (25.2 MW)- 2020	Equinor floating Canary Islands, Spain (200 MW)- 2025	
Nezzy2 Floating, Germany (testing-1.5 MW)- 2020	Donghae 1, South Korea (200 MW)- 2024	
Kincardine, UK (48MW)- 2020	Redwood Coast offshore wind project, USA (150 MW)	
TetraSpar Demo, Norway (3.6 MW)- 2020e	Sicilian Channel TetraSpar floating project, Italy (250MW)- 2025	

Figure 8: Demonstration, pilot, pre-commercial and commercial floating offshore wind projects (Global Wind Energy Council 2020, p. 88)

The markets for floating offshore wind are all around the world. In Europe, they include countries adjacent to deep waters with high wind speeds, e.g. in the northern North Sea or at the Atlantic coast like UK, Norway, Ireland, France, Spain or Portugal, as it can be seen in figure 9. For these countries, excluding the UK, floating wind will generally open up the offshore wind market as bottom-fixed wind turbines couldn't be installed in adjacent waters. On the other hand, the UK can profit from its experience in bottom-fixed offshore wind and transfer this expertise to the floating market. Future following markets could also lie in the Mediterranean Sea, for example, in Italy, Greece or Turkey, even though wind speeds are generally lower here (Carbon Trust 2020, p. 20).

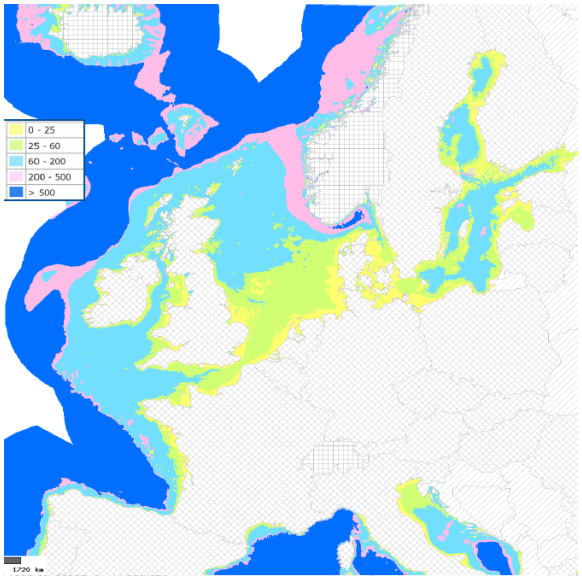

Figure 9: Water depth in northern and western Europe (Friends of Floating Offshore Wind 2018, p. 7)

Outside of Europe, floating offshore wind could be deployed at the pacific coast of the USA where water depth ranges between 600 m and 900 m or in Asian countries like Japan, Korea, Taiwan and China (Carbon Trust 2020, pp. 20–21). Additionally, floating wind can be utilised to decarbonise islands, which otherwise wouldn't have access to reliable renewable energy, like the Canaries or Hawaii (ETIP Wind 2020, p. 4).

Floating offshore wind farms are heavily dependent on the local supply chain. They can stimulate job growth in marine industries, especially those that are affected by the decline of the local shipbuilding industry (ETIP Wind 2020, p. 4). Additionally, they could enable a smooth energy transition with expertise coming from the oil & gas sector as well as technicians that can be retrained for floating wind purposes (Global Wind Energy Council 2020, p. 85).

The deployment of floating offshore wind projects will be highly dependent on the local government policies as a supportive regulatory framework engages industry participation and increases the pace of technological innovation (Carbon Trust 2020, p. 17; Global Wind Energy Council 2020, p. 90). Therefore, an accurate prediction of the deployment scale is not possible so far, as those frameworks were not created yet. Hence, either a slow, moderate or accelerated deployment is conceivable, which is also displayed in figure 10. Nevertheless, a large rise in floating offshore wind deployment is expected in every scenario.

Country	Installed (MW) by end 2020	Expected (MW) 2022	Estimated Deployment (MW) 2025	2030	2035	2040
EUROPE						
UK	80	80	142	1,100	3,800	7,400
France	2	116	116	1,550	5,100	8,900
Other Europe*	31	125	160	2,450	6,200	11,900
Europe (slow)	-	255	296	2,300	6,300	11,000
Europe (expected)	**113**	**320**	**420**	**5,100**	**15,100**	**28,200**
Europe (accelerated)	-	355	449	5,950	21,900	45,600
ASIA						
Japan	12	30	80	930	4,200	11,000
China	0	0	20	495	2,500	7,000
South Korea	0	3	320	1,600	5,000	10,000
Asia (slow)	-	25	210	1,800	5,900	12,900
Asia (expected)	**12**	**33**	**420**	**4,300**	**14,300**	**31,800**
Asia (accelerated)	-	40	520	5,300	21,200	56,200
UNITED STATES						
US (slow)	-	0	0	370	1,500	3,700
US (expected)	**0**	**12**	**12**	**1,270**	**4,300**	**9,800**
US (accelerated)	-	12	12	1,800	6,600	17,500
GLOBAL						
Global (slow)	-	280	511	4,500	13,800	27,800
Global (expected)	**125**	**365**	**848**	**10,750**	**34,000**	**70,300**
Global (accelerated)	-	407	971	13,100	50,100	120,200

**Other Europe includes Portugal, Spain, Norway, Greece and Turkey*

Figure 10: Deployment ambitions of FOWT with different deployment scenarios (Carbon Trust 2020, p. 18)

Another factor that will significantly improve the large-scale deployment of floating offshore wind is the rise of turbine capacity in the recent and coming years. In the past two decades, the average offshore wind nameplate capacity rose in Europe from 1.5 MW to 7.2 MW and significantly larger turbines were already announced like the 15 MW Siemens Gamesa SG14-222 DD model or the recently improved 13 MW GE Haliade-X (Global Wind Energy Council 2020, p. 81; GE Renewable Energy 2020). This rise in turbine capacity occurs to reduce the levelized cost of energy (LCOE) as the increase capital expenditure (CAPEX) of the turbine it outweighs through fewer foundations, cables and installations being required as well as fewer mandatory maintenance activities, which in turn reduces the operational expenditure (OPEX). Additionally, the availability of the turbine and the technical capacity factor will increase through a larger rotor diameter and increased tower height, which is increasing the annual energy production (AEP) (Global Wind Energy Council 2020, p. 81). The capacity growth of offshore wind turbines with different drive technologies as well as floating offshore wind turbines is displayed in figure 11.

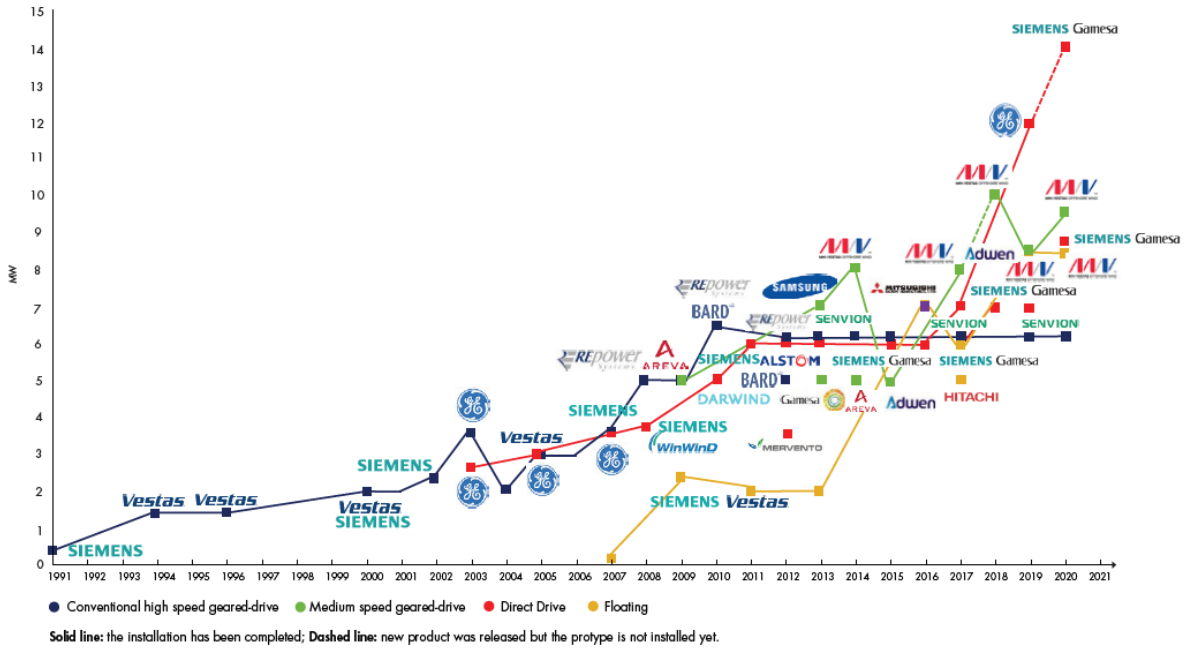

Figure 11: Capacity growth of offshore wind turbines (Global Wind Energy Council 2020, p. 83)

1.3 Cost of floating wind

Although floating offshore wind technology has improved significantly in recent years, its cost has made it uncompetitive to the established energy sources. Compared to bottom-fixed offshore wind, the substructure is a large contributor to the CAPEX as larger and more complex structures are required. Therefore, the cost of current floating offshore wind substructures could even be equal to the CAPEX of the turbines, like in the reference project by NREL in 2018, displayed in figure 12 (note that mooring and anchors cost are also included in the substructure & foundation cost). However, substructure costs are expected to reduce significantly with improved design and manufacturing. At the same time, turbine size and cost will increase, whereby turbines are expected to be the biggest cost contributor in future commercial-scale projects (Carbon Trust 2015, p. 126).

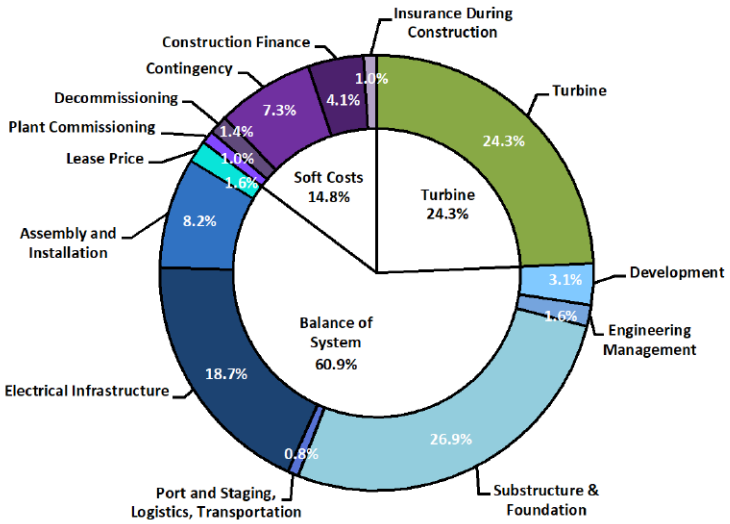

Figure 12: CAPEX breakdown of a FOWT in 2018 (National Renewable Energy Laboratory 2019, p. 24)

Additionally, the maintenance cost of FOWTs are expected to be higher than those of fixed-bottom wind turbines because more components are required to be maintained and other maintenance strategies are used (tow-to-port operations) (National Offshore Wind Research & Development Consortium 2019, p. 28).

By combining the CAPEX ($/kW) and OPEX ($/kW/year) with the fixed charged rate (FCR) (%) and the net AEP (MWh/MW/year), the LCOE ($/MWh) can be calculated (National Offshore Wind Research & Development Consortium 2019, p. 2):

$$LCOE = \frac{(CAPEX \cdot FCR) + OPEX}{(AEP_{net}/1.000)}$$

The LCOE is the determining factor in assessing the cost-competitiveness of an energy source. Currently, the LCOE of floating offshore wind is estimated to be around 143 $/MWh (Quest Floating Wind Energy 2020, p. 4). Those costs are expected to reduce significantly when the technological innovations associated with the deployment pre-commercial and commercial-scale wind farms will establish. Therefore, LCOE of FOWTs could already break even with bottom-fixed offshore wind by 2027 and they could already be in the range of 40 – 60 €/MWh (≈ 50 – 70 $/MWh) by 2030 (Friends of Floating Offshore Wind 2018, p. 8). However, like the deployment of floating wind, the price reduction is heavily reliant on the local policies like subsidies or tax credit and the regulatory framework. That leads to a broad range of potential LCOE, which is displayed in figure 13. Figure 14 shows the LCOE

estimation for floating wind of different organisations. For an overview of the LCOE of other energy sources compare appendix C.

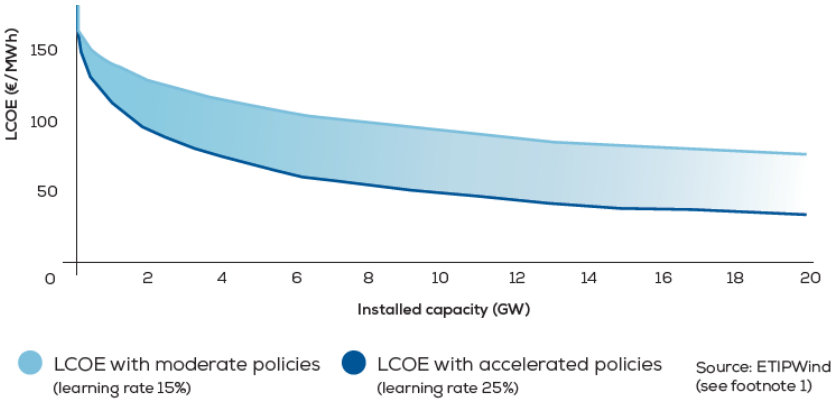

Figure 13: LCOE reduction with different policies (ETIP Wind 2020, p. 4)

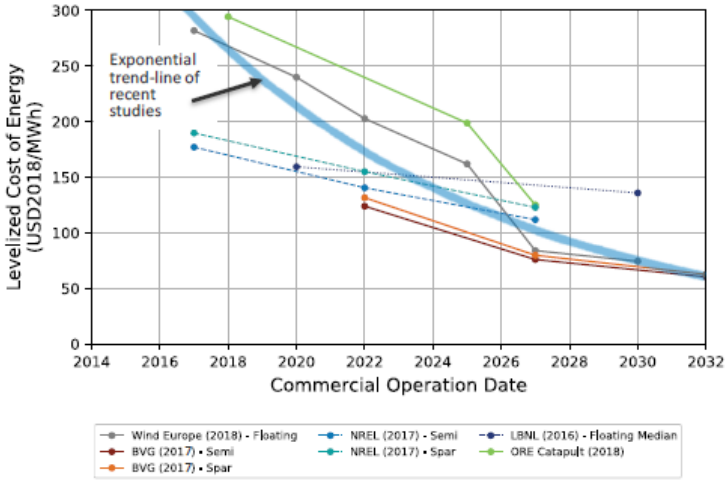

Figure 14: LCOE estimations of different organisations (U. S. Department of Energy - Office of Energy Efficiency & Renewable Energy 2018, p. 64)

Somewhen, the LCOE reduction is expected to stagnate, when the increase of turbine size plateaus due to regulatory or logistical barriers. Nevertheless, this is not likely to happen any time soon as technological innovations will significantly reduce LCOE in the coming years.

2 General

The following chapters 3 to 11 will portray the different technological innovations that can advance the floating wind technology to commercial readiness. Each chapter will cover one component or process that is relevant over the lifetime of the turbine and will examine the potential innovation of it in detail. The relevant components are the nacelle, the rotor, the substructure, the mooring system and the wind park cables and electronics. The processes are split in wind park development, installation process and the operation & maintenance (O&M) process. Not every innovation that will improve floating wind is explicitly bound to this use case but could also be beneficiary for bottom-fixed offshore and/or onshore wind technology and may also see the application in those areas before it is used in floating wind. In chapter 11, this thesis will also consider new use cases for floating wind technology to increase its suitability for different applications further.

The following innovations will not be evaluated on how much they might reduce the LCOE of floating wind turbines due to the limited scope of the thesis and uncertainties regarding the technological readiness and full market potential of the different innovations. However, it can be said that every following innovation has the potential to reduce LCOE in some form, hence reduce CAPEX or OPEX or increase the gross AEP. Note that not every innovation is compatible with other innovations introduced, e.g. due to different substructure types or assembly methods.

3 Nacelle components

The central components to convert the motion of the rotor into electricity are placed inside the nacelle. The entirety of the generation components is called drive train, which besides the generator and the gearbox, also includes brakes, couplings and shafts. The turbine controller, generator cooling and bearings are subsystems inside the nacelle and not considered as part of the drive train. A covering usually made out of aluminium or glass-reinforced plastics is used to protect the components of the nacelle against environmental influences (Bundesverband Windenergie, Maschinenhaus).

Since the first wind turbines were built in 1979, the drive trains improved significantly. However, as turbine ratings were increasing drastically in recent years, there is still room for improvement to the drive train. Generally, most of these improvements can be applied to any wind turbine of an appropriate size, however, some are specifically for floating wind.

3.1 Generator

There are two types of drive train designs: the conventional geared drive train and the direct drive train. In the conventional geared drive train, a gearbox converts the low speed of the incoming shaft connected to the rotor to a high-speed rotational movement, which is required by the generator to produce electricity. In contrast, direct drive generators are directly connected to the rotor and use permanent magnets to generate electricity from the low-speed rotational movement of the rotor. The size of the generator increases to generate the same amount of energy as the high-speed generator of the conventional drive train design. Still, the removal of the gearbox at least partially compensates this weight increase. In a conventional drive train, gearboxes are critical components as they are very susceptible to failure resulting in high maintenance cost.

Additionally, gearboxes decrease the efficiency of the drive train due to losses in the gear transmission. In consequence, the removal of the gearbox is the main advantage of direct drive technology. The reduced maintenance operations are especially important for offshore wind, as every maintenance operation is significantly more expensive than onshore (Net Zero Guide). Turbine manufacturers GE and Siemens Gamesa have already been relying on direct drive technology for their offshore wind

turbines for several years and further improvements of the technology are expected to happen based on the lessons learned from the current generation of direct drive technology (InnoEnergy 2018, p. 41).

One of the biggest downsides of the direct drive technology are the permanent magnets inside the generator. From a purely technical perspective, their use is favourable compared to the alternative coil drives due to their lower weight and lower copper demand, leading to a decrease in CAPEX and OPEX (Morris 2011). However, those permanent magnets usually consist of rare earth mainly found in China or in from China controlled countries, which leads to a less secure supply chain and potential high price fluctuations. Therefore, establishing non-rare earth permanent magnets like axial flux permanent magnets with ferrite material would make the wind industry less dependent on rare earth. Additionally, those alternative permanent magnets could also reduce overall cost due to their lower raw material cost. However, non-rare earth permanent magnets are a relatively new technology and need further research before they are used in new generations of wind turbines (Offshore Wind Innovation Hub, Turbines - Powertrain - Development of next generation generators)[1].

An increasingly important factor of the drive train is its weight, especially for turbines with a rating of 15 MW and above and for floating wind turbines. If the weight of the drive train can be reduced, the size and consequently the cost of the floater reduces, as less weight has to be lifted (van de Kaa et al. 2020, p. 5). A lighter drive train would also result in less fatigue of the tower, thereby reducing tower size and simplify the installation process as less weight that has to be lifted to the increasingly higher nacelle height (Offshore Wind Innovation Hub, Turbines - Powertrain - Development of next generation generators). One solution to reduce the drive train weight is using superconducting wire. This type of wire has almost zero resistance when it is cooled below the critical temperature and can carry substantially more current, whereby the required size of the generator decreases. With this technology, the weight of the generator can be reduced by up to 50% while the generator can be more efficient at the same time (Guan et al. 2017, p. 1).

Currently, direct drives and geared drives are relatively even in offshore market share. However, in the long-term, direct drive trains might have the lead as gearboxes are close to reaching their maximum technical potential, whereas the direct drive still has room for further improvements. With increasing turbine ratings, gearboxes would also require an additional stage, which consequently leads to an increased size and more importantly increased mechanical losses and more parts that are susceptible to failure. In contrast, direct drives remain their efficiency with bigger scale (van de Kaa et al. 2020, p. 5).

3.2 Drive Train

Besides the generator design, different innovations promise to optimise the design of the drive train itself. For instance, modularizing the drive train would shift the focus of the design process towards optimised OPEX as a modular design would improve the O&M procedures. One of these modular solutions could be parallel drive trains where several generator modules and convertor modules are connected along with each other, thereby making the drive train less susceptible to a failure of a single module as some redundancy would be provided. This design could increase the turbine availability when the smaller units have fewer failure rates than the bigger ones and when they could be repaired and replaced quicker. However, to be applicable for failure states, modules are required to be slightly overrated and the powertrain control will have to be able to adapt the torque-speed curve to the remaining modules. This new design approach is only feasible if the increased accessibility justifies the

[1] The Offshore Wind Innovation Hub is delivered jointly by the Offshore Renewable Energy Catapult and the Knowledge Transfer Network. The website provides an innovation roadmap with a tree structure. For clarity reasons, the path to the relevant information will be indicated in this thesis.

increased acquisition cost. Therefore, the application of a modular drive train is only expected for future high rated 20MW+ offshore turbines (Offshore Wind Innovation Hub, Turbines - Powertrain - Development of next generation convertors).

Drive train designs of bottom-fixed offshore wind turbines can be applied to floating wind solutions without the need for great adaptation. Nonetheless, in floating applications, components inside the nacelle have to resist accelerations and displacements that are not present in bottom-fixed offshore wind turbines, which could decrease the lifetime of the components. Therefore, sharing the learnings from the first demonstration, pilot and pre-commercial floating wind projects will improve the general drive train design. Combined with new knowledge from different industries like aerospace, heavy automotive or marine transport, the reliability of drive train components in FOWT thereby increases significantly (Offshore Wind Innovation Hub, Turbines - Powertrain - Floating Wind).

The reliability of floating offshore wind drive train components can also be improved by standardizing functional testing rigs explicitly built to test drive train components or entire drive trains in accurate loading scenarios. Thereby, the lifetime of the components can be quantified more accurately (InnoEnergy 2018, pp. 41–42; Offshore Wind Innovation Hub, Turbines - Powertrain - Floating Wind).

In the long term, once the floating wind technology established itself in a broad market, it may even be feasible to develop a wind turbine design specific for floating wind if facilitated savings can justify the increased developing costs. The reduction of nacelle and rotor weight would be a high priority to decrease the required size of the substructure. Furthermore, drive train components and the rotor could be re-designed to withstand higher loads from floater motions, therefore allow substructure designs to be lighter and enabling them to introduce more motions, accelerations and inclinations into the turbine (Carbon Trust 2020, p. 47).

Bearings are essential components in the entire drive train. Therefore, it is crucial to quantify the reliability of the bearings to have a predictable lifetime. However, current bearing testing often is insufficient when they are tested in on-ground drive train tests, not considering the critical failure modes taking place in practice. Future bearing testing should investigate the operating conditions in which these critical failures occur. Those conditions then should be taken into account in the testing environment to increase the reliability of the bearings (Offshore Wind Innovation Hub, Turbines - Powertrain - Advanced testing & validation).

A holistic optimisation tool that considers every component of the floating wind turbine could be useful to improve the design of the entire turbine. Currently, components are optimised by themselves, which could lead to constraints in combination with other elements of the turbine. If the correlation between the different parts were integrated into the optimisation software, it would lead to a re-thinking of the design of single components to optimise the turbine as a whole (InnoEnergy 2018, p. 39).

3.3 Convertor

In current wind turbines, the generator is producing variable frequency alternating current (AC), which in this form can't be fed into the grid, which is, depending on the country operated in, operating at a constant frequency at 50 Hz or 60 Hz. Therefore, it is necessary to transform the electricity produced from the generator to a grid suitable frequency. This work is done by converters, which at first convert the variable frequency AC to direct current (DC) and then back to AC at constant 50 Hz or 60 Hz (Blaabjerg et al. 2011, p. 711).

Silicon is commonly used in current converters, but new switches made from silicon carbide provide an area of improvement. High-temperature silicon carbide semiconductors operate with higher energy density, a higher switching capacity and a high voltage mode. Although they are more expensive then

silicon semiconductors, their properties result in fewer semiconductors and smaller cooling devices required in the converter (Wallmann 2016). However, the technology isn't established in a broad market yet and further testing of these switches is required (Offshore Wind Innovation Hub, Turbines - Powertrain - Development of next generation convertors).

Converters play a vital role in the wind turbine and it is essential to increase their reliability as their failure would result in a turbine switch off. Therefore, some redundancy and fault tolerance in the converter will be beneficial to increase the availability of the turbine. This redundancy can be provided by using several parallel-connected sub-converters, whereby the turbine still can operate at a lower rating until the next maintenance operation occurs. This maintenance operation then either takes place in the following scheduled maintenance routine or, if feasible, in an immediate maintenance operation (Offshore Wind Innovation Hub, Turbines - Powertrain - Development of next generation convertors).

In most wind farms, a medium voltage (MV) grid (66 kV) is connecting the turbines with the substation. To meet the demand of increasing turbine ratings and to minimise losses in the interarray grid, it might be sensible to establish a high voltage (HV) interarray grid. Therefore, converters need to increase the number of steps to accommodate the higher voltage. For this converter design, silicon carbide switches might be the best solution due to their ability to work in high voltage operations (Offshore Wind Innovation Hub, Turbines - Powertrain - Development of next generation convertors).

Wide bandgap semiconductors improved a broad range of electronic devices through their enhanced switching speed, operating temperature and their reduced losses and might also be applicable for offshore wind turbines. However, this type of semiconductor produces fast-fronted voltage transients which in return leads to a significant reduction of the lifetime of the insulation of the connected machines. Consequently, this will reduce the reliability and availability of the machines. Further research is required to develop an optimised power density as well as further recommendation for the use of wide bandgap semiconductors to increase the lifetime of the converter (Offshore Wind Innovation Hub, Turbines - Powertrain - Development of next generation convertors).

As an alternative to AC power take-off, the DC:AC converter could be removed and instead the direct current would be used in the interarray grid. Therefore, only one cable core is required, reducing the material cost and also lowering losses during the transfer to the substation (InnoEnergy 2018, p. 37). Furthermore, when using high voltage direct current (HVDC) export cables, this configuration only requires an HV DC:DC transformer on the substation instead of an additional HV AC:DC converter. To eliminate the need for a substation, an MV or HV DC:DC converter with a high-frequency power transformer could be placed inside every turbine. The electricity than would be fed from the turbine into a medium voltage direct current (MVDC) grid or an HVDC grid and would be exported directly. However, the impact of high voltage terminations inside the turbine needs further research before this technology would be permitted (Offshore Wind Innovation Hub, Electrical Infrastructure - Alternative Grid Solutions - Enabling technologies for HV DC Grids; Electrical Infrastructure - Offshore Substation Optimisation - Optimised Designs).

The discussed AC/DC-DC/AC converters have the downside in having losses of up to 5 %. In a different electrical configuration, the generator is directly connected to the constant grid, controlled by feedback control. However, this leads to a mismatch in optimal aerodynamics and turbine system loads. Synchronous generators without slip can't run in either of these setups because they need to be coupled with the grid. As a variant to the converters continuously variable transmission drive trains might be a solution. These devices continuously adjust the transmission ratio of input and output speed between the rotor and the generator on a mechanical, hydraulic or hydro-mechanical basis, allowing the generator to operate at its optimum in regards of rotational speed and performance.

Therefore, insufficient and costly converters are no longer needed (Yin et al. 2019, p. 327). While the gross AEP will be lower due to inefficiencies of the device, CAPEX and OPEX might be reduced significantly because of the removal of the converters (InnoEnergy 2018, p. 37).

3.4 Gearbox

Drive train designs with a gearbox have a lower CAPEX then direct drive solutions and therefore have a lower LCOE when operating reliably (van de Kaa et al. 2020, p. 5). Thus, turbine manufacturers like MHI Vestas still rely on this well-established technology with many potential suppliers. However, the reliability of gearboxes is their biggest constraint because the gears will experience high loads in variable wind speed conditions leading to gear failures and consequently to turbine shutdown and high unplanned service cost.

It is crucial to increase the reliability of gearbox solutions in wind turbines to compete with direct drive solutions. This could be realised by optimising the gear mesh loadings to lower the loads of the gear. An introduction of slower rotating gearboxes with the same or even higher loadings would also improve the reliability (InnoEnergy 2018, p. 40). The high-speed stage of the gearbox can even be removed completely, whereby the reliability of the gearbox would significantly increase and additionally mechanical losses would reduce. However, a mid-speed drive train solution requires a larger and more complex generator, which can result in increased inefficiencies (InnoEnergy 2018, pp. 40–41).

To decrease bearing failures of rolling element bearings, which are susceptible for premature failures, journal bearings could be used instead inside the gearbox and the entire drive train. They are not commonly used in offshore wind turbines but found successful application in other marine operations and have significantly higher reliability against early distressing bearing failures (Offshore Wind Innovation Hub, Turbines - Powertrain - Powertrain design).

As an alternative to conventional geared speed and torque transmission, hydraulic or magnetic non-contact torque-speed converters could be used. These gearbox designs would avoid several types of conventional gearbox failures and thereby significantly increase turbine reliability. However, they still need further research to prove their efficiency and reliability and decrease the cost of the technology (Offshore Wind Innovation Hub, Turbines - Powertrain - Powertrain design).

3.5 Controller

The controller of the wind turbine is installed inside the nacelle as part of the subsystems. The device controls the turbine to generate the maximum power in current wind conditions and at the same time, ensuring drive train safety. In floating offshore wind applications, the controller also must respond to the dynamical behaviour of the turbine and can change the angle of heel of the turbine (Offshore Wind Innovation Hub, Turbines - Powertrain - Powertrain design).

Further improvements of the controller for floating wind turbines are crucial to minimise loads of the turbine components. Data from turbine sensors combined with data from already existing floating wind turbines can be used to develop a less conservative controller design (InnoEnergy 2018, p. 40). However, even the bespoke controllers of early prototype scale floating offshore wind projects led to a significant decrease in tower pitch angle and consequently reduced loads to the turbine. This improvement can be seen in figure 15, which displays the numerical simulation of the bespoke controller of the Hywind demonstration project by Equinor (Proskovics 2018, p. 5).

The impact of the controller design for floating wind applications does affect not only the turbine and the substructure but also the moorings of the floating platform. With an optimal controller design, the

mooring fatigue can be minimised, leading to an improved mooring design and higher reliability of the moorings and hence lower LCOE (Corewind 2020, p. 85).

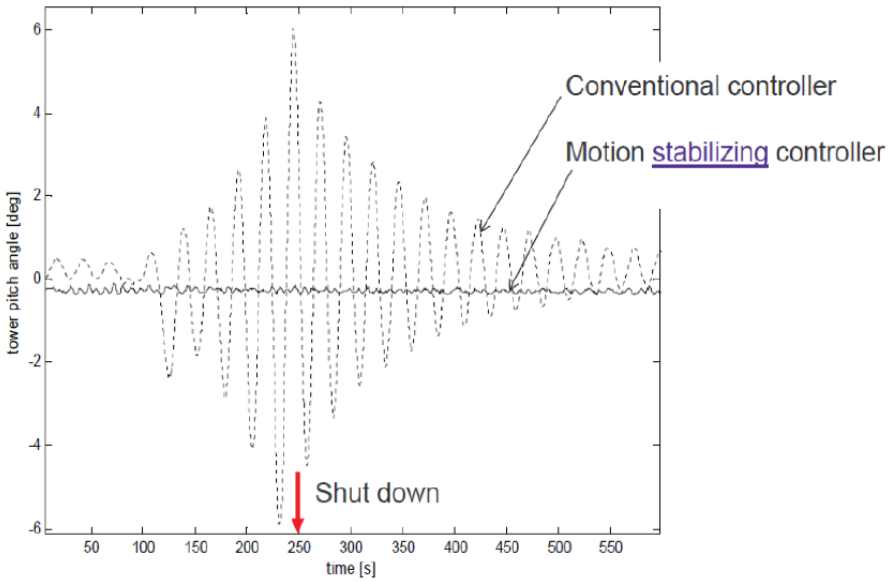

Figure 15: Comparison of the motion response of a conventional wind turbine controller and the bespoke Hywind controller (Proskovics 2018, p. 5)

3.6 Monitoring

The drive train has many crucial components, whose failure would result in turbine shutdown and high O&M cost. Those costs can be reduced by equipping the components with sensors that accurately observe the status of the component, detect failures early and precisely predict the remaining lifetime. This method is called condition monitoring (CM). With this monitoring method maintenance plans can be adapted to the status of the turbine components, leading to reduced downtimes through turbine failures (Offshore Wind Innovation Hub, Turbines - Powertrain - Advanced understanding and prediction of failure).

However, CM is not established for every component inside the nacelle and current monitoring methods aren't well suited for the specific use case. For example, methods like vibration monitoring detect surface failures in rolling bearings, but this cannot detect sub-surface damages. Alternatively, acoustic emission monitoring is theoretically able to detect those damages. However, further improvements in the reduction of background noise and operational vibrations are required before the technology will find implementation in the nacelle (Offshore Wind Innovation Hub, Turbines - Powertrain - Advanced understanding and prediction of failure).

CM could also be used inside the converter, more precisely the Insulated Gate Bipolar Transistors (IGBT), which are key components for the power conversion. Data from the CM of the IGBT can be used to minimise the loading of a single unit and balance it across all IGBTs inside the converter instead. Therefore, not only the lifetime of the single IGBT increases but also the lifetime of the entire converter (Offshore Wind Innovation Hub, Turbines - Powertrain - Advanced understanding and prediction of failure).

The lifetime and O&M cost of large direct drive generators can also be improved through CM. The large forces of the generator could deform the rotor and stator of the generator, whereby airgaps could be closed. Hence, monitoring of the airgaps would provide the operations team with crucial information and the generator operation could be changed accordingly (Offshore Wind Innovation Hub, Turbines - Powertrain - Advanced understanding and prediction of failure).

4 Rotor

Even though the rotor could be considered as one unit of the drive train, it is usually seen as a separate main component of the turbine due to its importance and its specific design. The rotor is consisting of the blades and the hub and is the key component to convert the power of the wind energy to mechanical energy. Inside the hub are the blade pitch controllers, which change the blade pitch angle of every individual blade depending on the wind conditions. The pitch controllers not only try to maximise the power generation by adjusting an optimal blade pitch angle but also minimise severe loads of the blades (Bundesverband Windenergie, Rotor).

4.1 Rotor components

As it was examined in chapter 1.2, the turbine nameplate capacity is rising. To enable this rise in capacity, the turbine size and especially the blade length is constantly increasing, e.g. the recently announced 14MW Siemens turbine will have a rotor diameter of 222m with blades of 108m length. Consequently, new challenges have to be solved, when the blade length, the nacelle height, the tower height and for floating applications the substructure size increase. Those challenges are examined in this chapter and the following ones.

The increase of blade size can only take place when the aeroelastic loads of the blade can be reduced. This can be enabled by using aeroelastic tailoring methods which can increase the directional stiffness of the structural design. The aeroelastic tailoring software is combining blade cross-section analysis tools, aeroelastic tools and blade failure analysis tools in one holistic software. This holistic modelling tool is providing developers with additional knowledge about the coupled behaviour of the blade properties, whereby the overall blade performance can be further optimised (Offshore Wind Innovation Hub, Turbines - Rotor - Disruptive blades).

With an increase in blade size, the weight of the blades also increases. However, current materials will reach a maximum point, where the increased weight would result in critical loads of the blade and potential blade failure. Also, the transport and installation of a heavy blade will be increasingly difficult. New light-weighted blade materials like textiles and improved structural design of the blade with structural stiffeners could be used to decrease blade weight (Offshore Wind Innovation Hub, Turbines - Rotor - Disruptive blades). Potentially even light-weighted materials from aerospace research could be used in future blades (InnoEnergy 2018, p. 48).

Another important task for future wind turbines is the further improvement of the aerodynamics of the wind turbine blades. Therefore, especially for high altitudes, the aerofoil can be improved. By having low solidity sections without sharps edges the lift and drag loading reduces substantially and combined with a circulation control the rotor could be up to 30% larger within the same loading envelop (Offshore Wind Innovation Hub, Turbines - Rotor - Disruptive architecture).

Flaps, slats and morphing enable a quick change of the shape of the blade whereby the aerodynamics of the individual blade can actively change in irregular winds. In contrast to common pitch control, these technologies can respond faster and consequently also reduce loads of the blade (Offshore Wind Innovation Hub, Turbines - Rotor - Disruptive blades). However, active aerodynamic control is yet to be proven on a commercial scale and there are still some uncertainties regarding their robustness and reliability in tough environmental conditions (InnoEnergy 2018, p. 49).

Current pitch control of the blades only focusses on maximising the power output. Yet, floating wind platforms bring in extra motions that have to be taken into consideration as well. Therefore, new pitch control specific for floating wind has to be designed to avoid structural resonance, regulate the rotor speed and control the platform pitching (Offshore Wind Innovation Hub, Turbines - Rotor - Floating Wind). Blades can be further optimised for floating offshore wind by direct collaboration between

blade and floater manufacturers. Through this collaboration, the design regulations slowly can relax as a further understanding of turbine performance is gathered. Furthermore, the rotor can be specified to handle a wider variety of wind speed over the rotor area as there is more movement in the wind turbine. This movement also has to be considered in blade deflection as tower contact has to be avoided (InnoEnergy 2018, p. 46).

Erosion at the leading edge of the blade results in a decrease in aerodynamic performance and consequently, a decrease in power generation. New materials will have to be developed that protect the blade from leading edge erosion over the entire lifetime of the blade and allow higher tip speeds (Offshore Wind Innovation Hub, Turbines - Rotor - Development of advanced materials).

This tip speed is usually limited by fatigue loading, uncertainties about the aerodynamic performance of the blade as well as the mentioned blade erosion. However, with improved structural design, sufficient blade erosion protection and possibly even active aerodynamic control, the blade tip speed could be improved which would result in an increase in power generated and reduce the turbine CAPEX. In contrast, the CAPEX of the support structure would increase, but it is expected to be outweighed by the other factors (InnoEnergy 2018, p. 48).

To protect the blade not only from erosion but also from icing, lightning and electromagnetic interference, a multi-functional device for these three threads is very applicable for the extreme conditions offshore. By combining the protections in one device, the weight decreases and manufacturing becomes less complex (Offshore Wind Innovation Hub, Turbines - Rotor - Development of advanced materials).

Enabling the manufacturing of the 100m+ long blades is also essential. One solution to overcome the logistical challenges of the very long blades is splitting one blade into two or more blade segments. This segmentation would reduce transport costs of the blade and would eliminate the necessity of expensive factory extension. However, it is yet to be determined if the increased production cost of segmented blades would predominate the savings in logistics (Offshore Wind Innovation Hub, Turbines - Rotor - Disruptive blades).

In current blade manufacturing, a lot of tasks like tape lay-up and fibre placement are done manually. Automation of some of these tasks could result in increased production speed and potentially increased blade quality (Mishnaevsky et al. 2017, p. 4). Blade quality can also be improved by using more pre-manufactured components, whose quality control is much easier than that of the entire blade. At the same time, they would improve the design and supply flexibility and, like the segmented blade, reduce manufacturing facility cost (InnoEnergy 2018, p. 50). Another blade quality concern are the adhesives used in manufacturing. Not only do they require mixing and expose workers to potentially harming chemicals, but adhesive bonding failures are common, especially at the trailing edge. New adhesives like structural tapes could provide higher properties and improve safety and applicability (Offshore Wind Innovation Hub, Turbines - Rotor - Development of advanced materials). Currently, blade moulds are almost bespoke and only manufactured by very few companies. A standardisation of blade mould components would not only improve the manufacturing but also bear the potential for significant blade cost reduction (Offshore Wind Innovation Hub, Turbines - Rotor - Advanced manufacturing).

Besides the blades, also the equipment within the hub can be improved. These improvements can regard the bearing concept, the hydraulic and electric systems and the backup energy sources for emergency response. Also, the design of the hub can be improved as well as its material properties (InnoEnergy 2018, p. 50).

4.2 Modelling & Testing

During the design of the rotor components, modelling software is used to predict the performance of the components. The more accurate and reliable this modelling software is, the better developers can adjust their design in early development stages and save cost in the long term. Reliable blade modelling tools exist, but they will have to be optimised for new longer blades (Offshore Wind Innovation Hub, Turbines - Rotor - Advanced understanding and prediction of failure).

One modelling tool that could be further improved is the blade structure modelling tool. It is currently based on the material maximum load acceptance limit and cannot be used to capture delamination or torsion stiffness of the blade. Some finite element codes that are based on the actual thickness of the material do already exist. However, the creation of the mesh is challenging and further improvements are required (Offshore Wind Innovation Hub, Turbines - Rotor - Advanced understanding and prediction of failure).

Blade testing has improved in recent years, but there is still room for improvement regarding the optimisation of aerodynamic performance and adaptation to the further increase in blade size. Also, in regards to floating wind, the testing should be improved to consider the additional movement of the floater (Offshore Wind Innovation Hub, Turbines - Rotor - Floating Wind). Also, the non-destructive testing can be improved for a better understanding of blade damages by penetrating deeper in composites and improving the accuracy of the damage interpretation inside the blade material (Offshore Wind Innovation Hub, Turbines - Rotor - Advanced testing & validation).

When the operator of the wind park wants to keep track of the status of the blades and predict their lifetime, he can use condition monitoring. However, the current fracture mechanic model, which interprets the data from the monitoring system, is only used on the bond-line of the blade and cannot be used on the composite structure. Therefore, it is essential to develop this model further to understand better the damage growth (Offshore Wind Innovation Hub, Turbines - Rotor - Advanced testing & validation).

Another monitoring method relevant for the rotor is the inflow wind measurement. Currently, anemometry is used on wind turbines to infer the inflow wind conditions. For a more complete and faster inflow wind measurement, LiDAR (Light Detection And Ranging) technology could be used in future applications. With improved knowledge about the inflowing wind, the blade pitch and aerodynamics can be adjusted accordingly, increasing the generated power. However, this technology would come at high acquisition cost as LiDAR units are costly. Also, the OPEX would rise because even if the units are built robust to the extreme conditions, unplanned failures of the LiDAR could occur (InnoEnergy 2018, p. 47).

4.3 Turbine configuration

Current offshore wind turbines that operate at a commercial scale are exclusively horizontal axis, upwind, three-bladed, mounted on a tubular tower and have a single turbine. However, different turbine configurations bear the potential to be sensible alternative solutions to the current wind turbines either by increasing the generated power or lowering the cost of the technology itself. Yet, neither of the concepts is currently fully developed, whereby large development costs are required, which is currently prohibiting the application for floating wind.

Most of the offshore wind turbines installed are horizontal axis. However, regarding floating wind, vertical axis turbines might be a possible alternative. Vertical axis turbines have a lighter tower-top mass resulting in a lower centre of gravity and a lighter substructure (Achard et al. 2017, p. 216). Furthermore, as the vertical rotor isn't mounted on a high tower, the major components of the turbine, e.g. the gearbox and the generator, are much more accessible for installation and maintenance (Achard

et al. 2017, pp. 216–217). Additionally, vertical axis wind turbines are insensitive to the wind direction, resulting in no need for yaw control and the potential for large rotor sizes where the wind direction changes with height (Achard et al. 2017, p. 217). However, a comparison between horizontal axis turbines and vertical axis turbines showed that the vertical axis generates about 17.6 % less energy under the same conditions than a conventional horizontal axis turbine (Zhengshun et al. 2017, p. 218). Furthermore, even though most of the fatigue loadings between a vertical and a horizontal axis wind turbine are similar, the maximum mooring fatigue of a vertical axis wind turbine is up to four times higher, resulting in increased mooring cost (Zhengshun et al. 2017, p. 218). Overall further research of the vertical axis wind turbine is needed before it is competitive for a broad market, even though its advantages are appealing for floating offshore wind. A prototype on a floating vertical turbine can be seen in figure 16.

Figure 16: Floating vertical turbine prototype by SeaTwirl (SeaTwirl 2015)

Another alternative to current wind turbines are two-bladed turbines. As wind turbine blades get longer, it might be feasible to reduce the number of blades to two and hence reduce transport, installation, O&M and manufacturing costs. Two-bladed turbines might be especially beneficial for floating wind applications. That is due to the decrease in turbine weight and the reduced fatigue loading of the platform implicated by the turbine design, both resulting in a reduction of substructure size and cost. A downside of this design is the increased fatigue loadings of the turbine that need to be controlled by a controller specifically designed for two-bladed turbines (Offshore Wind Innovation Hub, Turbines - Rotors - Disruptive blades).

Current wind turbines are usually upwind turbines, which does mean that their blades are positioned to face the incoming wind. In contrast, in downwind turbines, the blades are always on the lee side of the tower and the nacelle. So far, this configuration has not been widely adopted because the wake effect of the tower leads to some uncertainties and potentially less power generation. Additionally, downwind turbines produce more noise than upwind turbines, which made them unsuitable for onshore applications (Koh and Ng 2016, pp. 799–800). However, theoretically, downwind turbines have several advantages. First, upwind turbines need extra clearance between the tower and blade and stiffer blades to avoid contact between the bending blades and the tower. That is achieved by aligning the blades either with a cone angle, tilting or curving them or have an extra overhang. In contrast, downwind turbines do not need this additional clearance as the blades are bending away from the tower and are more flexible and lighter blade materials could be used which also reduces the loads on the hub and the drive train (Koh and Ng 2016, p. 800). Furthermore, the active individual pitch

control of the blades could be used to mitigate the adverse loading effects of the tower (Koh and Ng 2016, pp. 800–801).

Additionally, downwind wind turbines do not require active yaw control but yaw freely and faster through the incoming wind. With no active yaw system, the CAPEX decreases and the weight of the nacelle reduces, which is especially beneficiary for floating wind turbines (Koh and Ng 2016, p. 801). Through their tower wake effects downwind turbines generate up to 5% less power than upwind turbines. However, in floating wind applications, downwind turbines might even generate more power than upwind turbines. That is due to the tilting angle in upwind turbines, which, as the floating turbine is pitching in wind direction, leads to an increased angle of error between the rotor axis and the wind inflow. At the same time, it decreases in the downwind turbine (Koh and Ng 2016, p. 801). Another advantage of the lack of extra tower clearance is that more light-weighted lattice towers can be used, which is again advantageous for floating wind (Koh and Ng 2016, p. 801). Even though downwind turbines have already been implemented in floating concepts, which can be seen in figure 17, they still require more advanced research before they will be implemented on a commercial scale. This research has to regard an optimal design, the actual cost-benefit of downwind turbines, adjusted control strategies and especially the wake effect of the tower shadow (Koh and Ng 2016, pp. 803–805).

Figure 17: PivotBuoy concept with a downwind turbine (Ferraro 2020)

Multi rotor turbines are several smaller-scale turbines that are mounted onto one tower instead of one larger-scale rotor, compare figure 18. Through their smaller size, they have the advantage that their installation and maintenance is much easier because no big jack-up vessel is needed for the transport. Furthermore, the smaller size makes their blades less costly and easier to manufacture and transport. Their downside is that several turbines close to each other lead to inefficiencies through wake effects of the other turbines. Therefore, it is essential to maximise the distance between the rotors, e.g. with lattice towers. Besides the wake effect, this turbine configuration also is challenging in regards to active control and structural vibration (Offshore Wind Innovation Hub, Turbines - Rotors - Disruptive architecture).

Figure 18: Prototype of an onshore multi rotor turbine by Vestas (van der Laan et al. 2019, p. 253)

When future wind park developers try to operate in stronger and more consistent winds in high altitudes, kites might be a solution. This technology uses the mechanical energy of the kite moving in high altitudes which is then transferred to an either fixed or floating generator where the mechanical wind energy then is converted to electricity, which can be seen in figure 19. Kite technology is significantly cheaper to manufacture than conventional wind turbines as significantly smaller foundations will have to be built and it can be constructed and installed easily. However, the durability of the kite, its resistance against extreme weather conditions and the overall reliability of the kite requires further research before commercialisation can be expected (Offshore Wind Innovation HubTurbines - Rotors - Disruptive architecture).

Figure 19: Prototype of an energy kite on a floating platform by Makani (Garcia 2019)

5 Substructure

Floating substructures originally were used in the offshore oil & gas (O&G) industry, but the offshore wind developers adapted the concept to their technology. Even though many lessons were learned from the offshore O&G industry, there is still a lot of room for improvement in the floating offshore wind substructures.

5.1 Substructure design

According to Quest FWE, a data and market intelligence website that provides information about current floating offshore wind projects, currently 35 different substructure designs are under development, which is also an indicator for the broad interest in floating wind (Quest Floating Wind Energy). Even though the number of concepts will decrease through time and natural selection, a smaller number of competitive designs would be helpful to convince investors to invest in the technology. Therefore, an independent review of current designs would be beneficial to break down the number of designs to the most promising ones (Offshore Wind Innovation Hub, Substructures - Floating Wind).

As most of the basic substructures types came from O&G, they are not yet fully optimised for the floating wind sector and significant improvements in floater design will be seen through the lessons learned in the first floating offshore wind projects. These improvements are regarding a less conservative design with more efficient use of materials, resulting in a lower weighted substructure with reduced cost (Offshore Wind Innovation Hub, Substructures - Floating Wind; InnoEnergy 2018, p. 57). These improvements of next substructure generations can already be seen in the iterations of the WindFloat and Hywind projects (Quest Floating Wind Energy).

The lessons learned from the first floating wind projects can also be brought into better optimisation tools for the substructures, thereby having an already optimised substructure design early on and save cost in later project stages (Offshore Renewable Energy Catapult 2015, p. 12). Further research should also focus on the relationship between turbine size and the optimal size of the floater substructure as this is also a potential factor for a too conservative design (Offshore Renewable Energy Catapult 2015, p. 12). However, the up-scaling of substructures for bigger turbine ratings has shown to have positive scaling effects, e.g. a pilot project of Principle Power only required a 100% larger substructure for a 500% larger wind turbine (Proskovics 2018, p. 9).

Further collaboration between turbine suppliers and floater designers will lead to a holistic optimisation of the entire floating wind turbine and an improvement of project timelines. The substructure designers require early information about the wind turbine configuration but especially in early project stages turbine suppliers might not be willing to reveal detailed information. Therefore, it might be advantageous to work in early project stages with representative generic wind turbine models and communicate only inclination and acceleration limits and collaborate in load simulations and share the actual data later. The collaboration between both suppliers also has to be closer than in bottom-fixed offshore energy as the behaviour between the turbine and the substructure are significantly more coupled in floating wind (Carbon Trust 2020, pp. 46–47).

One floater-specific innovation is regarding the semi-submersible. The mooring design used in current concepts allows a floater movement of up to 50 m, which could result in heavy loading on the substructure. Therefore, it is essential to improve the station keeping response of the platform. Additionally, active ballasting systems can be installed in the floater to counteract the inclining moment that results from the aerodynamic thrust (Hannon et al. 2019, p. 18).

Also, the tower design could be improved for floating wind. When the stiffness, fatigue and damping performance are considered, an increase in tower mass could lead to a considerable decrease in

substructure mass and consequently, a significant cost reduction (InnoEnergy 2018, p. 58). A decrease in tower mass might also be beneficiary as long as the tower remains its stiffness. Thereby, the natural frequency of the tower would increase, which would improve the turbines operating limits and its fatigue life. Additionally, the decrease in tower mass would result in material cost savings (Offshore Wind Innovation Hub, Substructures - Tower - Reduce mass of towers).

Additionally, tower design will improve by using better tower dampers and single section towers instead of multi-section towers, thereby decreasing the number of flanges, that have to be manufactured, assembled and maintained (InnoEnergy 2018, p. 58). However, single section towers require higher transportation effort, especially with increasing turbine height. This problem could be solved by using concrete towers that are poured and cured in place, which not only eases the manufacturing but also eliminates the need for heavy lifting vessels for assembly. Furthermore, concrete towers would also reduce tower material cost as concrete is significantly cheaper than steel. However, the volume of concrete towers would have to increase compared to steel to ensure that the loads facing the tower can be supported (Offshore Wind Innovation Hub, Substructures - Tower - New towers constructions).

Lattice tower designs represent an alternative to the conventional cylinder-shaped tower design. The main advantage is their ability to better react to higher loads. So far, they were not the preferred tower design because the framework tower shape is more expensive to manufacture. However, they become more and more suitable as the turbine size increases and, consequentially, the conventional tower diameter and thickness also increases, leading to increased tower cost. Furthermore, lattice towers might enable new turbine configurations like multi rotor turbines and downwind turbines, as mentioned in chapter 4.3 (Offshore Wind Innovation Hub, Substructures - Tower - New towers constructions).

Another essential factor for the floating substructures is their manufacturing. Current bespoke and costly designs are not suitable as the number of substructures will increase drastically once the technology is commercialised. Therefore, the manufacturing process has to turn to cheaper, more efficient serial production methodologies that can handle several substructures in production at once (Offshore Wind Innovation Hub, Substructures - Floating Wind). In terms of manufacturability, through their uniform structures and no multi-plane joints, spar-buoys are the easiest and cheapest substructure designs to manufacture. TLPs generally have a more complex design than spar-buoys, but their low weight improves the manufacturability (Proskovics 2018, p. 6). Due to their large size and complex design, semi-submersibles are currently regarded as the most complicated substructure type to be manufactured (Global Wind Energy Council 2020, p. 86). Manufacturing costs could be reduced by designing the floater specifically to ease the manufacturing process. For example, the Tetraspar TLP-floater concept consists of modular components that are easy to transport and can be assembled with a conventional dock-side crane within two days (National Offshore Wind Research & Development Consortium 2019, p. 10). The main concern regarding the serial production of substructures is the required port infrastructure, which will be covered in chapter 9.1.

5.2 Substructure materials

Currently, most of the substructure concepts are made from steel as it is a well-established material used in the offshore industry. Therefore, the know-how regarding steel already exists and solutions and standards to avoid corrosion of the steel are well established. Additionally, the assembly of the substructure can be fastened up with the use of pre-fabricated components (Matha et al. 2017, p. 300). Steel is also a relatively recyclable material, which benefits the decommissioning and sustainability of the substructure (Proskovics 2018, p. 7). Nevertheless, as steel components are prefabricated, there will be issues with building and transporting such large parts. To assemble them at site, specialised

equipment is required at the shipyard like large scale welding machines. Furthermore, steel is a relatively expensive material and its price can fluctuate a lot, which means additional uncertainties in planning (Matha et al. 2017, p. 300).

As an alternative to steel, concrete can be used as the substructure material. In contrast to steel, concrete has a high local content because the batching plant can be installed as a mobile or a stationary unit at any construction site in the entire world. That makes the substructure independent of the steel price and is especially suitable for countries without own steel production or construction sites. Furthermore, instead of specialised workers and equipment, local workers and supply chains can be used (Matha et al. 2017, p. 301). Additionally, concrete has a lower material cost per ton than steel, even though this is slightly upset by the required increase in substructure mass and size to ensure that it can withstand the loads. As concrete does not have to deal with corrosion, the lifetime of a concrete substructure is significantly longer than the lifetime of steel substructures. They can potentially be even reused when the lifecycle of the turbine expires, but it is uncertain whether this is a feasible solution as the typical turbine size is expected to rise (Proskovics 2018, p. 7). Besides the casting process in-situ, which can be easily adjusted to special requirements, also pre-cast concrete parts could be used, which might be beneficial for serial production (Matha et al. 2017, p. 301).

However, until now, the offshore wind industry has not much experience with concrete structures leading to uncertainties regarding production steps, O&M and decommissioning. The increase in substructure size and weight will require higher investment in the port infrastructure, especially when the substructure production is aiming towards serial production. Additionally, the construction process is susceptible to several weather conditions like frost or heavy rain. As concrete is not able to bear tension loads, pre-tensioning is necessary and it is mandatory to avoid upending action during the construction (Matha et al. 2017, p. 301). Moreover, concrete requires curing time, so additional space at the port is necessary to cure the concrete before it can be placed inside the water (Proskovics 2018, p. 7).

As an alternative to concrete and steel, also new materials like wood, aluminium or composites or hybrid solutions can be considered. Even though those materials could come in at higher material and manufacturing cost, they could provide beneficial advantages like lighter structures or higher damage resistance (Offshore Wind Innovation Hub, Substructures - Enabling Research - New Materials). Those materials could also be better recyclable to maintain the value of the components longer and therefore save cost in the long term (Offshore Wind Innovation Hub, Substructures - Enabling Research - Design).

Corrosion protection for offshore steel structures is well established and advanced, yet, the best protection technique is to be found. All current systems have their disadvantages, in general, their reliability, operational procedure, air ventilation and water exchange requirements have to improve to increase the protection of the substructure (Offshore Wind Innovation Hub, Substructures - Materials and scour protection). Additionally, the coatings of the substructure can be improved to be more resistant to damages and corrosion, potentially even through self-healing materials, to increase the operational life and reduce repair and maintenance cost (Offshore Wind Innovation Hub, O&M and Windfarm Lifecycle – Maintenance – Reactive Maintenance – Planned Corrective).

6 Cables & electrics

The electricity transmission of an offshore wind park is an integral part of the CAPEX and OPEX of the park. If the cables or other electric devices don't work correctly or even fail, it will result in electricity losses and high maintenance costs. Therefore, it is essential to increase the reliability and quality of the electronic equipment used in an offshore wind park. Especially floating offshore wind parks require further research, as the dynamic behaviour of the platforms require cables which can handle these additional forces and dynamics themselves, i.e. fatigue of cables will be an issue.

6.1 Dynamic cables

Conventional subsea cables consist of several different layers, which can be seen in figure 20. The conductor is the central element of the power transmission and depending on the transmission type consists of one core (DC) or three cores (AC). The dielectric system consists of the conductor screen, the insulation and the insulation screen and is wrapped around the conductor, thereby preventing the electrical leakage of the cable. The metallic sheath is preventing the water ingression into the inner layers. But as water might penetrate the welding seams, a swelling tape underneath the sheath prevents the further penetration of the moisture. To protect the cable from mechanical loadings like anchors or fishing gear and to ensure structural integrity and tension stability, metal wires are wrapped around the sheath thus providing armour for the cable. Finally, an outer serving made from polymers covers the armour to reduce external stresses and corrosion of the armour. Additionally, optical cables can be installed inside of three cored cables to monitor the condition of the cable and to transmit data. (Weerheim 2018, pp. 21–24).

Figure 20: Elements of a static HV subsea cable with one core and three cores (Weerheim 2018, p. 21)

In contrast, dynamic submarine cables have a double armouring to increase the torsional stiffness of the cable, as it can be seen in figure 21. The cross-sectional area of the conductor of the dynamic cable also must increase due to thermal limitations of the bend stiffeners used for dynamic cables. Dynamic forces increase the friction between the different layers of the cable. Therefore, an additional friction layer can be introduced into the cable between the sheath and adjacent layers to reduce the friction force between them (Weerheim 2018, pp. 33–34).

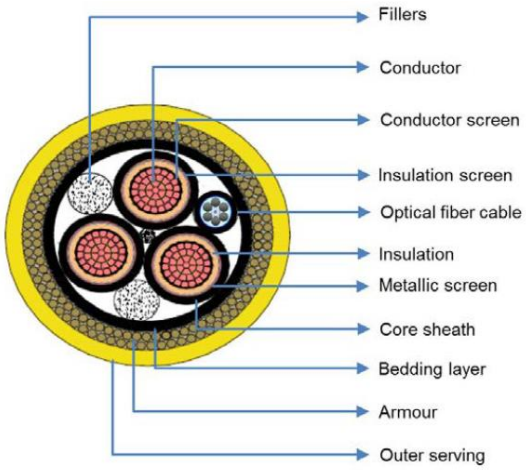

Figure 21: Cross-section of a dynamic subsea cable (Jensen et al. 2015, p. 139)

The sheath is the most fatigue sensitive component of the power cable. Therefore, HV dynamic cables use corrugated tubular sheathing, seen in figure 22, made of copper or steel instead of led, which is noticeably more resistant against fatigue and will increase the sheath lifetime substantially. Currently, this sheathing is suitable for depth up to 400 m, but as the depth increases, like on the North American pacific coast, the technology requires additional research. That is due to the varying loads inside the water column where the upper part of the cable suffers high fatigue through the movement of the platform and whereas the bottom part experiences high hydrostatic pressure (Weerheim 2018, pp. 44–45).

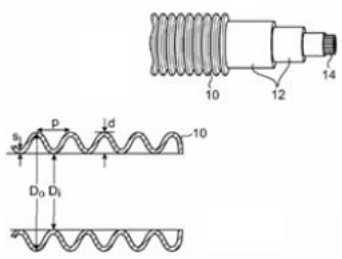

Figure 22: Profile of a metallic corrugated tubular sheathing (Weerheim 2018, p. 45)

Water ingression is a great danger for the cable when it is damaged by some external objects like fishing equipment or anchors. Future power cables might use self-healing materials inside the outer serving, the armour and the sheath to prevent the water ingression and remain structural integrity (Offshore Wind Innovation Hub, Electrical Infrastructure - Enabling Research - Design and materials).

Over its lifetime, the dynamic cable suffers a lot of different loads. Especially in the upper, warmer and oxygen-rich parts, marine growth will bring in additional loads. These loads alter the buoyancy of the cable and shifts the distribution of fatigue loads of the cable (Carbon Trust 2018, p. 34). However, the actual impact of marine growth onto the performance of dynamic subsea cables is not yet entirely determined (Offshore Wind Innovation Hub, Electrical Infrastructure - Component Reliability Improvement - Cables). Therefore, further research will show if it might be feasible to use autonomous marine growth cleaning devices to ensure reliable operation (Carbon Trust 2018, p. 40).

There are not many flexible subsea cables on the market yet, especially cables suitable for HV. As the floating wind market further progresses, the understanding of the different influences on the dynamic cables improves. That will result in an optimal cable core size, insulation thickness, and mechanical

protection and therefore increased reliability and potentially even efficiency, resulting in lower cable cost (InnoEnergy 2018, p. 59).

The reliability of the cables can be increased by improving the testing procedure of the cable. Through improved testing in every stage of the cable design and manufacturing process, the failure mechanisms can be better understood and mitigation measures and solutions can be recommended for the design process (Offshore Wind Innovation Hub, Electrical Infrastructure - Component Reliability Improvement - Cables). Those testing methods involve mechanical, electrical and non-electrical testing, where some of those testing procedures like full-scale fatigue testing or heating cycle voltage test have very long testing timelines up to several months (Carbon Trust 2020, p. 59).

As the dynamic cables are then well understood, a standardisation of the cables will be severely beneficial. A standardised design will increase their reliability and lower the manufacturing cost, especially when cables are produced in large numbers for large offshore wind parks. It would also bring down the cable maintenance cost as the workers only need training and tools for a single cable design (Offshore Wind Innovation Hub, Electrical Infrastructure - Floating Wind).

Currently, a cable joint connects the dynamic and the static section of the cable. This joint is flexible and made out of the core joints, the fibre-optical cable joint and the usual sheath and armouring (Weerheim 2018, p. 37). However, due to the free movement of the dynamic section of the cable, cable joints are prone to failure (Weerheim 2018, p. 41). Therefore, it is essential to improve the subsea connectors. It will also be beneficial if the cable joints are standardised to not only cheapen the connector itself but also improve the efficiency and cost of cable maintenance and replacement and reduce the wind farm downtime (Offshore Wind Innovation Hub, Electrical Infrastructure - Component Reliability Improvement - Components). Alternatively, the static section of the cable could be replaced by having a fully dynamic cable, which would eliminate the need for cable joints and reduces the required accuracy in construction (InnoEnergy 2018, p. 59).

The accessibility of the dynamic cable connector needs to be as easy as possible to ensure a flawless installation and O&M operation. If the floating wind turbine should be towed to port for a major repair, a 'plug-and-play' connector might be suitable. However, those connectors haven’t been tested at full scale and over the entire lifetime of the floater (Carbon Trust 2018, p. 39). Despite marine growth, corrosion and splash zone fatigue, the connectors still need to be operable even after the potential 25 to 30 years of operation. Additionally, those connectors require a concept for their disconnected status. The first possible solution is to connect the cable to a female connector and then lay them down at the seabed. Alternatively, the cable could be connected to a floating structure, either a floater structure that is installed temporally instead of the substructure as a mooring or cable connection or a small electrical buoy that is permanently stored at the substation. However, it is yet to be determined if the 'plug-and-play' is feasible for floating offshore wind turbine as it is highly dependent on the O&M strategy. They are suitable when several major repairs at a port are done over the lifetime of the turbine. But suppose only a few tow-to-port-operations will be done during the turbines lifetime, cable connectors might only be an increased failure risk and an additional cost factor as they are more expensive than standard cable terminators (Carbon Trust 2018, p. 36).

Dynamic cables experience critical fatigue loadings at the top and bottom part of the cable, where it is connected to the floating platform and the static cable. These loads can be reduced by using rigid bend stiffeners at those sections. At the static section of the cable, the bend stiffeners are used to avoid the over bending and fatigue failure. On the opposite, the dynamic bend stiffener connects the cable of the floater to the dynamic cable. It should enable a smooth transition between the floating structure, which has heavy axial loads, and the dynamic cable as it is increasing the local stiffness of the cable gradually (Weerheim 2018, pp. 37–38). However, no bend stiffeners exist yet for high voltage dynamic

cables because those stiffeners need to be larger and more rigid as HV dynamic cables experience heavier fatigue loads. Additionally, their manufacturability needs to increase (Carbon Trust 2018, p. 35).

It is undesirable to have a free-hanging configuration of the dynamic cable as the motions of the floater are coupled from the touchdown point, leading to high tensions at the hanging point. Therefore, buoyancy modules are used to decouple the floating structure and the touchdown point and reduce cable fatigue significantly (Weerheim 2018, p. 45). The buoyancy modules can be installed in different configurations, which can be seen in figure 23.

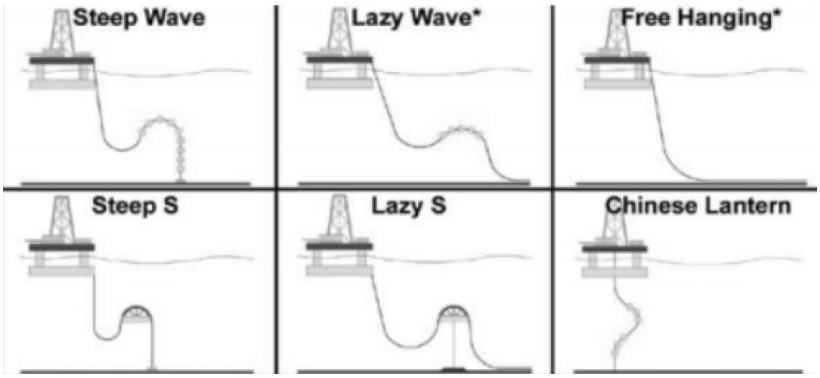

Figure 23: Different hanging configurations of a dynamic cable (Weerheim 2018, p. 35)

The most suitable solutions for dynamic cable are the Lazy Wave, the Lazy S and the Steep Wave configuration. However, as the Steep Wave configuration requires more subsea infrastructure and the Lazy S might have compression problems at the touchdown point when the floater experiences high motions, Lazy Wave is usually the preferred configuration. The Lazy Wave configuration also reduces the maximum tension force, minimises the dynamic cable response and has fewer fatigue cycles (Weerheim 2018, pp. 35–36). The configuration can be still optimised for floating offshore wind by varying the buoyancy modules configuration to minimise the cable fatigue at the touchdown point (Weerheim 2018, p. 43).

When the floating wind structures are installed in deep waters and the distance between the structures is relatively close, a mid-water hanging configuration might be suitable. In this configuration, the cable does not lay on the seabed but is only supported by buoyancy modules, as it can be seen in figure 24. This configuration reduces the cable length required and hence the total cable cost. However, as this configuration has not been applied to a floating wind project so far, there is still a lack of experience and further research is required to ensure the operability of this design, especially for higher voltages (Carbon Trust 2018, p. 35).

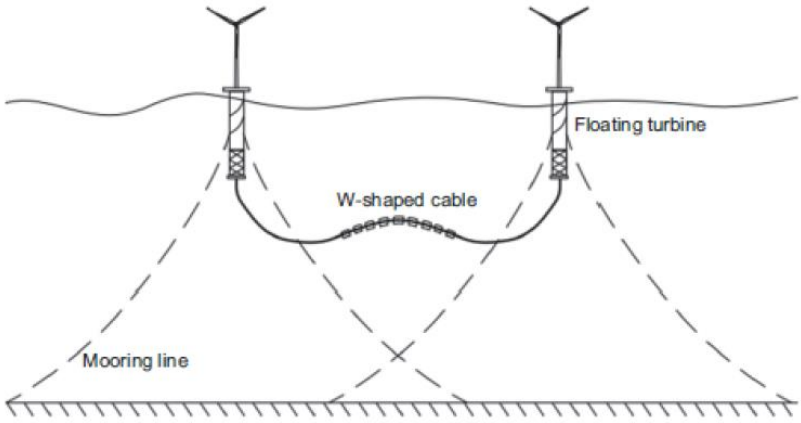

Figure 24: Mid-water cable configuration for floating wind turbines (Weerheim 2018, p. 36)

6.2 Substations

Currently, the offshore substation is usually bottom-fixed. But as the water depth extents the suitable 100 m, the substation, like the wind turbines, will have to float as well. Floating substations are generally not a major problem. Still, there is a lot of room for improvement for them to be optimised for floating applications. Through the wave motions and wave slam, the substation equipment is experiencing additional inclinations and vibrations, whereby the insulation liquid of the transformers could cause rolling (Weerheim 2018, p. 16). However, the suitability of the electrical equipment for those additional forces was proven by the only current floating substation at the Fukushima Kizuna project as well as the seismic qualification of some equipment and the floating transport and installation of some fixed-bottom platforms.

Nevertheless, further testing and development of the equipment is required to increase its reliability. Those critical components of the transformer are the tank, the internal supports and accessories like the Buchholz relays and bushings (Carbon Trust 2018, pp. 33–34). Besides the transformer, the power converter and the circuit breaker also have to be optimised. When testing, not only the fatigue cycles over the entire lifetime have to be considered, but also the high accelerations events and the low-frequency resistance of the devices (Offshore Wind Innovation Hub, Electrical Infrastructure - Floating Wind).

As the substation is very heavy, the floating platform will be costly as well. Therefore, it is desirable to reduce the substation weight (Weerheim 2018, p. 16). It is also essential to optimise the hull form and structural stiffness to minimise the impact of wave slam and the maximum accelerations of the substation (Carbon Trust 2018, p. 33; Offshore Wind Innovation Hub, Electrical Infrastructure - Floating Wind). However, the weight even increases, when the floating offshore wind farm is located further from shore and heavy AC/DC converter are installed on the substation to minimise the electrical losses by using HVDC transmission (Weerheim 2018, p. 16). Alternatively, as mentioned in chapter 3.3, MVDC could be used as an interarray solution and thus reducing the weight of the substation by requiring less equipment for power conversion. However, those DC arrays also need further development, especially regarding cost-effective protection methods. Those methods will increase the availability of the wind farm, while at the same time reduce the total cost. That can be done by reducing the electrical stresses of the MVDC grid and reduce the number of required components of the protection grid to decrease costs. In the long term, even HVDC interarray grids might establish, but currently, MVDC is further developed and can be used as an intermediate step to HVDC grids (Offshore Wind Innovation Hub, Electrical Infrastructure - Offshore Substation Optimisation - DC Arrays).

The cost of offshore substations (15-20% of wind farm CAPEX) can be brought down by standardising the mostly individual substations to more modular repetitive solutions. Those designs should be as autonomous as possible to have less personnel at the site for OPEX work and reduce the cost of ancillary services (Offshore Wind Innovation Hub, Electrical Infrastructure - Offshore Substation Optimisation - Optimised Designs).

As the floating substations will supply increasingly bigger wind farms, the cable management of the connected floating wind turbines will be an essential task, to reduce the risk of entanglement and risk of damages to the dynamic cables (Weerheim 2018, p. 16). The size of the substation, which is substantially bigger and heavier than the floating wind turbines is another issue, as not every port infrastructure can manufacture such a giant substation (Offshore Wind Innovation Hub, Electrical Infrastructure - Offshore Substation Optimisation - Optimised Designs).

Current research also investigates alternative solutions to floating substations. A subsea substation would eliminate the need for the large substructure of the substation as well as potentially reducing the cable cost. However, the concept is relatively young, has not proved in a bigger project scale so far and additional research is needed (Carbon Trust 2018, p. 40).

As mentioned in chapter 3.3, the need for a substation could be eliminated by having modular substations, that are built within the wind turbines, which could reduce the cost significantly. As a transformer within every turbine of the park might be redundant, instead a distributed transformer could be placed on the last substructure of each row of the wind turbines. Even though the increased weight contributes to an increased substructure cost, this solution might be cheaper than the smaller transformer within every wind turbine (Weerheim 2018, p. 16).

6.3 Monitoring

As the dynamic cables are relatively expensive and have a high risk to fail, it should be feasible to use condition monitoring techniques to track the failures, dynamic thermal rating or the mechanical loading histories in real-time. Not only would this procedure enable predictive maintenance and reduce downtimes, but also improve the handling and installation of the dynamic cables, particularly the stiffer HV cables (Carbon Trust 2020, p. 60).

Different measurement instruments that can be used for the CM of dynamic cables include distributed temperature measurement system (DTS), partial discharge monitoring (PDM) and distributed strain sensing (DSS). In DTS the temperature profile along the length of the cable is measured by a fibre either inside or alongside the cable to determine unforeseen issues inside the cable. The same fibre material used for DTS can also be used for DSS, even though two separate fibres are used to avoid the mixture of the measurement data. In contrast to DTS, DSS uses the natural phenomena of the backscattering of a small amount of light inside the fibre to determine locations of strain inside the cable accurately. Most suitable for the DSS sensor is a geotextile with integrated optical fibre. PDM can detect damages in the insulation and in cable joints, but is not able to detect them over distances over a few kilometres, therefore, not suitable for export cables, but can be used for the interarray cables on-site (Weerheim 2018, p. 48).

Those CM procedures will improve the knowledge about the failure rates of flexible cables and thereby decrease the cost of potentially too conservative cable designs in the long term, even though sensors bring in additional acquisition cost that are expected to be outweighed by the cost savings. Additional research is required to improve the measurement methods and to investigate the suitability of currently used optical fibre cores for monitoring purposes (Carbon Trust 2020, p. 67).

Currently, all electrical equipment components are handled separately. However, to reduce data and overall cost, it might be feasible to develop one holistic CM platform for the entire electrical equipment of the wind turbine (Offshore Wind Innovation Hub, Electrical Infrastructure - Component Reliability Improvement - Components).

6.4 Electrical grid

Even though floating offshore wind farms could operate far from shore in more consistent wind conditions than farms near shore, the intermittency of the wind is still an issue for the electrical grid it is operating in. This problem might be solved by developing a more flexible, decentralised HVDC supergrid, that operates over national borders. Such a supergrid would be able to flexibly adapt to the intermittency of the rising number of renewable energies (Offshore Wind Innovation Hub, Electrical Infrastructure - Alternative Grid Solutions - Alternatives to Grid).

The control strategies of the wind farm will have to be more responsive to the grid it is operating in, as an increase in windfarms will reduce the grid inertia and therefore increase the level of required available response. Thus, wind farm control is needed to be able to change the generation characteristics of the wind farm to balance the grid. At the same time, the wind farm control will have to be smarter to maximise power generation and reduce the losses. Therefore, technologies like data prognosis, cloud computing can be used to operate at a more automated, faster-responding stage (Offshore Wind Innovation Hub, Electrical Infrastructure - Alternative Grid Solutions - Grid flexibility).

Currently, a lot of industry research is focussing on the establishment of HVDC export cables for long-distance transmission. A promising alternative to HVDC is low-frequency AC transmission at 16.7 Hz, which depending on the power rating is suitable for distances from 80 to 107 km and could reduce the transmission cost and efficiency (Xiang et al. 2016, p. 4). However, the current AC equipment is not suitable for this type of transmission and it might also impact the generation characteristics of the wind turbine. Further research is required to improve the technology and develop improved testing, standards and a regulatory framework for low-frequency AC transmission (Offshore Wind Innovation Hub, Electrical Infrastructure - Alternative Grid Solutions - Alternatives to Grid).

7 Moorings

Mooring lines are an essential part of floating offshore wind turbines. They keep the FOWT in station and thereby ensure the optimal electricity generation and the reliable electricity transfer to either the adjacent wind turbine or the substation. Two main types of mooring systems exist, the catenary mooring and the taut mooring, which is displayed in figure 25. With catenary moorings, the movement of the floater is limited by the large weight of the lower section of the mooring line lying on the seafloor. Taut moorings maintain stability and position through a high tension in the mooring cables, which consequently results in high loads on the anchors. The taut mooring system could also be implemented with vertical cables, whereby the footprint becomes even smaller and less cable is required but at the same time the vertical forces on the anchor increases, resulting in more costly anchor design. Vertical taut moorings are used in floating wind for TLPs, whereas spar-buoys and semi-submersibles use catenary moorings (Corewind 2020, pp. 10–11).

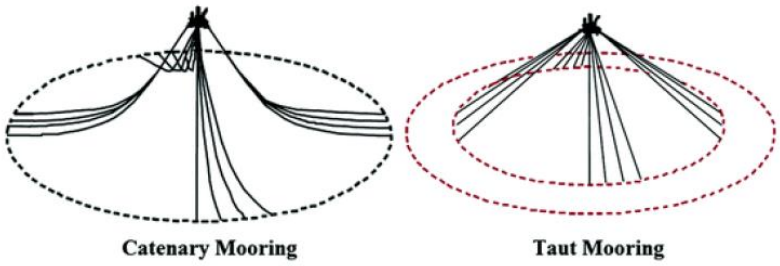

Figure 25: Catenary and taut mooring configuration (Corewind 2020, p. 10)

7.1 Mooring design

Moorings for floating offshore structures are well-established in the O&G industry. However, the current mooring designs are costly and an improved understanding in mooring fatigue, materials and installation methods is required to apply the knowledge in large scale floating offshore wind farms (Carbon Trust 2018, p. 42).

The mooring costs are highly dependent on the water depth the FOWT is operating in. In shallow waters (< 100 m) the mechanical properties and dynamic loadings are very high, thereby the moorings have to be larger and consequently more expensive, especially when the moorings are made out of chains entirely. Additionally, when the catenary mooring configuration is used, the footprint of the moorings will have to increase to achieve the required restoring forces, whereby the mooring cost continue to rise. As can be seen in figure 26, the optimal depth for mooring cost ranges from 100 m – 250 m, but with increasing depth, the material cost increases. However, even in water depths up to 800 m, the material cost increase is still less than the cost of shallow water chain moorings that have to withstand the high loads (Carbon Trust 2018, pp. 42–43).

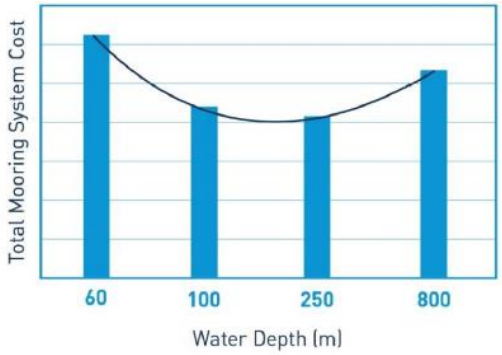

Figure 26: Total mooring system cost with increasing water depth (Carbon Trust 2018, p. 42)

Taut moorings are more advantageous in shallow waters as they are less depth sensitive and have a linear cost increase with water depth, but they have their challenges regarding anchoring. In terms of environmental conditions, moorings are not only dependent on the water depth but also the met-ocean conditions it is operating in. In a harsh environment, the dynamical forces are higher, leading to an increase in mooring size, especially in shallow waters (Carbon Trust 2018, p. 43). Therefore, it is vital to increase the research about low-cost shallow water moorings, where first steps can be seen by recent industry projects (Principle Power 2020).

Even though the fundamental mooring design remains the same as in the O&G sector, the coupled behaviour of a FOWT results in additional mooring loadings that don't occur in O&G. Those coupled behaviours like the additional fatigue load cycles that are transferred from the wind turbine impact the performance and reliability of the moorings. However, as current standards used for FOWT moorings are based on the O&G standards, those additional loadings are not considered. Therefore, mooring design standards have to be adjusted for floating wind (Carbon Trust 2018, pp. 43–44).

Peak loads that occur in extreme weather conditions are an essential factor in mooring design. Those peak loads decrease the reliability of the mooring and lead to a conservative design. Therefore, modelling tools have to take those extreme weather conditions into account and mooring line configuration has to improve to minimise those loads (Carbon Trust 2018, p. 44; Corewind 2020, p. 16).

Currently, either chain, steel wire or synthetic fibre ropes is used as mooring material. Chains are the most common material and are well established as they have good abrasion properties, preferable bending properties and are heavy, which is good for catenary moorings. They are the best suitable solution for areas near the surface and near the seabed, as their bending properties are ideal for the high dynamic forces and their weight increases the restoring force of the FOWT. Yet, their weight is not beneficial in the water column and potential corrosion has to be considered in the design process. Steel wire is lighter than chains and has higher elasticity and durability. However, wires are more likely to be damaged or corroded (Corewind 2020, p. 17). Therefore, it will be beneficial for wires and chains, when additional research on corrosion protection can be used to increase their reliability (Corewind 2020, p. 41).

Moorings made from synthetic materials are light weighted, have a high fatigue performance, require shorter mooring lines and have a smaller mooring configuration footprint. Some synthetic materials are well-proven in O&G, but ongoing research projects enabled the increased suitability of synthetic moorings for FOWT (Carbon Trust 2018, p. 44). Polyester ropes are the most proven ones with a track record in O&G of over 30 years and should be applicable for FOWT without problems. However, in contrast to steel chains or wire, polyester experience axial load elongation characteristics that are nonlinear, which might be a disadvantage in mooring fatigue (Corewind 2020, p. 17). Nylon has a very high elasticity, which makes it especially suitable for shallow waters where other materials become too stiff to adapt to the dynamic forces. So far, nylon moorings have only been applied for short term applications due to low durability, but recent improvements in their fatigue performance made them suitable for long-term use (Corewind 2020, p. 17). HMPE has good abrasion resistance and high strength and stiffness, which makes it suitable for deep-water uses, especially for TLPs. A downside of HMPE is its susceptibility for creep, which could lead to sudden rope failures (Corewind 2020, p. 17). The installation procedure of some synthetic rope is more complex than the installation of steel chains due to required pre-stretching of materials and some synthetics being more sensitive during handling and load out. Nevertheless, if the mentioned challenges of synthetic moorings are overcome, significant overall mooring cost savings are expected (Carbon Trust 2018, p. 44).

Catenary moorings are usually not made from steel wire or synthetics ropes exclusively as the advantages of steel chain predominate at the top and bottom part of the mooring. With steel chain,

the line length can be easily adjusted to the currently required length at the top. At the bottom section, neither wire nor synthetic rope has the same resistance against being dragged over the seabed like chains. However, a hybrid solution of chain and wire or rope in between is suitable for many floating wind applications, which was already proven in the first Hywind project that used a combination of chain and wire (Corewind 2020, p. 18).

Besides the mooring line and the anchors, clump weights and buoyancy modules can be used as additional mooring components. Clump weights are weights made from cast steel, that are especially useful in shallow waters as they increase the vertical loading and total tension in the mooring line, thereby increase the restoring force and reduce the amplitude of tension peak. In contrast, buoyancy modules decrease the weight of the moorings as they create an upward force and decouples the mooring line dynamics from the dynamics of the floater, which makes them especially suitable in deep waters (Corewind 2020, p. 18).

When a mooring line fails, it is important to assure that the other moorings and anchors remain their stability by some sort of redundancy or increased mooring reliability (Corewind 2020, p. 57). Those mooring line failures are not only a possibility but are likely to occur in a large-scale wind farm. According to Rambøll, over half of the mooring damages occur outside of the operation. Therefore, improved handling and manufacturing would be beneficial to increase the reliability of moorings. Additionally, a risk management plan could also reduce mooring failure risk (Carbon Trust 2018, p. 43).

First pre-commercial floating offshore wind farms will gather essential information regarding mooring failure risk and mooring design. Therefore, it is necessary to share those lessons learned to understand the key challenges of moorings (Carbon Trust 2018, p. 47). This knowledge then can be used to create a framework for the assessment of mooring failure, which could ease the determination of mooring design and robustness and thereby reduce cost. Furthermore, this knowledge can be used to improve the inspection standards for FOWT moorings and thus reduce failure probability (Carbon Trust 2020, p. 67). In terms of standards, appropriate levels of redundancy and safety levels should be defined as well as a standard for moorings in TLPs (Carbon Trust 2018, p. 47). It also would be beneficial when more research focuses on the cost risk benefits of the various mooring designs as well as their inspection requirements and fault-tolerance to determine the most suitable design for every condition (Carbon Trust 2020, p. 67).

Those mooring designs will also have to consider the avoidance of clashing between the moorings and the dynamic cables. Current mooring design process prioritises the effective offset control and minimised mooring cost and only provide a spatial envelope for the cable configuration to avoid any clashing. But in floating wind, the dynamic cables have increased importance and especially the use in shallow waters complicates the mooring and cable placement as the connection placement and the relaxed mooring lines will result in smaller envelopes for the cables. Clashing is also an issue when the substructure sizes decreases and the number of wind turbines increases (Corewind 2020, p. 68). Therefore, a combined design loop for cables and moorings is beneficial to increase the envelope and additionally maximise the allowable cable offset. This cable offset is usually a limiting factor for the mooring design as it gives the mooring only a certain amount of tolerance. Leaving this tolerance would induce peak loads into the mooring whereby the moorings have to increase in size (Corewind 2020, p. 84).

The placement of the mooring might also play a vital role in the overall mooring cost. Usually, the mooring lines are spread at various positions around the substructure. In contrast, several moorings could also be installed at a single point at the substructures centre of rotation in a taut mooring configuration. This concept could potentially reduce the cost of moorings and the floater as well as

reduce installation time, especially when combined with a downwind turbine (Corewind 2020, p. 12; DTU Wind Energy 2019).

For maintenance activities, where a failed mooring must be replaced, it is vital to develop a mooring replacement method. This replacement could either be a derrick barge or an anchor handling vessel (AHV), which could also replace the mooring. However, the mooring replacement requires several modifications to the AHV like subsea cutting tools to remove the failed mooring (Corewind 2020, p. 58). Additionally, the top connectors of the moorings will have to improve in regards of cost and simplicity as a fast connect and disconnect procedure is essential for installation and tow-to-port O&M activities (Carbon Trust 2018, p. 45).

7.2 Anchors

The type of anchor used for the floating wind turbine depends on the mooring configuration, installed water depth, the soil type and the required holding capacity. Some different anchor types for different water depth (shallow to deep water) and seabed condition (hard to soft soil) are shown in figure 27.

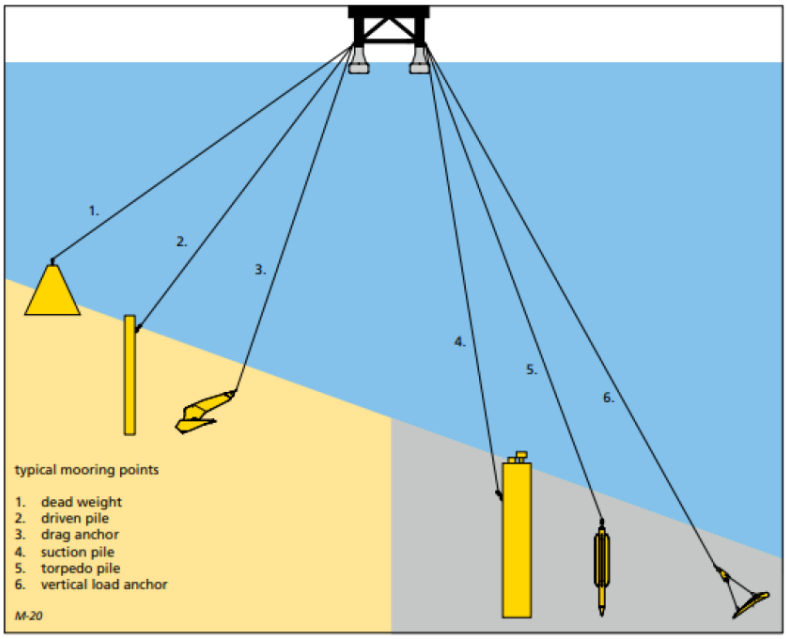

Figure 27: different anchor types (Corewind 2020, p. 24)

An issue of those anchors is their reusability, e.g. suction anchors are not reusable after being decommissioned and new anchors are required to be installed if the turbine moves to a different place (Corewind 2020, p. 41).

Some attractive floating offshore wind markets like Japan, Taiwan or the U.S. West Coast are in active seismic regions. For those regions, the anchor design standards will have to improve to remain anchors holding capacity even when soil liquefaction takes place. To achieve this, the anchor size and penetration depth will have to increase, resulting in increased anchor cost, especially for TLPs due to their large vertical forces (Carbon Trust 2018, p. 47). Research should emphasise not only the seismic behaviour of the TLP anchors but also their tendons, as they are essential to maintain the stability of the TLP (Carbon Trust 2018, p. 50).

One disadvantage of using single turbine floaters are their high anchor cost. To reduce those cost, either the anchor and/or the moorings could be shared. A mutualised anchor reduces the anchor and installation cost and requires less geotechnical surveys. However, it might only have a small impact as a shared anchor also implies some restrictions. Those restrictions regard higher anchor positioning

requirements, less optimised mooring due to distance constraints are leading and wind turbine array layouts and mutualised anchors being not feasible for complex bathymetry of the site or difficult seabed conditions (Carbon Trust 2018, p. 46).

In shared mooring configurations, several smaller wind turbines are placed on a floater to reduce mooring and cable cost (Corewind 2020, p. 12). The downside of those multi-turbine floaters is their decreased electricity generation due to the wake effects of the adjacent wind turbine, similar to the multi-rotor turbines mentioned in section 4.3 (Offshore Wind Innovation Hub, Turbines - Rotors - Disruptive architecture). Large scale demonstration projects are currently planned for these multi turbine floater concepts like the Nezzy^2 project of aerodyn and EnBW and the Donghae TwinWind project by Hexicon.

Additionally, interarray moorings require additional research. In this concept, only a few floater mooring lines are anchored to the seabed, while the other floaters are connected to each other without direct connection to the seabed (Carbon Trust 2018, p. 50).

7.3 Monitoring

In O&G mooring lines are inspected in short intervals. This procedure cannot be applied in floating offshore wind as the farms are located far from shore and large-scale wind farms will have over 100 mooring lines installed. Therefore, improved monitoring methods will have to be used to move to a risk-based inspection approach. Additionally, the mooring inspection standards and guidelines are required to improve, to enable a risk-based inspection plan (Carbon Trust 2018, p. 46).

Monitoring techniques have already been developed for O&G. They can detect failed moorings (sonar probe), measure the mooring line angle and derive the mooring line loading (inclinometer, indirect in-line tension monitoring) or detect the floater positioning, thereby determine the mooring loading (GPS). Other methods can directly measure the mooring line loading to detect failure, overloading or assess fatigue (Load Cell) or monitor the current floater and mooring motions and conditions, whereby the mooring loadings can be forecasted (Integrated Monitoring and Advisory System) (Corewind 2020, pp. 51–57). However, they are costly and potentially not effective enough for an application in floating wind (Carbon Trust 2018, p. 46). Additionally, their overall implementation needs to improve, especially in components that experience significant changes in material characteristics. To ensure the reliable operation of the monitoring sensors, suitable power systems need to establish to supply the subsea sensors (Carbon Trust 2020, p. 67).

8 Wind park development

Before a wind farm can be installed, operated and maintained, it must be planned. The planning process is one of the vital areas of improvement as important parameters of the floating offshore wind farm are set here, which influences the entire wind park performance.

8.1 Planning process

Currently, the layout of a wind farm is planned relatively manual and is an iterative process. A multi-variable layouting software that can optimise the layout for the lowest lifetime cost, the maximum yield or the most extended lifetime will be very beneficial for the planning process and could reduce cost significantly. Those tools can consider wake effects, electrical array cost and sizing, support structure cost, substation placement, geotechnical and environmental constraints (InnoEnergy 2018, p. 29; Offshore Wind Innovation Hub, O&M and Windfarm Lifecycle - Project Development - Project Development). If the tool is optimised explicitly for floating wind, additionally mooring cost and the dynamic cable configuration can be considered (Offshore Wind Innovation Hub, O&M and Windfarm Lifecycle - Project Development - Floating Wind).

Most of the current wind farm layouts have rows of wind turbines in a radial design around the substation as it can be seen in figure 28, which displays the layout of the Danish Horns Rev 2 wind farm (Baring-Gould 2014, p. 6). However, floating offshore wind farm has different constraints than bottom-fixed offshore wind farms like the mooring lines and anchors. The EERA DTOC proposed a hypothetical layout of a floating offshore wind farm in the Dogger Bank with no regards to the bathymetry of the site (water depth ranges from 20 m to 60 m). They assumed a wind park of 104 wind turbines with three mooring lines per anchor and used shared anchors with tree mooring lines per anchor which resulted in a celluloid layout of the wind farm. This celluloid shape was then split into two clusters due to substation limitations, which can be seen in figure 29 (Schepers et al. 2015, pp. 114–116).

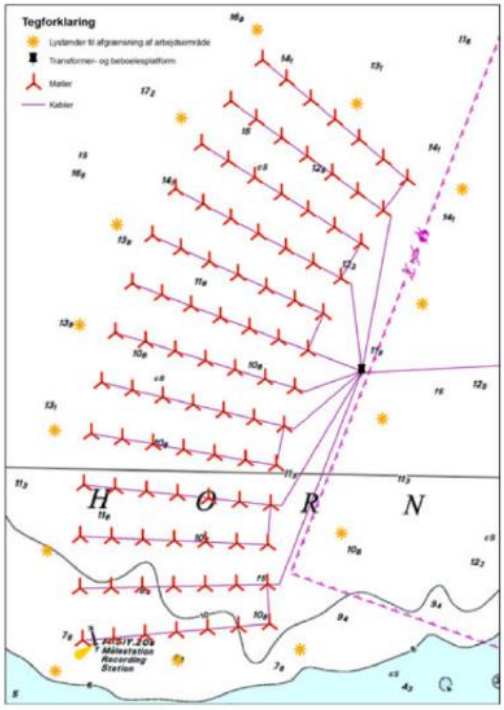

Figure 28: Layout of the Horns Dev 2 wind farm (Baring-Gould 2014, p. 6)

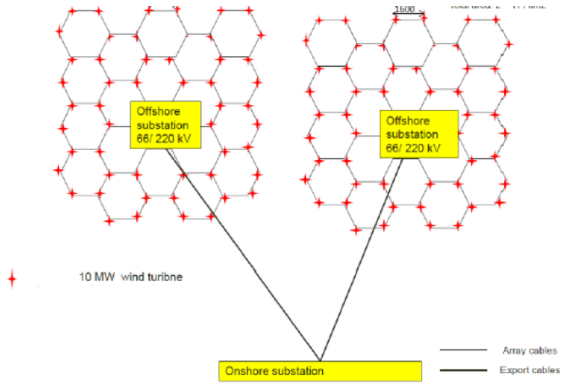

Figure 29: Layout for a floating offshore wind farm (Schepers et al. 2015, p. 115)

Wake effects of adjacent wind turbines have a significant impact on the performance of the wind turbine. The turbine efficiency can be increased through a mooring configuration and a layout that allows increased manoeuvrability of the turbine. With this increased manoeuvrability, the entire turbine could be positioned by a control system according to the wind direction and wake effects instead of yawing the nacelle accordingly. However, this layout variation has not been applied yet, even though it has shown theoretical benefits (Rodrigues et al. 2015, pp. 939–940).

One of the decisive steps during the planning process is the front-end engineering design which is conducted after the conceptual design and a feasibility study. In this stage, engineers will perform various studies to determine technical problems and provide a first approximate forecast of the overall cost. However, for floating wind farms, more surveys should take place to reduce the cost of later design changes. Those studies can provide additional data from geotechnical and geophysical surveys and provide the best installation strategy for different turbine and foundation design. Additionally, this optimisation of front-end engineering design is increasing the accuracy of the estimated cost of the wind farm (InnoEnergy 2018, p. 30).

Additionally, the cost could be brought down by improving met-ocean monitoring during the planning process. With increased knowledge about the wind speeds across the site, wind farm layout can be improved as well as the modelling of the wave effects (InnoEnergy 2018, p. 30). Meanwhile, improving the sea condition monitoring could lead to a less conservative, site-specific substructure design with reduced cost and improve the installation and O&M plans (InnoEnergy 2018, p. 32). The cost of met-ocean monitoring for floating wind could be brought down by developing a floating meteorological station. Compared to the current bottom-fixed stations they can be installed faster and also could measure relatively cheap above hub height (InnoEnergy 2018, pp. 31–32).

The costs of anchoring and electrical cabling are heavily linked to the geophysical and -technical conditions of the site. Therefore, improvements in the surveying of those conditions lead to a less conservative design, improved anchor positioning and selection and installation cost (InnoEnergy 2018, pp. 30–31). Presently, static subsea cables require to be buried as they need to be protected against fishing equipment and anchors. Yet, in floating wind, those damages don't happen that often due to the increased water depth and wind farm access restrictions. Thus, the necessity of the subsea cable burial should be investigated and, if the burial is necessary, investigate the required buried depth as different soils have different protection capabilities (InnoEnergy 2018, p. 31).

Interests of local stakeholders often influence the construction of a new offshore wind park. Therefore, it is essential to involve those stakeholders like the fishing and shipping industry and national defence sector early on in the planning process to avoid conflict of interest and find compromises which satisfy all sides (Proskovics 2018, p. 8).

One area of improvement to avoid the social and economic conflicts is assessing the impact of floating offshore wind farms on the shipping industry and fishing grounds. When standardised assessment procedures are established, the additional shipping cost and the ability of local fishers to sustain with displaced fishing levels can be evaluated more precisely (Offshore Wind Innovation Hub, O&M and Windfarm Lifecycle - Project Development - Social and economic impact).

During the different project stages of a floating offshore wind farm, important data and information is passed between several different parties, who all use different software which can lead to a lot of inefficiencies and wastes. Therefore, a common data platform or tool that enables the seamless flow between the various project states and contractors would significantly improve the entire process (Offshore Wind Innovation Hub, O&M and Windfarm Lifecycle - Project Development - Project Development).

For the planning process, it would be favourable if the developers and supply chain provides a prediction of the number of required workers to carry out the project as well as indicative timescales. Thereby, the cumulative social and economic impact can be estimated. That is especially important when offshore wind established as a broad sector and the general demand for technicians increases (Offshore Wind Innovation Hub, O&M and Windfarm Lifecycle - Project Development - Social and economic impact).

8.2 Environmental impact

Every structure built has some impact on the environment in which it was constructed. This impact is determined by environmental studies, that usually require a lot of time. However, the tools to pursue those studies in offshore wind are not yet optimised for floating wind as FOWT have a fundamentally different impact on the environment compared to bottom-fixed offshore wind. While piling operations required for bottom-fixed offshore wind significantly impact the environment through the noise and the disruption of the seabed, FOWTs are influencing the environment through the mooring lines which float in the water column and drag over the seafloor as well as the anchors that have to be installed. It is still uncertain how much those factors, as well as turbine noise, affect the environment, especially in large scale wind farms, hence further research dedicated to floating wind is required (Offshore Wind Innovation Hub, O&M and Windfarm Lifecycle - Project Development - Floating Wind).

Additionally, the overall modelling and monitoring of the marine and the ornithological environment must improve. The models have to separately assess the impact of the floating wind turbine on individual marine life behaviour (by a single turbine), the population changes (entire wind farm) and the ecosystem changes (several adjacent wind farms). Spatial scales to coordinate the data collection also are beneficial as well as using an open database with a determined roadmap to collate the data, thereby avoiding the “sample everything” approach. If a suitable environmental monitoring method has been developed, standardisation of this method will be beneficial (Offshore Wind Innovation Hub, O&M and Windfarm Lifecycle - Project Development - Reducing ecological impact uncertainty).

In terms of monitoring techniques, ornithological monitoring should be improved to monitor bird behaviour accurately and thereby avoid too conservative approaches, delays, cost increases or potentially even refusal of consents. Marine life monitoring can be improved by also considering indirect environmental effects. For example, the floater extracts energy from the water column, especially in combination with wave or tidal energy. This extraction impacts the water column mixing, which in turn influences the primary production and thereby the food chain (Offshore Wind Innovation Hub, O&M and Windfarm Lifecycle - Project Development - Reducing ecological impact uncertainty).

9 Installation and infrastructure

As it is generally a necessity to minimise the cost in a large scale commercialised floating offshore wind farm, the assembly and installation procedures of FOWT require several innovations and improvements. Those innovations affect the turbine assembly, the installation of the moorings, anchors, the cables and as well as the procedures taking place offshore in genera.

9.1 Turbine assembly

In contrast to the previous innovations, which were mostly independent of the floater design, its design is highly influential on the assembly process. Generally, turbine and substructure components are fabricated in low personal cost countries and then will be transported to the port or site as single or pre-assembled parts. When a semi-submersible floater is used, the turbine assembly takes place at a suitable port by a crane with high lift height like a crawler crane. The assembled turbine then is towed to the site and connected to the moorings and cables. Spar-buoys have a large draft and therefore cannot be installed at a port. They require a sheltered location, where a heavy lift vessel (HLV) assembles the different turbine parts. Afterwards, the turbine is towed to site and connected to the pre-assembled mooring and cabling system. If a TLP is used and it is inherently stable enough to be towed to site, it can be assembled at the port-site like the semi-submersible FOWT. Otherwise, all parts require to be brought to site, then connect the substructure to the moorings and then assemble the tower onto the moored substructure with a floating dynamically positioned installation vessel (Carbon Trust 2018, p. 53). An overview of the different installation methods is shown in figure 30. However, those procedures are subject to change as the floater concept evolves. Barges are installed similarly like semi-submersibles.

Key Features	Semi-sub	TLP	Spar
Substructure Fabrication	Multiple Site(s)	Multiple Site(s)	Multiple Site(s)
Substructure Assembly & Loadout	Quay + Trailer	Quay + Trailer	Quay + Trailer
Turbine Assembly & Integration			
Lower Tower Integration	Quay	Quay	Inshore/offshore
Turbine Assembly	Pre-assembled rotor	Pre-assembled rotor	Pre-assembled rotor
Turbine Integration	Quay/Inshore/Offshore	Offshore	Inshore/Offshore
Transit			
Substructure	Wet tow/On-deck	Wet tow/On-deck	Wet tow/On-deck
Substructure-Turbine Integrated	Wet tow/On-deck	Not Possible	Wet tow
Specific Operations	None	Tendon Tensioning	Upending
Mooring System	Pre-Installed	Pre or Post	Pre-Installed

Figure 30: Different installation methods for floater designs (Carbon Trust 2018, p. 53)

When large commercial-scale wind parks (50+ turbines) need to be installed within one summer campaign (200 days), it is essential to have a substructure design that is compatible with serial fabrication methods. Additionally, port infrastructure is required to be able to handle the production of several units at once as substructure construction is expected to require 7-15 days per unit. However, to meet timelines, a fully assembled substructure is needed every four days. Therefore, at least four substructures have to be assembled in the production line at a time. Additionally, the throughput can be increased by using two parallel assembly lines. However, not every port is capable of producing at such a large scale. Therefore, substructure production may spread across several port facilities to ensure the delivery timelines (Carbon Trust 2018, p. 55).

Even though using dry docks to produce semi-submersibles might be a feasible option, it would severely limit the serial production of them. There are only a limited number of dry docks with

sufficient size and draft for a semi-submersible production globally. Furthermore, in dry docks, the substructures would have to be produced simultaneously, which isn't suitable for mass production. Alternatively, the substructure could be assembled on a submersible barge at dockside. However, regarding serial production, this procedure isn't compatible either. Probably the most suitable assembly approach is a serial assembly line at the quayside with a load-out by a trailer. This procedure not only optimises the throughput time but additionally mitigates the need for heavy lift operations and decreases crane capacity requirements. Large dry docks still could be beneficial for serial production as they can be utilised as wet storage for completed structures and as a production buffer (Carbon Trust 2018, pp. 55–56).

Some early investments in port infrastructure will significantly increase the availability of suitable ports for floating offshore wind production. Those investments regard the soil bearing capacity, improvements in available crane capacity, onshore set-down area and wet storage (Offshore Wind Innovation Hub, O&M and Windfarm Lifecycle - Installation - Floating Wind; Carbon Trust 2018, p. 52). More ports would also become suitable for FOWT production when the draft of the structure minimises. Therefore, developers should increase their focus on draft minimisation to improve the suitability of their design (Carbon Trust 2018, p. 54). Alternatively, if the draft of a semi-submersible becomes too large, it could also be installed in a sheltered area like a spar-buoy (Carbon Trust 2018, p. 56). Port availability would even increase if a large crawler crane can be brought to the port-side. However, those cranes are logistically challenging, expensive and are globally only available in limited numbers. To decrease those cost, smaller jack-up vessels, that have become too small to handle large scale bottom-fixed turbines, could become an alternative. They can be jacked-up above quay-side level, thereby lift in heights typical port cranes cannot operate in and replace the need for large crawler cranes (Carbon Trust 2018, p. 55).

The installation process itself can also be improved. For example, improvements in rapid steel welding and the use of quick-setting concrete is fastening up the serial production (Carbon Trust 2018, p. 61). Using slip joints instead of flange to flange connections at the base of the tower decreases the installation time and bumpers, guides and installation aid can be helpful to control the relative motions of the floater (Carbon Trust 2020, p. 56).

When spar-buoys should be installed in a sheltered area or when TLPs are assembled offshore or for maintenance activities (floating) heavy lift vessels (HLVs) are required. However, current HLVs are large structures that are not yet optimised for floating wind as they have to be flexible to increase their usage (Carbon Trust 2020, p. 50). Future optimised HLVs could increase the working conditions of the spar-buoy assembly from a maximum wave height of 1.4 metres to 2.5 m as well as improve capable windspeeds for a component lift for speeds higher than 12 m/s, which would not reduce risk during the lifting but also minimise the HLV usage time (InnoEnergy 2018, p. 66). The installation time can also be reduced by using feeder barges, that supply the HLV with the required components (InnoEnergy 2018, p. 67). Nevertheless, the feasibility of a new HLV specific for floating wind is not determined, yet (Carbon Trust 2020, p. 54).

The lifting operations could be minimised by lifting the entire assembled turbine in one single lift onto the spar-buoy (InnoEnergy 2018, p. 68). However, no crane currently installed on an HLV can single lift turbines over 6 MW due to height constraints. The maximum hub height, which could range from 162 to 190 m in future 20 MW turbines, is an important factor for the heavy HLV selection. Currently, only a few HLV are capable to lift that high as most of the HLVs are focussing for flexibility reasons on a high lift radius instead of extreme lift height (Carbon Trust 2020, p. 50). Alternatively, HLVs with two cranes could be used as they enable larger single lifts. To reduce LCOE, a practical optimum turbine size and a consensus upper bound hub height will be beneficial (Carbon Trust 2020, p. 55).

HLVs can also be further improved regarding motion compensation (MoCo), especially for floating to floating operations. Those motions include a crane tip MoCo, crane base MoCo, an active or passive heave compensation or a full 3D MoCo to improve the walk to work system. Usually, heave compensation is done by lowering the HLV onto the seafloor to increase the speed of the hook movement of the crane. Walk to work systems improve the walking transfer between two floating structures or a floating structure and a fixed structure by removing the relative motions of the floating vessel (Carbon Trust 2020, pp. 51–52).

When HLVs or cranes used at the port-side are not capable of lifting in the required heights and scale, climbing cranes might be a feasible alternative in future floating offshore wind applications. Climbing cranes use the tower as their support, drive along it and assemble the required components without limit to lift height. However, they have only been tested in onshore wind context yet, currently are limited in lifting capacity and require an adjusted tower design. Nevertheless, small adjustments in their support points can increase their lifting capacity. Additionally, they are well suited to perform maintenance work offshore as they are significantly cheaper than floating HLVs (Carbon Trust 2020, p. 52).

Generally, the open engagement between turbine manufacturers and supply chain has to increase to ease the installation and maintenance of floating offshore wind turbines, which is hindered by the additional motions of the floater, and thereby reduce the cost significantly (Carbon Trust 2020, p. 55).

9.2 Cable installation

One of the first floating offshore wind projects, Fukushima FORWARD, used the following cable installation method: At first, a cable laying vessel (CLV), which can carry up to 160 km of cable, installed the static section of the cable. Afterwards, the dynamic cable was installed through the dynamic bend stiffener to the floater (either the substation or the FOWT). The termination points of both cables were pulled upwards by a remotely operated vehicle (ROV) or a grapnel, connected on the CLV with the transition joint and the static bend stiffener and then lowered to the seabed by an ROV. Even though this procedure is subject to change as new, low-cost cable installation methods will be developed, it is expected to stay similarly (Weerheim 2018, pp. 45–46).

Several dynamic cable failures can occur during installation, that has to be mitigated to ensure cable lifetime. Those failures are caused by (Weerheim 2018, p. 27; p. 41):

- loosing dynamic positioning, which might lead to undesired strain, bending and choking of the cable.
- anchors of the CLV that damage previously laid cables, when the CLV moors itself during the installation process.
- too small bending radius which induces in residual tensions in the cable that result in movement of the cable over the seabed.

Additionally, static cables can be damaged during installation by (Weerheim 2018, p. 27; p. 41):

- kinks induced by the inadequate forward motion of the floater.
- damages during loading and re-loading of the cable by bad handling.
- inappropriate trenching methods or equipment.

Improvements in the accuracy of vessel control, the overview of the vessel surroundings, the cable handling methods and the vessel equipment and size will be beneficial to improve the cable laying procedure and reduce cost (Weerheim 2018, p. 27; p. 41).

Cable installation cost can also be reduced by increasing the range of working conditions the CLV can operate in. This maximises the vessel utilisation cost and thereby reduce CLV charter rates (InnoEnergy 2018, p. 68).

As mentioned in chapter 6.1, the cable connection and disconnection procedure is an essential task in the cable installation process and maintenance. Simplifying the cable connectors could decrease installation time significantly and thereby reduce cost.

9.3 Mooring installation

The mooring installation procedure is different for every project as it depends on several factors. These factors include the mooring type, used material as well as the floater design and the port and site characteristics. Generally, the moorings, anchors and connectors are pre-assembled at the harbour. Following, they are loaded onto an anchor handling vessel (AHV), installed at the site and when the floater is assembled then hooked up to the substructure (Corewind 2020, pp. 39–40).

Due to its complexity, the mooring installation is a large cost contributor, particularly in large scale wind farms with a large number of moorings and anchors that have to be installed. Additionally, these costs rise when TLPs are used due to their instability and high-tension moorings, even though those additional costs are countered by decreased procurement cost. Essential factors in the mooring installation are (Carbon Trust 2018, p. 45):

- the connection time and simplicity of mooring top connectors as well as their met-ocean limitations
- the required precision and the installation time of the anchors and potential anchor piling requirements
- requirements of the mooring materials like pre-tensioning and handling of hybrid mooring lines
- the mooring line dimensions resulting in specific handling and vessel requirements
- the platform stability and the mooring connection points
- the site met-ocean conditions as well as its distance from the port
- the handling capacity, bollard pull, charter rate and general availability of the used AHV
- the set-down area and load-out of the port
- the number of mooring lines and anchors used in the project and the project timeline

When all of those factors are considered in early project planning stages, the installation cost can reduce significantly (Carbon Trust 2018, p. 45).

It will be highly beneficial when future improvements could increase the speed and accuracy of the mooring installation as it will significantly reduce the required time at sea for large scale wind farms and consequently the associated cost (InnoEnergy 2018, p. 65). However, they need to be safer simultaneously because, according to Rambøll, flawed installation methods are currently contributing to 22% of all mooring damage (Carbon Trust 2018, p. 43).

The mooring installation for future large scale floating offshore wind farms could also require new AHV specific for those applications. Those new AHVs can improve installation by having a larger mooring capacity and being able to install larger mooring lines and anchors, as well as having a high bollard pull to ease mooring hook-up (Carbon Trust 2018, p. 57).

9.4 Offshore operation

For all floating offshore installation activities like heavy lift operations, mooring and anchor installation or cable laying, it is essential to operate as accurate as possible. Dynamic positioning (DP) is a crucial tool to enable this accuracy. It has been expensive so far, but recent and future improvements to DP are expected to significantly reduce the price and solve several challenges (Carbon Trust 2018, p. 56).

Improving DP for rougher environmental conditions could also increase the maximum operable average weight height from 2.0 m to 3.0 m, thereby increasing the weather window for offshore operations. Additionally, the optimisation of connectors and substructures ensures the installation during harsh conditions (InnoEnergy 2018, p. 67).

The towing operation of the assembled FOWT is restricted to weather conditions and limited to slow towing speeds up to 5 knots. Additionally, it requires a port of refuge for extreme weather conditions, especially when the tow operation has a longer transit time than the maximum forecast period (72 hours, equivalent to ~ 360 miles). In those long-distance tows, the vessel and floater have to be designed to withstand the 10-year storm events, as the weather cannot be forecasted accurately (Carbon Trust 2018, p. 57). Further research on the acceleration limits of the FOWT will improve the tow speed, and additionally fasten up the turbine assembly. Currently, blades need to rotate during transport and installation, eliminating this need will be beneficial (Carbon Trust 2020, p. 56).

Offshore installation scheduling is highly dependent on met-ocean conditions. To be able to respond to the current conditions and on-site challenges quickly, an extensive installation vessel will be beneficial to adapt swiftly scheduling plans (InnoEnergy 2018, p. 66).

10 Operation & Maintenance

Floating offshore wind farm operators and owners are not only interested in efficient and well-built wind farms, but they also want them to operate as reliably and conveniently as possible over the longest possible lifetime with minimal OPEX. Therefore, O&M strategies and maintenance operations need to be as cost-efficient as possible.

10.1 Operational strategies

Currently, wind turbines are controlled individually to maximise the power generation of every single unit. However, wind farms lack a control tool that optimises the performance of the wind farm as one entity. This controller could provide an improved energy production as it considers the wake effects of the turbines in one row, reduce the turbine loadings and can consider the impact of the wind turbines onto the grid balance. Additionally, it could control the wind farm in separate clusters which provides further flexibility in turbine operation. A holistic controlling approach might also be beneficial to maintenance as it could provide valuable information about the site condition and turbine status. The turbine status might also be considered in the control strategy of the wind farm as it might be more profitable when a turbine generates less electricity but thereby increases its lifetime and the profit in the long-term (Offshore Wind Innovation Hub, O&M and Windfarm Lifecycle - Operations – Assets & Technical – Control Optimisation).

The profitability of the wind farm can increase additionally as not only the weather forecast but also the forecast of expected electricity prices is included in the day to day operational decisions. If the maintenance operation is executed during low electricity price periods, the downtime losses will decrease significantly (Offshore Wind Innovation Hub, O&M and Windfarm Lifecycle - Operations - Commercial & Strategy - Trade & Yield Optimisation).

For a reliable long-term operation of floating offshore wind farm, it would be valuable when standardised methods can be developed to assess the remaining life of turbines, foundations, anchoring and mooring lines. An accurate assessment of the lifetime of the different wind turbine components will not only reduce the number of required inspection but also might justify the extension of the FOWT lifetime beyond the expected 25 – 30 years. Those standardised assessments require the early involvement of the original equipment manufacturers. Still, they are only expected to be developed when the installation of FOWT ramps up and standards have been established for bottom-fixed turbines (Offshore Wind Innovation Hub, O&M and Windfarm Lifecycle - Operations – Floating Wind).

Additionally, lifetime management tools might be used to analyse the monitoring data, perform predictive maintenance operations based on those analysis and thereby eventually even increase the expected lifetime of the wind turbine (Offshore Wind Innovation Hub, O&M and Windfarm Lifecycle - Operations – Assets & Technical – Lifetime Management).

10.2 Maintenance strategies

The inspection and maintenance rate of offshore wind farms is currently based on determined schedule plans without regarding the actual condition of the wind turbine. In contrast, condition-based maintenance uses the data of the condition monitoring sensors to plan the maintenance activities based on the current status of the turbine components. Thereby the turbine downtime decreases, which results in increased AEP and reduces OPEX since technicians get no longer send to the site for maintenance work that is not required. Even though the turbine acquisition cost will increase as more sensors are needed, the reduction in OPEX is expected to outweigh those cost (InnoEnergy 2018, p. 74). Figure 31 displays the differences between predetermined maintenance and condition-based maintenance as well as corrective maintenance.

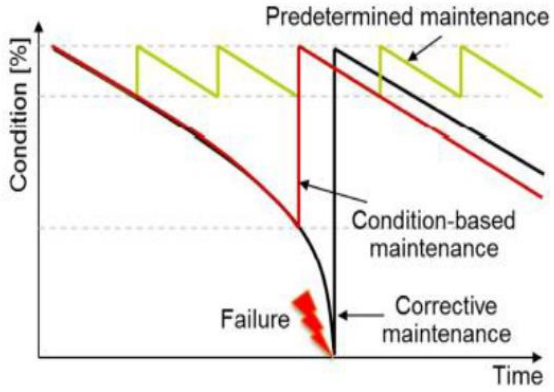

Figure 31: Objects condition in different maintenance types (Corewind 2020, p. 42)

However, maintenance activities are still expected to be significantly more frequent in floating wind than in bottom-fixed offshore wind. Besides the regulatory uncertainties of the relatively new technology that result in more conservative maintenance plans, FOWT components experience additional loads through the motion of the floater, which results in more frequent intervention and inspection rates. Additionally, floating wind turbines consist of more components that are sensitive to those motions than its bottom-fixed counterpart (Offshore Wind Innovation Hub, O&M and Windfarm Lifecycle - Operations – Floating Wind). Currently, this results in 120 hours of annual in-person inspection for floating wind compared to 20 hours annually for a monopile foundation and 60 hours annually for jacket foundations in a predetermined maintenance plan (InnoEnergy 2018, p. 76). Therefore, it is essential to improve the understanding about the motion effects of a FOWT onto its components and to loosen the conservative requirements accordingly (Offshore Wind Innovation Hub, O&M and Windfarm Lifecycle - Operations – Floating Wind).

Bespoke maintenance planning software tools promise to improve the efficiency of currently human planned maintenance strategies as the software optimises those plans based on available resources and expected outcome. Additionally, it is crucial to clarify the technicians the influence of their activities on the efficiency of the maintenance strategy (Offshore Wind Innovation Hub, O&M and Windfarm Lifecycle – Maintenance – Service – Planning).

Currently, various countries have various maintenance approaches. A more streamlined global maintenance strategy could improve technician training, as well as the certification process, national policies, best practices and the safety of the workers. Thereby, the efficiency of maintenance activities would increase and their cost would reduce (Offshore Wind Innovation Hub, O&M and Windfarm Lifecycle – Maintenance – Service – Statutory inspections).

Early integration of the maintenance strategies into the floater design will be beneficial as well. Those design variations can include the implementation of active ballasting systems, which not only benefits the stability of the floater but also could be a feasible solution to support the offshore lift operation, or the integration of a support structure for climbing cranes into the tower (Carbon Trust 2020, p. 56).

One of the large benefits of floating offshore wind turbines on paper is their ability to be disconnected from the site and towed to port for major repairs. However, the viability of those tow-to-port strategies is not yet fully determined. Besides the costly and complex mooring and cable top connectors, which were examined in chapter 6.1 and 7.1, there are uncertainties regarding the port infrastructure and the out-of-service arrangements. Tows-to-port require a sufficiently large quayside area with capable crane capacity to perform the major repair that must be available when required. Additionally, a buoy, a substructure-like floater or an additional electrical cable is required to connect the disconnected cable and moorings to and to maintain the electrical flow of power even when the turbine is removed.

If research shows that tow-to-port strategies are not feasible, floating heavy lift vessels or alternative crane solutions are required to perform the major repairs offshore (Carbon Trust 2018, p. 60; Offshore Wind Innovation Hub, O&M and Windfarm Lifecycle - Operations – Floating Wind).

Those mentioned crane solutions usually are very expensive, especially for high hub heights as it was examined in chapter 9.1. In recent offshore wind projects, blade exchange was performed craneless by some rigging solutions. Even though those rigging solutions require certain scaling for offshore wind, they should be viable for floating offshore wind as well. They would be especially appealing when the use of a crane vessel is too expensive, for example, when only a single turbine blade needs to be exchanged (Carbon Trust 2020, p. 52).

If blades only require a repair or usual maintenance, it would be beneficial for technician safety as well as repair quality, when a suitable repair and maintenance habitat would be developed. This habitat is not only protecting the technicians and material from environmental impact and therefore increase the working conditions of those activities, but also would control humidity and temperature to assure the required quality (Offshore Wind Innovation Hub, O&M and Windfarm Lifecycle – Maintenance – Reactive Maintenance – Major Repairs).

10.3 Crew transport & Access

Floating offshore wind farms are expected to be installed far from shore. Therefore, it is important to improve not only the maintenance activities itself but also improve the crew transfer vessel (CTV) to ensure best possible technician access to the turbines and to make maintenance activities as efficient as possible.

Technician access can be improved by advancing the dynamic positioning of the CTV to decrease the relative motions between the floating to floating operation and thereby decrease the personnel risk during the transfer and access a wider range of weather conditions, which decreases OPEX (Offshore Wind Innovation Hub, O&M and Windfarm Lifecycle - Operations – Coordination & People – Vessels & Access). For example a CTV with a passive or active heave compensated walkway or lifting pod that increases the operability to a maximum wave height of up to 2.5 m would increase the accessibility of an offshore wind farm in the North Sea from 70% to 95% (InnoEnergy 2018, p. 74).

Additionally, CTVs should increase their maximum payload capacities to transport more material and tools to site to be more flexible and to decrease OPEX as it would reduce the number of required CTVs. Improvements in the comfort of the CTV would maximise the technicians' productivity on-site and thereby increase maintenance efficiency and decrease the OPEX. However, the number of required technicians per turbine is expected to decrease as the automation of O&M is increasing (InnoEnergy 2018, p. 75). New CTV designs might also have a more efficient hull shape, could use new propulsion methods or alternative fuels like electric drives or hydrogen to meet market demands (Offshore Wind Innovation Hub, O&M and Windfarm Lifecycle - Operations – Coordination & People – Vessels & Access).

If the CTV is not capable of accessing the wind turbine due to high wave heights, helicopters are an alternative to ensure personnel access even in harsher conditions. However, they are very costly and not justifiable if they have high standby rates. Therefore, it is essential to maximise its utilisation by sharing one helicopter for multiple adjacent sites and improving the weather resistance and maximum payloads of the helicopter to make it more suitable for several maintenance activities (Offshore Wind Innovation Hub, O&M and Windfarm Lifecycle - Operations – Coordination & People – Vessels & Access).

If a large scale floating offshore wind farm is deployed far from shore, it might not be feasible and efficient anymore to have long-distance travels to perform maintenance activities. For those applications, motherships or service operation vessels promise to reduce OPEX significantly. Those vessels are stationed at site for several weeks and technicians live for this period on the service operation vessel. They are then sent from the mothership to the turbines with a smaller vessel to minimise travel distance. Supposing the wind farm is sufficiently large and requires continuous maintenance activities, it might also be feasible to build a floating or fixed offshore base that also can be utilised as material storage for O&M activities. Alternatively, retired O&G platforms in proximity to the wind farm can be used as a base for technicians (Offshore Wind Innovation Hub, O&M and Windfarm Lifecycle - Operations – Coordination & People – Vessels & Access).

Staff and vessel utilisation will be significantly improved by the accurate met-ocean condition forecast of an area of approximately 100 km^2 for a time period beyond five days. Those improvements provide a reduced downtime of the turbine as routes can be planned accordingly (InnoEnergy 2018, p. 75; Offshore Wind Innovation Hub, O&M and Windfarm Lifecycle - Operations – Coordination & People – Vessels & Access). Route planning is very site-dependent and no best fit for all sites can be determined. Therefore, route planning can be improved by using innovative tools that utilise AI and machine learning to develop the best routes specific to the site (Offshore Wind Innovation Hub, O&M and Windfarm Lifecycle - Operations – Coordination & People – Marine coordination).

As floating wind establishes the knowledge about the required tools and parts for turbine maintenance increases resulting in a decrease of OPEX. Research and experience will also improve the knowledge about turbine fault patterns whereby the repair time and consequently also the turbine downtime decreases (InnoEnergy 2018, p. 76). OPEX can be further reduced by using a data-driven warehousing and logistics approach that increases the efficiency and productivity of the inventory management system. Additionally, it reduces stock levels and the cost of holding space (Offshore Wind Innovation Hub, O&M and Windfarm Lifecycle - Operations – Coordination & People – Marine coordination).

10.4 Automated O&M

It is always a large cost contributor to send technicians offshore to perform an inspection, maintenance or repair activity and it will risk technicians health and safety, even if CTVs are optimised. The use of remotely controlled or autonomous vehicles that can carry out those tasks instead could reduce OPEX significantly (Offshore Wind Innovation Hub, O&M and Windfarm Lifecycle - Operations – Coordination & People – Vessels & Access). The largest cost reduction is expected when fully autonomous systems are used. Still, remote-controlled robots offer some cost reduction as well (Offshore Wind Innovation Hub, O&M and Windfarm Lifecycle - Operations – Coordination & People – Human factors).

Those autonomous units like drones or robots are very useful to perform redundant, remotely diagnosable tasks like bolt torquing or lubrication replenishment. Thereby, not only personnel cost and transit cost are reduced, but it also enables technicians to focus more on troubleshooting and performance optimisation and reduces the annual service downtime (InnoEnergy 2018, p. 73; Offshore Wind Innovation Hub, O&M and Windfarm Lifecycle – Maintenance – Service – Servicing).

Drones are particularly promising to improve blade inspection and repair. Currently, three technicians that access the blades via rope require one entire day to inspect the blades of one turbine. In contrast, a remotely controlled or even autonomous drone can perform this inspection reliably three times faster. Thereby, only one operator is required that operates the drone and analyses the inspection data (InnoEnergy 2018, p. 73) (Offshore Wind Innovation Hub, O&M and Windfarm Lifecycle - Operations – Assets & Technical – Survey & Inspection). Automated systems can also be used to repair smaller blade defects like erosion or surface defects or to routine check the lightning protection system (Offshore Wind Innovation Hub, O&M and Windfarm Lifecycle – Maintenance – Reactive Maintenance

– Planned Corrective). Additionally, systems might be developed that remotely perform non-destructive testing of the blades or substructure and the operator only is informed when an anomaly occurs or an event that requires additional attention (Offshore Wind Innovation Hub, O&M and Windfarm Lifecycle - Operations – Assets & Technical – Survey & Inspection).

ROVs can be used to perform subsea inspections of the substructure. It will be beneficial to improve the cameras and sensors of the ROV to increase its suitability for those operations and reduce the need for human divers to inspect substructures. Additionally, ROVs can be used to inspect cables and moorings (Offshore Wind Innovation Hub, O&M and Windfarm Lifecycle - Operations – Assets & Technical – Survey & Inspection).

Another benefit of the autonomous inspection systems is their ability to perform several tasks at once when they are used as teams or swarms. Those teams might be stationed in unmanned vehicle hubs, that can transport the robots to the turbine and deploys, recovers and recharges them. Those hubs should be a fully encompassing solution that is flexible and expandable (Offshore Wind Innovation Hub, O&M and Windfarm Lifecycle - Operations – Coordination & People – Human factors).

The robotic solutions must become easy to interact with for the technicians. Additionally, new technologies might support the technicians on site. E.g. augmented reality headsets could provide them with additional maintenance information to increase the efficiency of the offshore operations. Another solution could be natural language translations that can be used to ease the interaction between the very internationally diverse technicians (Offshore Wind Innovation Hub, O&M and Windfarm Lifecycle - Operations – Coordination & People – Human factors).

10.5 Monitoring

As it was examined in previous chapters, condition monitoring of the wind turbine components is essential to reduce the required annual personnel maintenance hours and to predict the lifetime of the component accurately.

Besides the component-specific monitoring techniques, some monitoring methods also help to track the overall wind park status. Satellites can be used to monitor the visual status of the farm, the sea state, ground conditions vessel movements. Improvements in the cost of the met-ocean condition measuring sensors will enable deployment of those sensors at a larger scale across the wind farm and thereby improve the met-ocean data which results in optimised offshore operation planning and an improve forecast of the electricity generated (Offshore Wind Innovation Hub, O&M and Windfarm Lifecycle - Operations – Assets & Technical – Monitoring).

The introduction of CM sensors in a variety of turbine components will result in a vast amount of data that has to be analysed. Therefore, machine data analysis like machine learning and artificial intelligence will be beneficial to process this data, identify sub-optimal performance and notice failures and issues earlier (Offshore Wind Innovation Hub, O&M and Windfarm Lifecycle – Maintenance – Reactive Maintenance – Major Repairs).

However, as not the data analysis might be the critical cost factor but the required server storage to store all those data, the necessity, purpose and number of sensors used for CM require to be evaluated carefully (Corewind 2020, p. 57).

10.6 Decommissioning

Decommissioning is a vital part of all O&M strategies that must be included in the early development stage of every component. After the expiration of the turbine lifetime of usually 25 to 30 years, components either should be able to be reused, recycled or in the worst case used to generate energy by burning it.

One crucial area of improvement is the recycling of blades which consist of large-scale composites that currently cannot be recycled. An alternative recyclable blade material might be thermoplastic. However, this material has not been used on a larger scale so far and requires an alternative design and manufacturing process (Offshore Wind Innovation Hub, Turbines - Rotor - Disruptive blades).

Currently, there is no method to sufficiently recycle nacelle components. The overall turbine cost can be decreased by developing nacelle decommissioning procedures as some nacelle components consist of critical materials like rare earth (Offshore Wind Innovation Hub, O&M and Windfarm Lifecycle – Decommissioning).

Buried components of the offshore wind farm like some of the anchors and static cables are usually left behind when a wind park gets decommissioned. Nevertheless, those components consist of valuable materials or potentially even could be re-used entirely, whereby it will be beneficial when decommissioning methods are established for those components (Offshore Wind Innovation Hub, O&M and Windfarm Lifecycle – Decommissioning).

Decommissioned substructures might be feasible to be re-used with larger new wind turbines even though additional research that investigates the suitability of this application is required. Alternatively, a new large-scale rotor could be deployed onto an old drive train. However, the limitations of this configuration are not yet thoroughly investigated (Offshore Wind Innovation Hub, O&M and Windfarm Lifecycle – Decommissioning).

11 Use cases

National grid limitations may slow down the large-scale deployment of floating offshore wind farms as a large proportion of renewable energies negatively affects the grid balance. Therefore, it is essential to develop new use cases for FOWT, which are independent of the electrical grid connection. Additionally, the utilisation of wind farm space could be improved by combing floating wind with other suitable solutions.

One alternative use case for floating wind is combining it with Power-to-X (PtX) technologies. In PtX, electricity gets converted through electrolysis and other synthesis processes into liquid or gaseous chemical energy sources, most commonly hydrogen. PtX is expected to play a vital role in the decarbonisation of fossil fuel-dependent sectors, therefore is an enormous opportunity for offshore wind, which is particularly suitable for hydrogen production because it is carbon neutral. Currently, gas or coal is used to produce hydrogen and the resulting carbon is either emitted (grey hydrogen) or stored (blue hydrogen). In contrast, offshore wind does not require fossil fuels and does not emit any carbon, whereby the hydrogen produced by wind energy and other renewable energies is called green hydrogen.

Additionally, the offshore wind farm doesn't have to be connected to the grid anymore, which reduces the balancing cost, the risk of electricity suppliers and decouples it from transmission restrictions, thereby increases the availability of the wind farm. Those cost savings could even offset the additional required CAPEX for hydrogen production. When the technical innovations introduced are implemented, the price of offshore wind is expected to decrease significantly. Thereby, the green hydrogen price could drop from current $2.50 - $6.8/kg to $0.8 – $1.6/kg by 2050, which would make it price-competitive with fossil fuels (Global Wind Energy Council 2020, pp. 91–92).

Hydrogen production may also enable the deployment of far from shore offshore wind parks which have a distance of around 200 km to shore. Those distances make electrical cable costs too high to make a grid connection justifiable, whereby a non-grid connected system with a hydrogen production is more suitable. However, research has shown that the far from shore floating offshore wind farms are only feasible when the capacity factor is above 60%, what could be achievable as the Hywind Scotland has already an annual capacity factor of 56% (Ioannou and Brennan 2019, pp. 4–5). In early applications, before non-grid connected systems with exclusive hydrogen production will establish, PtX could also be used to process the surplus wind energy that otherwise would be curtailed (Global Wind Energy Council 2020, p. 93).

The hydrogen production could take place at different sites. The first solution is a purposely built PtX facility that is installed offshore, where hydrogen or another energy carrier is stored in tanks that are then transported to shore by ship, which can be seen in illustration 1 a) in figure 32. If the ship transport isn't feasible, the generated electricity alternatively can be transported to an onshore hydrogen facility, which is especially suitable for near-shore wind parks, compare 1 b) in figure 32. When the wind farm is built close to an O&G platform, the platform can be utilised to produce hydrogen. The hydrogen then is transported to shore via the gas pipeline with a hydrogen proportion of up to 20%. This solution, which can be seen in 2 in figure 32, is suitable for decarbonising the energy sector entirely but could be useful for the transition period (Global Wind Energy Council 2020, p. 93).

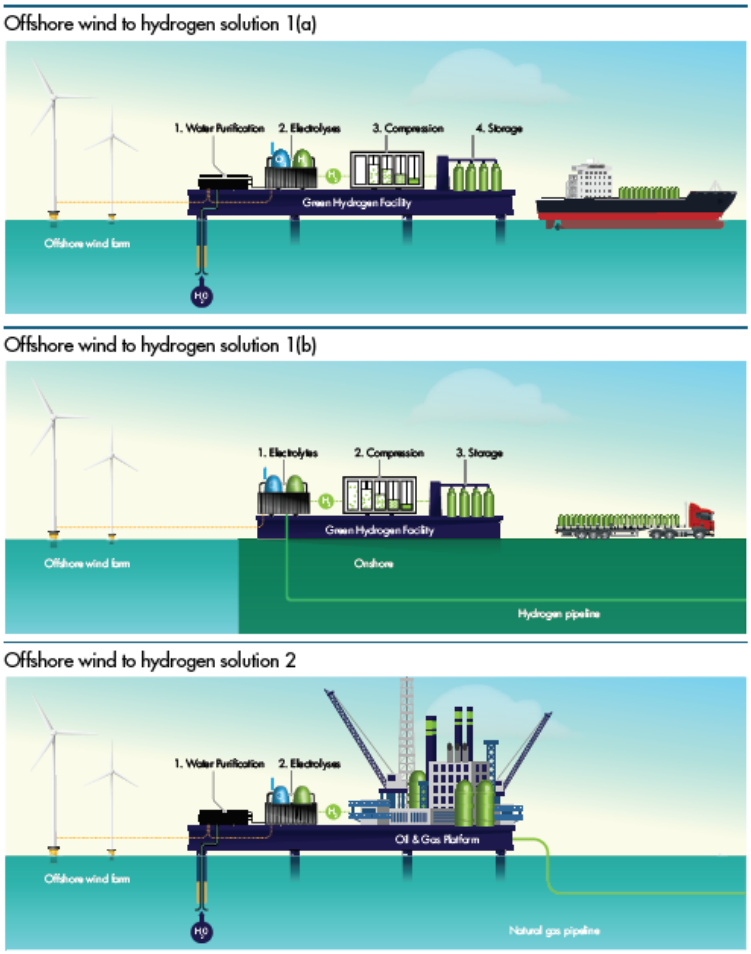

Figure 32: Different solutions for hydrogen production (Global Wind Energy Council 2020, p. 93)

Another alternative for a hydrogen facility is installing the equipment on the substructure itself which could bring down the cost as no additional platform is required. The first floating offshore wind with a hydrogen production is currently planned by ERM and funded by the British government. In this project, a prototype with a 2 MW turbine on a semisubmersible by Principle Power is planned to be installed in 2023 at the east coast of Scotland. In the next step, a scaled-up 10 MW pre-commercial turbine is planned for 2026. The first commercial offshore wind hydrogen farm with 100 MW should be deployed in 2032 and could be extended up to 4 GW in 2037 (Caine et al. 2019, p. 46).

When the hydrogen production facility is installed offshore and seawater is used to produce hydrogen, the electrolysers have to be more robust and weatherproof to be suitable for the offshore environment. Additionally, the electrolysis cost will have to be brought down and the efficiency has to increase (Offshore Wind Innovation Hub, Electrical Infrastructure - Flexible Offshore Wind Solutions - Cross-sector renewable integration).

Hydrogen (H_2) is the smallest existing molecule, which complicates transport and storage as it can penetrate several materials. Therefore, hydrogen is combined with natural gas when it is transported in pipelines. Those pipelines can be improved for hydrogen transport when they are made from Polyethylene, yet, additional research is required (Offshore Wind Innovation Hub, Electrical Infrastructure - Flexible Offshore Wind Solutions - Energy storage).

Generally, energy storage systems, to which hydrogen also belongs, are a viable solution to increase the revenue of the wind farm. With those systems, surplus electricity that either is not meeting demand in low peaks or would imbalance the grid can be stored in the energy storage systems and

then can be dispatched during high peak periods (Offshore Wind Innovation Hub, Electrical Infrastructure - Flexible Offshore Wind Solutions - Energy storage). For floating wind, different concepts of energy storage systems with the technology of a compressed air energy storage or hydro-pneumatic energy storage recently have been evaluated in the first studies and tested in prototype scale. In those studies, the energy storage system was integrated into the substructure of a TLP and a spar floater, which significantly increases the floater weight and would change the floater design but still could be feasible (Sant et al. 2017, 10; Buhagiar et al. 2019, p. 11). Still, there are uncertainties regarding scaling up energy storage systems, integrating them in existing infrastructure and the required support of the grid (Offshore Wind Innovation Hub, Electrical Infrastructure - Flexible Offshore Wind Solutions - Energy storage).

Currently, most of the O&G platforms use gas turbines installed on the platform to supply the required electricity. However, through the decarbonisation of the O&G sector, alternative solutions are needed. One of these solutions might be the installation of FOWTs close to the O&G platforms, which could supply the platforms with clean, renewable energy. (Offshore Wind Innovation Hub, Electrical Infrastructure - Flexible Offshore Wind Solutions - Cross-sector renewable integration). Equinor is already planning the first electrification of its O&G platforms and the final investment decision has already taken place. For the Hywind Tampen project in 2022, floating offshore wind turbines with a capacity of 88 MW should be installed in the northern North Sea, whereby 35% of the required annual electricity of the adjacent Snorre and Gullfaks oil fields will be provided (Equinor).

The utilisation of the space of the offshore wind farm is a vital factor for offshore wind farms. Therefore, wave energy generators could be integrated into the substructure design. Not only would this hybrid solution improve the production rates of wind, but they also could share infrastructure, lower the overall O&M cost and reduce the environmental impact. Additionally, as the wave energy generators would extract energy from the waves, the wave height would decrease, whereby the accessibility increases (Offshore Wind Innovation Hub, Substructures - Floating Wind). However, those hybrid solutions are in an earlier stage of development. More precisely, there is a lack of knowledge about the hybrid dynamics of the more complex system and it is still uncertain whether it is feasible to combine both technologies or if they instead should operate independently (Watson et al. 2019, pp. 6–7).

As mentioned in chapter 8.1, wind farms could significantly impact the survivability of the local fishing industry when essential fishing grounds are taken through the required wind farm area. Therefore, combining floating offshore wind farms with aquaculture could significantly contribute to sustaining the local fishing industry (Offshore Wind Innovation Hub, Electrical Infrastructure - Enabling Research - Design and materials). Aquaculture and floating wind could even benefit from another by reducing the site surveying cost, sharing anchors and installation cost and having shared vessel charter cost for O&M activity. Yet, those vessels cannot be utilised optimally as both activities have different O&M demands. When combined with floating wind, new nets are required for the aquaculture as traditional nets are not designed to be potentially damaged by mooring collision. Additionally, both activities have sup-optimal conditions and the availability of the wind turbines could reduce through aquaculture operations (Verschoof 2018, p. 131).

12 Wave loads and motions acting on a FOWT

Floating structures like semi-submersibles are exposed to large wave loads when they are installed and operating in an offshore environment. This chapter should determine the wave-induced loads on an exemplary floater by using the Morsion equation for different wave heading angles as well as the resulting response amplitude operators (RAOs).

12.1 Definition of the floater

The National Renewable Energy Laboratory (NREL) has been testing existing models and developed new models for offshore wind turbines for several years in the OC projects. During the OC5 project, the NREL validated a semi-submersible FOWT, called the OC5 DeepCwind Floating Wind System, which was selected as the basis for this thesis. The semi-submersible consists of three large outer columns that have a large submerged volume to stabilize the wind turbine that is placed in the centre of the substructure on a fourth smaller column, as it can be seen in figures 33, 34 and appendix D.

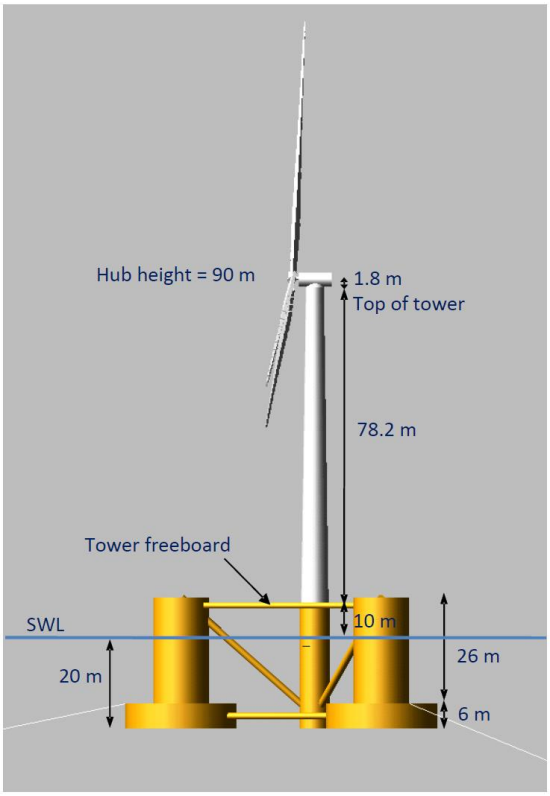

Figure 33: Complete OC5 DeepCwind Floating Wind System (Robertson et al. 2016, p. 4)

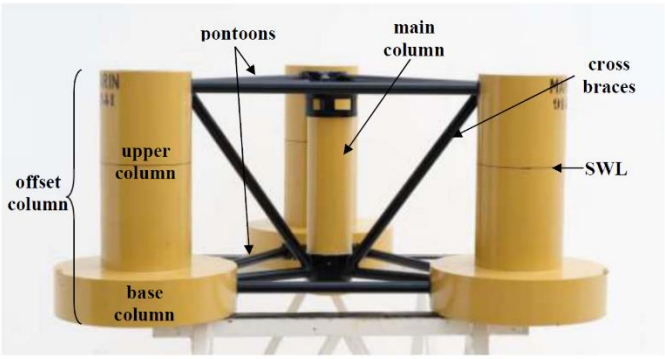

Figure 34: Description of the floater (Robertson et al. 2016, p. 23)

As it can be seen in figure 34, the outer columns of the floater are called offset columns, which are split into the larger diameter base column (BC) and the smaller diameter upper column (UC). It was unclear whether the base column can be regarded as a column or caisson. Therefore, both cases are investigated. For the caisson case, the cylinder will be called base caisson (BCS). The central column is called the main column (MC) and is connected to the offset columns through cross braces, while the offset columns are connected among themselves with pontoons. For simplicity reasons, the cross braces and pontoons are not taken to account for the following calculations. Additionally, only the foundation of the FOWT is considered, whereby the influences from the turbine, tower or moorings on the hydrodynamic movement are neglected. Table 1 displays the structural properties of the system as well as its hydrodynamic properties.

Table 1: Structural and hydrodynamic properties of the system (Robertson et al. 2016, p. 17)

description	symbol	value
Complete system mass	m_{tot}	1.2919E+7 kg
Draft	h_D	20 m
Draft of main column	h_{MC}	20 m
Thickness of base column/caisson	h_{BC}/h_{BCS}	6 m
Draft of upper columns	h_{UC}	14 m
Radius of main column	R_{MC}	3.25 m
Radius of upper columns	R_{UC}	6 m
Radius of base column/caisson	R_{BC}/R_{BCS}	12 m
Distance between offset columns and main column	a	28.87 m
Spacing between offset columns	b	50 m
Water density	ρ	1025 kg/m^2
Water depth	h	200 m

The wave loads and RAOs should be determined for five different wave heading angles: 0°, 45°, 90°, 135° and 180°. As the phase shift of the wave at every column will change with the wave heading angle, an additional coordinate system x', y' is introduced. This coordinate system can be described with $x' = x \cdot cos(\beta) + y \cdot sin(\beta)$ and $y' = x \cdot sin(\beta) + y \cdot cos(\beta)$ with β as the wave heading angle. The different wave heading angles are displayed in figure 35, where the offset columns and the corresponding upper and base columns are numbered according to appendix D.

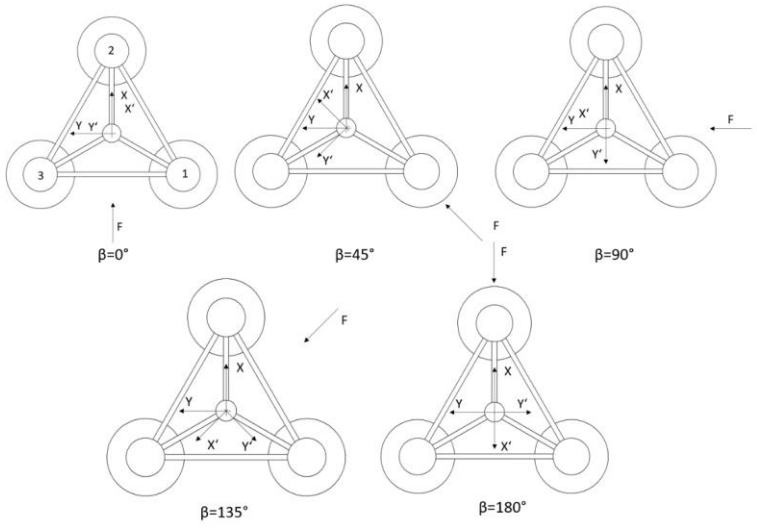

Figure 35: Different wave heading angles facing the floater

12.2 Hydrodynamic Model

To calculate the wave loads on the floater, a velocity potential $\phi(x, y, z, t)$ is provided, which exists, when an inviscid and incompressible fluid is assumed. Furthermore, small displacements and rotations are considered, whereby the body boundary conditions and free surface conditions can be linearized and the time dependency of the velocity potential can be linearized to (Ferri et al. 2020, p. 3)

$$-\omega^2\varphi + g\frac{\partial\varphi}{\partial z} = 0. \tag{1}$$

Here ω is the circular frequency, g is the gravity acceleration, z the vertical coordinates and φ the time-independent part of the velocity potential.

The Morsion equation can be used to calculate the inline forces of a body in an oscillation flow relatively accurate, even though it is empirically based and has several limitations. Those limitations include not accounting fluctuating lift forces, inaccurate capture of the inline force and ignoring memory effects (Benitz 2015, pp. 701–702). Additionally, to be applicable for the Morison equation, the structure has to be assumed as hydrodynamically transparent (Benitz 2015, p. 701). Hydrodynamic transparent structures are slender objects with the ratio $\frac{D}{\lambda} \leq 0.2$ with D as the objects diameter and λ as the wavelength which marginally disturbs the wave field, thereby normally occurring diffraction and radiation forces can be neglected (Ferri et al. 2020, p. 4). The inertia and drag forces dominate on those objects, which can be expressed by the Morison equation for a section of a bottom-fixed cylinder in the horizontal direction with (Clauss et al. 1992, p. 232)

$$dF_h = (f_m + f_d)dz = C_m\rho\frac{\pi D^2}{4}\frac{\partial u}{\partial t}dz + C_d \cdot \frac{\rho}{2}D|u|udz. \tag{2}$$

u is the vertical component of the velocity potential, the inertia coefficient $C_m = 1 + C_a$ is proportional to the added mass coefficient C_a and C_d describes the drag coefficient of the non-linear drag force f_d. To be applicable for floating structures, Clauss modified (2) to

$$dF_h = \underbrace{\rho d\forall\dot{u}}_{Froude-Krylov-Force} + \underbrace{\rho C_{a,h}d\forall(\dot{u}-\dot{v})}_{Added\ Mass\ Force} + \underbrace{\frac{1}{2}\rho C_d dA(u-v)|u-v|}_{Viscous\ Drag\ Force} \tag{3}$$

with $d\forall = \pi R^2 dz$ and $dA = 2Rdz$ for a submerged body (Clauss et al. 1992, p. 232). R is the radius of the cylinder and ∀ is the submerged volume of the cylinder. The Froude-Krylov force describes the force on the cylinder in a simplified pressure field without wave scattering and can generally be calculated with $F^{FK}(t) = -\rho\int\int\frac{\partial\phi}{\partial t}\,ndS$, however, for a submerged object this can be simplified to $F^{FK}(t) = \rho d\forall\dot{u}$ (Clauss et al. 1992, pp. 223–224). When the body is already moving with the velocity v, this velocity and its corresponding acceleration are considered in the added mass force and viscous drag force (Benitz 2015, p. 702).

Besides being inviscid, incompressible and irrotational, the waves are further simplified by using linear wave theory. For this theory, the wave is additionally assumed as being a two-dimensional, progressive gravity wave with a constant period, height and length, travelling over a horizontal, flat seabed. Furthermore, it has no temperature gradient through salinity gradients, no wind and no surface tension effect (Benitz 2015, pp. 695–696). Also, small amplitude waves where the wave height is much smaller than the wavelength and the water depth, whereby the non-linear terms of the velocity potential can be neglected ($\frac{H_w}{\lambda} \leq 0.02$) (Benitz 2015, pp. 695–696). Then the velocity potential can be simplified to

$$\phi(x,z,t) = \frac{\zeta_a g}{\omega}\frac{cosh\big(k(z+h)\big)}{cosh(kh)}sin(kx' - \omega t). \tag{4}$$

Here, $\zeta_a = \frac{H_W}{2}$ is the amplitude of the wave height H_W, $k = \frac{2\pi}{L}$ is the wavenumber depended of the wavelength L and h is expressing the water depth. In the complex form, the potential is

$$\phi_c(x,z,t) = -i\ \frac{\zeta_a g}{\omega}\frac{cosh\big(k(z+d)\big)}{cosh(kd)}e^{i(kx'-\omega t)} \tag{5}$$

with

$$\begin{aligned} -ie^{i(kx'-\omega t)} &= -icos(kx' - \omega t) - i^2\sin(kx' - \omega t) \\ &= \sin(kx' - \omega t) - icos(kx' - \omega t). \end{aligned} \tag{6}$$

As the floater is assumed to operate in deep water ($\frac{h}{L} \geq 0.5$) with a water depth of 200 m, the velocity potential can be further simplified as kh is reaching infinity and the hyperbolic tangent goes to one (Benitz 2015, p. 696). In deep waters, the wavenumber k can be expressed by rearranging the dispersion equation to $k = \frac{\omega^2}{g}$. Thereby the complex velocity potential in deep waters is

$$\phi_c(x,z,t) = -i\frac{\zeta_a g}{\omega}e^{kz}e^{i\theta_i}. \tag{7}$$

With the simplified velocity potential, the particle velocity and acceleration in the horizontal and vertical direction can be expressed as

$$u_c = \frac{\partial \phi_c}{\partial x} = \zeta_a \omega e^{kz}e^{i\theta_i}, \tag{8}$$

$$w_c = \frac{\partial \phi_c}{\partial z} = -i\zeta_a \omega e^{kz}e^{i\theta_i}, \tag{9}$$

$$\dot{u}_c = \frac{\partial u_c}{\partial t} = -i\zeta_a \omega^2 e^{kz}e^{i\theta_i}, \tag{10}$$

$$\dot{w}_c = \frac{\partial w_c}{\partial t} = -\zeta_a \omega^2 e^{kz}e^{i\theta_i}, \tag{11}$$

$$p_{dyn,c} = -\rho\frac{\partial \phi_c}{\partial t} = \rho g \zeta_a e^{kz}e^{i\theta_i}. \tag{12}$$

As the phase θ is shifting over the distance between the origin of the incoming wave and the next column i (i=1…7) in wave heading direction x', the phase can be written as

$$\theta_i = kx_i' - \omega t. \tag{13}$$

Substituting (8) and (10) in (3) the Morsion equation in the horizontal direction with a complex potential can be expressed as

$$\begin{aligned} dF_h = &-i\rho\pi R^2 \zeta_a \omega^2 e^{kz}e^{i\theta_i}dz + \rho C_{a,x}\pi R^2\big(-i\zeta_a\omega^2 e^{kz}e^{i\theta_i} - \dot{v}\big) \\ &+\frac{1}{2}\rho C_d 2R\big(\zeta_a \omega e^{kz}e^{i\theta_i} - v\big)\big|\zeta_a \omega e^{kz}e^{i\theta_i} - v\big|. \end{aligned} \tag{14}$$

12.3 Calculation of wave forces

With the Keulegan-Carpenter number, the importance of the drag and inertia forces of a structure can be evaluated with $KC = \frac{\pi H}{D}$. When KC ≤ 20 the inertia forces of the wave loads dominate, when 20 < KC < 40 both inertia and drag forces influence the maximum wave force and for KC ≥ 40 the drag forces dominate (Clauss et al. 1992, p. 242). The wave height, which would make drag forces on the cylinders influential on the smallest diameter, is $H_{W,20} = \frac{20 \cdot 2 \cdot R_{MC}}{\pi} = 41.3803\ m$, which is not realistic as the highest wave ever measured was 25.6 m high (Bard 2018). Therefore, the viscous drag forces on the structure can be neglected. As the floater is moored to a specific location, the structure is not in motion as long as it is not excited by wave loads, thereby $v = \dot{v} = 0$. With these simplifications, the horizontal wave loads on the floater are calculated with

$$\begin{aligned} dF_h &= -i\rho\pi R^2 \zeta_a \omega^2 e^{kz} e^{i\theta_i} dz - i\rho C_{a,h} \pi R^2 \zeta_a \omega^2 e^{kz} e^{i\theta_i} dz \\ &= -i\rho C_{m,h} \pi R^2 \zeta_a \omega^2 e^{kz} e^{i\theta_i} dz. \end{aligned} \tag{15}$$

As all structures are cylinders, the added mass coefficient $C_{a,h}$ in the horizontal direction is equal to 1, thereby $C_{m,h} = 2$ (Clauss et al. 1992, p. 227). When all cylinders are regarded as columns, the horizontal wave forces on the different columns are

$$\begin{aligned} F_{h,MC} &= -i2\rho\pi {R_{MC}}^2 \zeta_a \omega^2 e^{i\theta_{MC}} \int_{-h_{MC}}^{0} e^{kz} dz = -i2\rho\pi {R_{MC}}^2 \zeta_a \omega^2 \left(\frac{1 - e^{-kh_{MC}}}{k}\right) e^{i\theta_{MC}} \\ &= -i2\rho\pi {R_{MC}}^2 \zeta_a \frac{\omega^2}{k} \left(1 - e^{-kh_{MC}}\right) e^{i\theta_{MC}} \\ &= -i2\rho\pi {R_{MC}}^2 \zeta_a g \left(1 - e^{-kh_{MC}}\right) e^{i\theta_{MC}}, \end{aligned} \tag{16}$$

$$F_{h,UC,j} = -i2\rho\pi R_{UC}^2 \zeta_a \omega^2 e^{i\theta_{UC,j}} \int_{-h_{UC}}^{0} e^{kz} dz = -i2\rho\pi R_{UC}^2 \zeta_a g \left(1 - e^{-kh_{UC}}\right) e^{i\theta_{UC,j}}, \tag{17}$$

$$\begin{aligned} F_{h,BC,j} &= -i2\rho\pi R_{BC}^2 \zeta_a \omega^2 e^{i\theta_{BC.j}} \int_{-h_D}^{-h_{UC}} e^{kz} dz \\ &= -i2\rho\pi R_{BC}^2 \zeta_a g \left(e^{-kh_{UC}} - e^{-kh_D}\right) e^{i\theta_{BC,j}}. \end{aligned} \tag{18}$$

When the base column is regarded as a caisson, the Froude-Krylov-force and added mass force are no longer integrated over the entire caisson height but are now only related to the centre of the column in the z-direction $h_{CS} = h_D - h_{BCS} = 17m$. Therefore, with $z = -h_{CS}$ the horizontal force on the caisson is

$$F_{h,BCS,j} = -i2\rho\pi R_{BCS}^2 \zeta_a \omega^2 e^{i\theta_{BCS,j}} e^{-kh_{CS}} \int_{-h_D}^{-h_{UC}} dz = -i2\rho\pi R_{BCS}^2 \zeta_a \omega^2 e^{-kh_{CS}} h_{BCS} e^{i\theta_{BCS,j}}. \tag{19}$$

For the three offset columns j=1…3 the distances between the origin of the incoming wave and the upper column j and the base column j are the same. Consequently, their phase shift is also the same $x'_{OC,j} = x'_{UC,j} = x'_{BC,j} = x_j \cdot cos(\beta) + y_j \cdot sin(\beta)$ and $\theta_{OC,j} = \theta_{UC,j} = \theta_{BC,j}$. The distances x_j and y_j for the different columns are displayed in table 2.

Table 2: Distances between the origin and the different columns

	x_j	y_j
OC 1	-14,435 m	- 25 m
$OC\ 2$	28,87 m	0 m
$OC\ 3$	-14,435 m	+ 25 m
MC	0 m	0 m

For the main column, the phase thereby can be simplified to $e^{i(kx_{MC}-\omega t)} = e^{-i\omega t}$ as the phase shift for every wave heading angle is always zero. For every offset column with base columns, the horizontal force is

$$\begin{aligned} F_{h,OC,C,j} &= F_{h,UC,j} + F_{h,BC,j} \\ &= -i2\rho\pi\zeta_a g\left(R_{UC}^2\left(1-e^{-kh_{UC}}\right)+R_{BC}^2\left(e^{-kh_{UC}}-e^{-kh_D}\right)\right) \\ &\cdot e^{i\left(kx'_{OC,j}-\omega t\right)} \end{aligned} \tag{20}$$

and with base caissons it is

$$\begin{aligned} F_{h,OC,CS,j} &= F_{h,UC,j} + F_{h,BCS,j} \\ &= -i2\rho\pi\zeta_a(R_{UC}^2 g\left(1-e^{-kh_{UC}}\right)+R_{BCS}^2 h_{BCS}\omega^2 e^{-kh_{CS}})\cdot e^{i\left(kx'_{OC,j}-\omega t\right)}. \end{aligned} \tag{21}$$

With $e^{x-y} = \frac{e^x}{e^y}$ the total horizontal wave force on the structure

$$\begin{aligned} F_{h,tot,C} &= F_{h,MC} + F_{h,OC,C,1} + F_{h,OC,C,2} + F_{h,OC,C,3} \\ &= -i2\rho\pi {R_{MC}}^2\zeta_a g\left(1-e^{-kh_{MC}}\right)e^{-i\omega t} \\ &- i2\rho\pi\zeta_a g\left(R_{UC}^2\left(1-e^{-kh_{UC}}\right)\right. \\ &\left.+R_{BC}^2\left(e^{-kh_{UC}}-e^{-kh_D}\right)\right)\left(e^{i(kx'_{OC,1}-\omega t)}+e^{i(kx'_{OC,2}-\omega t)}\right. \\ &\left.+e^{i(kx'_{OC,3}-\omega t)}\right) \\ &= -i2\rho\pi\zeta_a g\left({R_{MC}}^2\left(1-e^{-kh_{MC}}\right)\right. \\ &\left.+\left(R_{UC}^2\left(1-e^{-kh_{UC}}\right)+R_{BC}^2\left(e^{-kh_{UC}}-e^{-kh_D}\right)\right)\left(e^{ikx'_{OC,1}}+e^{ikx'_{OC,2}}\right.\right. \\ &\left.\left.+e^{ikx'_{OC,3}}\right)\right)\cdot e^{-i\omega t}, \end{aligned} \tag{22}$$

$$\begin{aligned} F_{h,tot,CS} &= -i2\rho\pi\zeta_a\left(g{R_{MC}}^2\left(1-e^{-kh_{MC}}\right)\right. \\ &+\left(R_{UC}^2 g\left(1-e^{-kh_{UC}}\right)+R_{BCS}^2 h_{BCS}\omega^2 e^{-kh_{CS}}\right)\left(e^{ikx'_{OC,1}}+e^{ikx'_{OC,2}}\right. \\ &\left.\left.+e^{ikx'_{OC,3}}\right)\right)\cdot e^{-i\omega t}. \end{aligned} \tag{23}$$

For the vertical forces of the wave, the Morison equation of the structure differs for the submerged base column/caisson and the surface piercing main and upper columns. The base column/caisson has both ends of the cylinder wetted, whereby the Morison equation can be written similarly to the horizontal direction

$$dF_z = \rho\pi R^2\dot{w}_c dz + \rho C_{a,z}\pi R^2\dot{w}_c dz = \rho C_{m,z}\pi R^2\dot{w}_c dz = -\rho C_{m,z}\pi R^2\zeta_a\omega^2 e^{kz}e^{-i\theta_i}dz. \tag{24}$$

In contrast, the piercing columns only have one wetted surface in vertical direction, whereby the Froude-Krylov force is

$$F_z^{FK}(t) = \rho\int\int\frac{\partial\phi}{\partial t}\,ndS = -\int\int p_{dyn}\,(-1)dS = \rho g\pi R^2\zeta_a e^{-kh_i}e^{i\theta_i}. \tag{25}$$

To determine whether the hydrodynamic added mass is considered in the Morison equation, the added mass coefficients in the vertical direction are determined with figure 36. When all cylinders are considered as columns the factors α are

$$\alpha_{C,MC} = \frac{\pi R_{MC}}{4h_{MC}} = 0.1276, \tag{26}$$

$$\alpha_{C,UC} = \frac{\pi R_{UC}}{4h_{UC}} = 0.3366, \tag{27}$$

$$\alpha_{C,BC} = \frac{\pi R_{BC}}{4h_{BC}} = 1.5708. \tag{28}$$

With the base caisson, it is

$$\alpha_{C,BCS} = \frac{\pi R_{BCS}}{2h_{BCS}} = 3.1416. \tag{29}$$

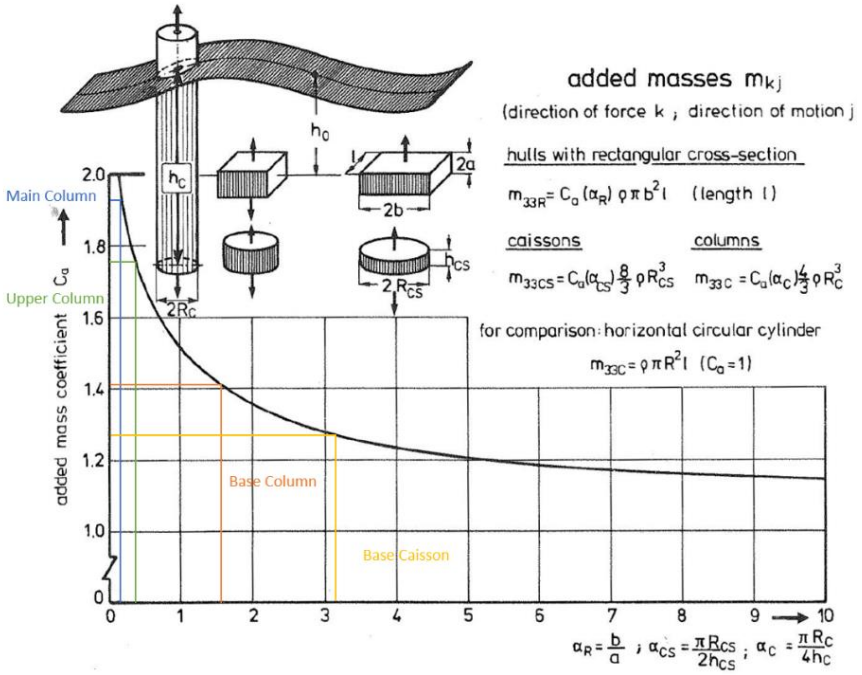

Figure 36: Vertical added mass coefficients of the different cylinders (Clauss et al. 1992, p. 281)

Thereby, the resulting added mass coefficients in the vertical direction are $C_{a,z,MC} = 1.93$, $C_{a,z,UC} = 1.755$, $C_{a,z,BC} = 1.41$ and $C_{a,z,BCS} = 1.271$ and the corresponding inertia coefficients are $C_{m,z,MC} = 2.93$, $C_{m,z,UC} = 2.755$ and $C_{m,z,BC} = 2.41$ and $C_{m,z,BCS} = 2.271$. Thereby the added masses of the cylinders are

$$m_{33,MC} = C_{a,z,MC}(\alpha_{C,MC})\frac{4}{3}\rho R_{MC}^3 = 90.5462\ t, \tag{30}$$

$$m_{33,UC} = C_{a,z,UC}(\alpha_{C,UC})\frac{4}{3}\rho R_{UC}^3 = 518.076\ t, \tag{31}$$

$$m_{33,BC} = C_{a,z,BC}(\alpha_{C,BC})\frac{4}{3}\rho R_{BC}^3 = 3329.856\ t, \tag{32}$$

$$m_{33,BCS} = C_{a,z,MC}(\alpha_{C,BCS})\frac{8}{3}\rho R_{BCS}^3 = 6003{,}1872\ t. \tag{33}$$

As the added mass in the vertical direction is significantly larger for the base cylinders than for the other columns, especially when considered as a caisson, the added mass forces for the upper and main column are neglected (Clauss et al. 1992, p. 271).

The vertical forces on the different columns and caissons are thereby

$$F_{v,MC} = \rho g\pi R_{MC}^2 \zeta_a e^{-kh_{MC}} e^{i\theta_{MC}}, \tag{34}$$

$$F_{v,UC,j} = \rho\pi R_{UC}^2 \zeta_a g e^{-kh_{UC}} e^{i\theta_{UC,j}}, \tag{35}$$

$$F_{v,BC,j} = -\rho C_{m,z,BC}\pi R_{BC}^2 \zeta_a \omega^2 e^{i\theta_{BC,j}} \int_{-h_D}^{-h_{UC}} e^{kz} dz \tag{36}$$
$$= -\rho C_{m,z,BC}\pi R_{BC}^2 \zeta_a g e^{i\theta_{BC,j}} \left(e^{-kh_{UC}} - e^{-kh_D}\right),$$
$$F_{v,BCS,j} = -\rho C_{m,z,BCS}\pi R_{BCS}^2 h_{BCS} \omega^2 e^{i\theta_{BC,j}} e^{-kh_{CS}}. \tag{37}$$

Analogous to the total horizontal force, the total vertical force is

$$F_{v,tot,C} = F_{v,MC} + F_{v,OC,1} + F_{v,OC,2} + F_{v,OC,3} = \tag{38}$$
$$= \rho\pi\zeta_a g \Big({R_{MC}}^2 e^{-kh_{MC}}$$
$$+ \left(R_{UC}^2 e^{-kh_{UC}} - C_{m,z,BC} R_{BC}^2 \left(e^{-kh_{UC}} - e^{-kh_D}\right)\right)\left(e^{ikx'_{OC,1}} + e^{ikx'_{OC,2}}$$
$$+ e^{ikx'_{OC,3}}\right)\Big) \cdot e^{-i\omega t},$$
$$F_{v,tot,CS} = \rho\pi\zeta_a \Big(g{R_{MC}}^2 e^{-kh_{MC}} \tag{39}$$
$$+ \left(gR_{UC}^2 e^{-kh_{UC}} - C_{m,z,BCS} R_{BCS}^2 h_{BCS} \omega^2 e^{-kh_{CS}}\right)\left(e^{ikx'_{OC,1}} + e^{ikx'_{OC,2}}\right.$$
$$\left. + e^{ikx'_{OC,3}}\right)\Big) \cdot e^{-i\omega t}.$$

For harmonic waves the complex force is $\underline{F} = \underline{\hat{F}} e^{-i\omega t}$. To display the force profile, both total forces are normalized with the reference force $G_{\zeta_a} = \rho g A_{wl} \zeta_a$ which is the weight force of the displaced water of the cylinder at the height ζ_a (Clauss et al. 1992, p. 270). A_{wl} is the waterline area of the cylinder, which is for the floater $A_{wl} = \pi \cdot R_{MC}^2 + 3 \cdot \pi \cdot \mathrm{R}_{UC}^2 = 372.4751 m^2$. The normalized total horizontal and vertical forces are

$$\frac{F_{h,tot,C}}{G_{\zeta_a}} = \frac{\hat{F}_{h,tot,C}}{G_{\zeta_a}} e^{-i\omega t} \tag{40}$$
$$= \frac{-i2\rho\pi\zeta_a g}{\rho g A_{wl} \zeta_a} \Big({R_{MC}}^2 \left(1 - e^{-kh_{MC}}\right)$$
$$+ \left(R_{UC}^2 \left(1 - e^{-kh_{UC}}\right) + R_{BC}^2 \left(e^{-kh_{UC}} - e^{-kh_D}\right)\right)\left(e^{ikx'_{OC,1}}\right.$$
$$\left. + e^{ikx'_{OC,2}} + e^{ikx'_{OC,3}}\right)\Big) e^{-i\omega t}$$
$$= \frac{-i2}{R_{MC}^2 + 3 \cdot \mathrm{R}_{\mathrm{OC}}^2} \Big({R_{MC}}^2 \left(1 - e^{-kh_{MC}}\right)$$
$$+ \left(R_{UC}^2 \left(1 - e^{-kh_{UC}}\right) + R_{BC}^2 \left(e^{-kh_{UC}} - e^{-kh_D}\right)\right)\left(e^{ikx'_{OC,1}}\right.$$
$$\left. + e^{ikx'_{OC,2}} + e^{ikx'_{OC,3}}\right)\Big) e^{-i\omega t}$$

$$\frac{F_{h,tot,CS}}{G_{\zeta_a}} = \frac{\hat{F}_{h,tot,CS}}{G_{\zeta_a}} e^{-i\omega t} \tag{41}$$
$$= \frac{-i2}{g(R_{MC}^2 + 3 \cdot \mathrm{R}_{\mathrm{OC}}^2)} \Big(g{R_{MC}}^2 \left(1 - e^{-kh_{MC}}\right)$$
$$+ \left(R_{UC}^2 g\left(1 - e^{-kh_{UC}}\right) + R_{BCS}^2 h_{BCS} \omega^2 e^{-kh_{CS}}\right)\left(e^{ikx'_{OC,1}}\right.$$
$$\left. + e^{ikx'_{OC,2}} + e^{ikx'_{OC,3}}\right)\Big) \cdot e^{-i\omega t},$$

$$\frac{F_{v,tot,C}}{G_{\zeta_a}} = \frac{\hat{F}_{v,tot,C}}{G_{\zeta_a}} e^{-i\omega t} \tag{42}$$
$$= \frac{1}{R_{MC}^2 + 3 \cdot \mathrm{R}_{\mathrm{OC}}^2}\Big(C_{m,z,MC} {R_{MC}}^2 e^{-kh_{MC}} + \Big(C_{m,z,UC} R_{UC}^2 e^{-kh_{UC}} - C_{m,z,BC} R_{BC}^2 \big(e^{-kh_{UC}} - e^{-kh_D}\big)\Big)\Big(e^{ikx'_{OC,1}} + e^{ikx'_{OC,2}} + e^{ikx'_{OC,3}}\Big)\Big) \cdot e^{-i\omega t},$$

$$\frac{F_{v,tot,CS}}{G_{\zeta_a}} = \frac{\hat{F}_{v,tot,CS}}{G_{\zeta_a}} e^{-i\omega t} \tag{43}$$
$$= \frac{1}{g(R_{MC}^2 + 3 \cdot R_{OC}^2)}\Big(g {R_{MC}}^2 e^{-kh_{MC}} + \big(gR_{UC}^2 e^{-kh_{UC}} - C_{m,z,BCS} R_{BCS}^2 h_{BCS} \omega^2 e^{-kh_{CS}}\big)\Big(e^{ikx'_{OC,1}} + e^{ikx'_{OC,2}} + e^{ikx'_{OC,3}}\Big)\Big) \cdot e^{-i\omega t}.$$

To display the forces profiles, their absolute value of the normalized amplitude is determined with $\left|\frac{\hat{F}_{x',tot}}{G_{\zeta_a}}\right| = \sqrt{\left(Re\left(\frac{\hat{F}_{x',tot}}{G_{\zeta_a}}\right)\right)^2 + \left(Im\left(\frac{\hat{F}_{x',tot}}{G_{\zeta_a}}\right)\right)^2}$. With $e^{ikx'} = cos(kx') + isin(kx')$ and $ie^{ikx'} = -sin(kx') + icos(kx')$ the real and imaginary part of the normalized force are

$$Re\left(\frac{\hat{F}_{h,tot}}{G_{\zeta_a}}\right) = \frac{2}{R_{MC}^2 + 3 \cdot \mathrm{R}_{\mathrm{OC}}^2}\Big({R_{MC}}^2\big(1 - e^{-kh_{MC}}\big) + \Big(R_{UC}^2\big(1 - e^{-kh_{UC}}\big) + R_{BC}^2\big(e^{-kh_{UC}} - e^{-kh_D}\big)\Big)\Big(sin\big(kx'_{OC,1}\big) + sin\big(kx'_{OC,2}\big) + sin\big(kx'_{OC,3}\big)\Big)\Big), \tag{44}$$

$$Im\left(\frac{\hat{F}_{h,tot}}{G_{\zeta_a}}\right) = \frac{-2}{R_{MC}^2 + 3 \cdot R_{OC}^2}\Big({R_{MC}}^2\big(1 - e^{-kh_{MC}}\big) + \Big(R_{UC}^2\big(1 - e^{-kh_{UC}}\big) + R_{BC}^2\big(e^{-kh_{UC}} - e^{-kh_D}\big)\Big)\Big(cos\big(kx'_{OC,1}\big) + cos\big(kx'_{OC,2}\big) + cos\big(kx'_{OC,3}\big)\Big)\Big), \tag{45}$$

$$Re\left(\frac{\hat{F}_{v,tot}}{G_{\zeta_a}}\right) = \frac{1}{R_{MC}^2 + 3 \cdot \mathrm{R}_{\mathrm{OC}}^2}\Big({R_{MC}}^2 e^{-kh_{MC}} + \Big(R_{UC}^2 e^{-kh_{UC}} - C_{m,z,BC} R_{BC}^2\big(e^{-kh_{UC}} - e^{-kh_D}\big)\Big)\Big(cos\big(kx'_{OC,1}\big) + cos\big(kx'_{OC,2}\big) + cos\big(kx'_{OC,3}\big)\Big)\Big), \tag{46}$$

$$Im\left(\frac{\hat{F}_{v,tot}}{G_{\zeta_a}}\right) = \frac{1}{R_{MC}^2 + 3 \cdot \mathrm{R}_{\mathrm{OC}}^2}\Big({R_{MC}}^2 e^{-kh_{MC}} + \Big(R_{UC}^2 e^{-kh_{UC}} - C_{m,z,BC} R_{BC}^2\big(e^{-kh_{UC}} - e^{-kh_D}\big)\Big)\Big(sin\big(kx'_{OC,1}\big) + sin\big(kx'_{OC,2}\big) + sin\big(kx'_{OC,3}\big)\Big)\Big). \tag{47}$$

The real and imaginary parts of the total force with caissons is determined analogously. Figure 37 is displaying a comparison of the horizontal and vertical forces of the model with base columns and caissons at a wave heading angle of 0°.

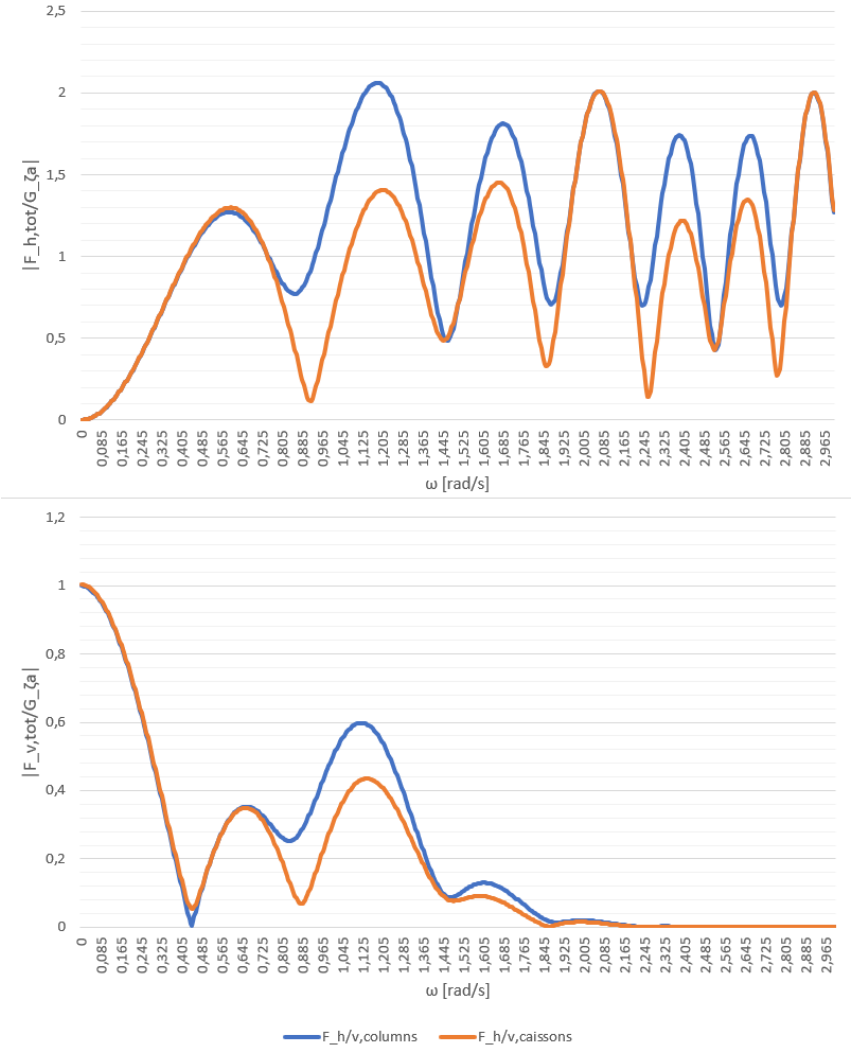

Figure 37: Comparison of the absolute values of the normalized horizontal and vertical forces with columns and caissons for $\beta = 0°$

As can be seen, the maximum values of the normalized horizontal and vertical forces are significantly higher for the base columns. As the maximum forces and displacements on the DeepCwind floater are the interest of the thesis, the thesis will mainly focus on the base column.

When compared to the horizontal forces determined in (Clauss et al. 1992, p. 273) for a semisubmersible with four legs, displayed in figure 38, the normalized horizontal force for 0° seems not to fit as its absolute value increasing with the frequency and decreases asymptotically after passing a maximum, but has no zero crossings. However, this is due to the behaviour of the real and imaginary part for this specific case where the sum of both parts is always positive, as it can be seen in figure 39. For the case when the total force is zero, the columns experience counteracting transverse forces of the same magnitude, but still is experiencing structural loadings. Generally, the horizontal force is zero for long waves as the decay terms $(1 - e^{-kh})$ are zero and the force is oscillating due to the phase differences of the forces on the different columns (Clauss et al. 1992, p. 270).

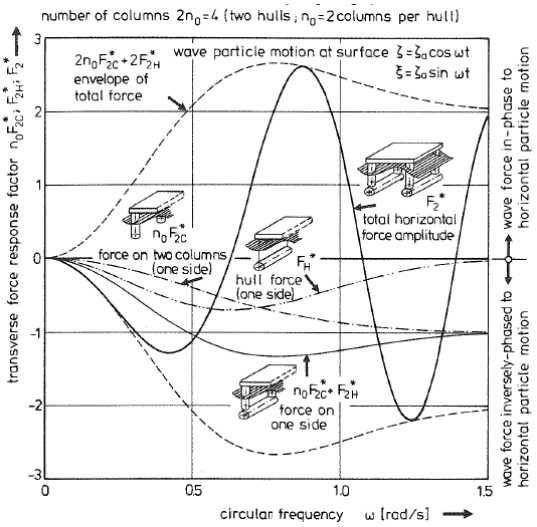

Figure 38: Horizontal forces on a semisubmersible with four legs (Clauss et al. 1992, p. 273)

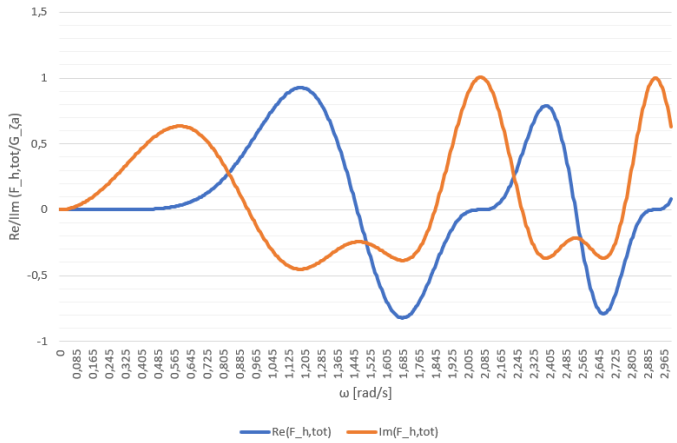

Figure 39: Normalized real and imaginary parts of the horizontal force with base columns for β = 0°

The force profiles in the vertical direction are similar to the force profile displayed for n=3 in figure 40, especially for the base caissons. For small frequencies, the Froude-Krylov force of the surface piercing columns dominates the force profile as the force on the base columns is near zero. The force on the piercing columns has the same phase of the wave elevation but decreases exponentially when the wave frequency rises. As higher the frequency gets, the forces of the base columns begin to dominate. Those forces are proportional to the vertical particle acceleration and inversely phased to the wave elevation. When the force on the base columns and the piercing columns cancel each other, the cancellation frequency ω_c occurs. In contrast to figure 40, the vertical force with the base caissons in figure 37 has no cancellation frequency as also the main column is considered, which has no base column/caisson at its end.

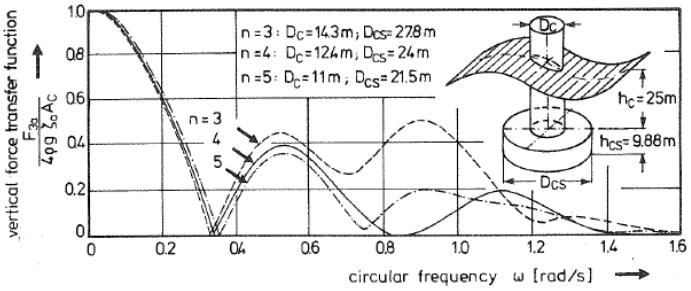

Figure 40: Heave exciting forces of a caisson-type semi-submersible with n columns (Clauss et al. 1992, p. 284)

For the different wave heading angles, the normalized horizontal and vertical wave forces can be seen in figure 41.

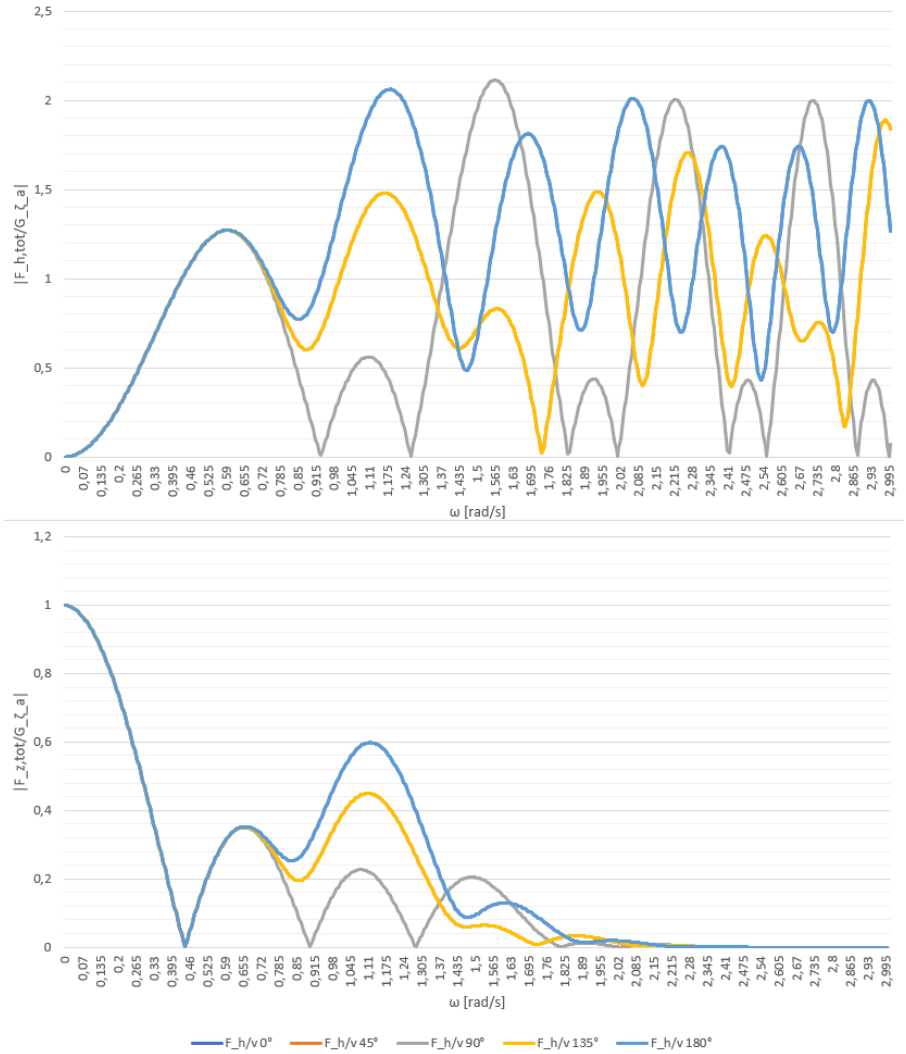

Figure 41: Normalized horizontal and vertical wave forces on the floater for different wave heading angles

The horizontal and vertical forces for 0° and 180° and for 45° and 135° overlap each other. Until the first local maximum, the horizontal and vertical forces are equal, independent of the wave heading angle. The horizontal force profile for 45°/135° has one zero crossing and generally smaller forces occur than for 0°/180°. However, it is not intuitive that the maximum continues to rise after the zero crossing and doesn't decrease asymptomatically. Thus far, no explanation was found for this phenomenon. For a wave heading angle of 90°, the force profile has several zero crossings, meaning that horizontal forces

on the columns regularly cancel themselves. After the first pair of zero crossings, the horizontal force for 90° exceeds its maximum, which is even slightly higher than the maximum for 0°/180°.

The vertical forces for 45°/135° behave similarly to 0°/180°. However, the forces are smaller after reaching the first maximum and the forces profile is declining faster to zero. For 90° the vertical forces on the structure are cancelled several times after the cancellation frequency. In these cases, the sum of the different phases is zero. It only once exceeds the local maximum of the 0°/180° where the force profile of 0°/180° is already declining. Otherwise, the forces are smaller after the first local maximum.

Generally, for the five different wave heading angles, the floater is experiencing the maximum horizontal force for 90° and the maximum horizontal force for 0° and 180°.

12.4 Determination of RAOs

The floater has theoretically all six degrees of freedom, three transitional (surge, sway, heave) and three rotational (roll, pitch, yaw), which can be seen exemplary for a buoy in figure 42. However, for simplicity reasons, the coupled behaviours of the floater are neglected, whereby main influences on the rotational DOF would be omitted for which reason this thesis is only focussing on the transitional degrees of freedom.

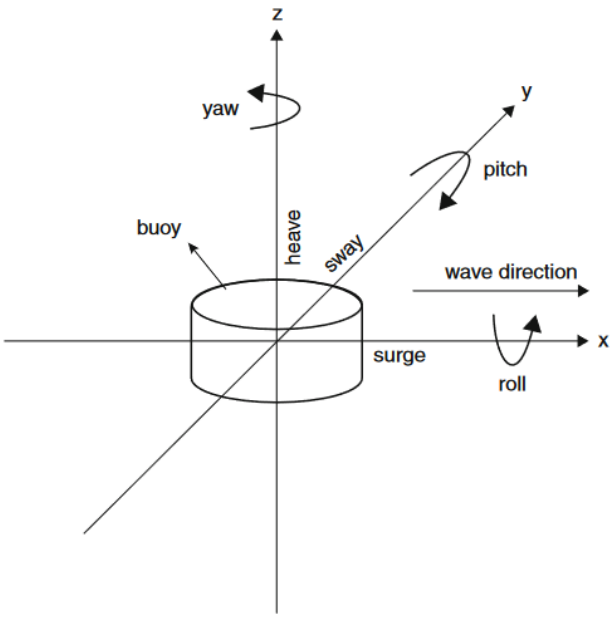

Figure 42: Degrees of freedom of a buoy (Pecher and Kofoed 2017, p. 140)

The general equation of motion is expressed with

$$\underline{F_E} = \left(\underline{M} + \underline{A}\right) \cdot \ddot{\underline{s}} + \underline{B} \cdot \dot{\underline{s}} + \underline{C}\underline{s}. \tag{48}$$

In the equation of motion, F_E is the excitation force, M is expressing the mass matrix, A the added mass matrix of the floater, B is the linear damping coefficient matrix, and C is the restoring coefficient matrix. As drag forces are neglected due to KC≤20, damping forces are set to zero. The excitation force in the respective direction can be expressed with $F_1 = F_h cos(\beta), F_2 = F_h sin(\beta)$ and $F_3 = F_v$. As the coupled behaviour of the floater and rotational DOFs are neglected, the mass matrix can also be expressed with $\underline{M} = m_{tot} = m = 1.2919 \cdot 10^7$ kg. According to Lewis, the added mass coefficients in the respective can be expressed with the equations displayed in table 3 (Lewis 1989, p. 56).

Table 3: Added mass coefficients

Added mass coefficient	Equation
m_{11}	$\int a_{11}\mathrm{dz}$
m_{22}	$\int a_{22}\mathrm{dz}$
m_{33}	$\int a_{33}\mathrm{dz}$

The two-dimensional added masses of the cylinder which are rotational symmetric around the z-axis can be expressed with $a_{11} = a_{22} = \pi\rho r^2$ (Newman 2017, p. 145). m_{33} was already calculated for the individual columns in formulas 30 to 33. The three-dimensional added mass coefficients are displayed in table 4.

Table 4: Three-dimensional added mass coefficients

	Main Column	Upper Column	Base Column	Total
$m_{11} = m_{22}$	$6.8025 \cdot 10^5\ kg$	$4.7618 \cdot 10^5\ kg$	$2.7822 \cdot 10^6\ kg$	$1.1068 \cdot 10^7\ kg$
m_{33}	$9.0546 \cdot 10^4\ kg$	$5.1217 \cdot 10^5\ kg$	$3.3299 \cdot 10^6\ kg$	$1.1617 \cdot 10^7\ kg$
$m_{44} = m_{55}$	$1.2073 \cdot 10^7\ kg \cdot m^2$	$3.3462 \cdot 10^7 kg \cdot m^2$	$9.7232 \cdot 10^8\ kg \cdot m^2$	$3.0294 \cdot 10^9\ kg \cdot m^2$

Only the heave direction has a restoring force, which can be calculated with (Newman 2017, p. 293)

$$C_{33} = \rho g A_w = 3.7453 \cdot 10^6\ \frac{N}{m} \tag{49}$$

The resulting equations of motion in for the different transitional DOFs can be seen in table 5.

Table 5: Equation of motion for the different transitional DOFs

DOF	equation of motion
Surge	$F_h cos(\beta) = (m + m_{11})\ddot{s}_{11}$
Sway	$F_h sin(\beta) = (m + m_{22})\ddot{s}_{22}$
Heave	$F_v = (m + m_{33})\ddot{s}_{33} + C_{33}s_{33}$

Harmonic waves are assumed whereby the structural movements can be written as $\underline{s(t)} = \underline{\hat{s}} e^{-i(\omega t - \epsilon)}$, $\underline{\dot{s}(t)} = -i\omega\underline{\hat{s}} e^{-i(\omega t-\epsilon)}$, $\underline{\ddot{s}(t)} = -\omega^2\underline{\hat{s}} e^{-i(\omega t-\epsilon)}$ and $\underline{F_E} = \underline{\hat{F}_E} e^{-i\omega t}$ with the phase ϵ. Thereby, the complex equation of motion can be formulated as

$$-\omega^2 \cdot \left(\underline{M} + \underline{A}\right) \cdot \underline{\hat{s}} \cdot e^{-i(\omega t-\epsilon)} - i \cdot \omega \cdot \underline{B}\ \underline{\hat{s}} \cdot e^{-i(\omega t-\epsilon)} + \underline{C} \cdot \underline{\hat{s}} \cdot e^{-i(\omega t-\epsilon)} = \underline{\hat{F}_E} \cdot e^{-i\omega t}. \tag{50}$$

The RAO is generally written as $H(\omega) = \frac{\hat{s}}{\zeta_a} e^{i\epsilon}$, if the complex equation of motion is converted accordingly the general RAO can be written as

$$\underline{H}(\omega) = \frac{\underline{\hat{s}}}{\zeta_a} e^{i\epsilon} = \frac{\underline{\hat{F}_E}}{\zeta_a\left(-\omega^2\left(\underline{M} + \underline{A}\right) - i\omega\underline{B} + \underline{C}\right)}. \tag{51}$$

Thereby, the different RAOs are

$$H_1(\omega) = \frac{\hat{F}_h cos(\beta)}{-\zeta_a \omega^2 (m + m_{11})} \tag{52}$$
$$= \frac{-i2\zeta_a \rho\pi g cos(\beta)}{-\zeta_a \omega^2 (m + m_{11})} \Big({R_{MC}}^2 \big(1 - e^{-kh_{MC}}\big)$$
$$+ \Big(R_{UC}^2 \big(1 - e^{-kh_{UC}}\big) + R_{BC}^2 \big(e^{-kh_{UC}} - e^{-kh_D}\big) \Big) \Big(e^{ikx'_{OC,1}} + e^{ikx'_{OC,2}}$$
$$+ e^{ikx'_{OC,3}} \Big) \Big)$$
$$= \frac{i2\rho\pi g cos(\beta)}{\omega^2 (m + m_{11})} \Big({R_{MC}}^2 \big(1 - e^{-kh_{MC}}\big)$$
$$+ \Big(R_{UC}^2 \big(1 - e^{-kh_{UC}}\big) + R_{BC}^2 \big(e^{-kh_{UC}} - e^{-kh_D}\big) \Big) \Big(e^{ikx'_{OC,1}} + e^{ikx'_{OC,2}}$$
$$+ e^{ikx'_{OC,3}} \Big) \Big).$$

$$H_2(\omega) = \frac{i2\rho\pi g sin(\beta)}{\omega^2 (m + m_{22})} \Big({R_{MC}}^2 \big(1 - e^{-kh_{MC}}\big) \tag{53}$$
$$+ \Big(R_{UC}^2 \big(1 - e^{-kh_{UC}}\big) + R_{BC}^2 \big(e^{-kh_{UC}} - e^{-kh_D}\big) \Big) \Big(e^{ikx'_{OC,1}} + e^{ikx'_{OC,2}}$$
$$+ e^{ikx'_{OC,3}} \Big) \Big)$$

$$H_3(\omega) = \frac{\rho\pi g}{\omega^2 (m + m_{33}) - C_{33}} \Big(C_{m,z,MC} {R_{MC}}^2 e^{-kh_{MC}} \tag{54}$$
$$+ \Big(C_{m,z,UC} R_{UC}^2 e^{-kh_{UC}} - C_{m,z,BC} R_{BC}^2 \big(e^{-kh_{UC}} - e^{-kh_D}\big) \Big) \Big(e^{ikx'_{OC,1}}$$
$$+ e^{ikx'_{OC,2}} + e^{ikx'_{OC,3}} \Big) \Big)$$

To display the RAO, its absolute value and phase are determined with

$$\left|\underline{H}(\omega)\right| = \sqrt{Im\left(\underline{H}(\omega)\right)^2 + Re\left(\underline{H}(\omega)\right)^2}, \tag{55}$$

$$\epsilon = arctan\left(\frac{Im\left(\underline{H}(\omega)\right)}{Re\left(\underline{H}(\omega)\right)}\right). \tag{56}$$

At first, the real and imaginary parts of the RAOs are determined

$$H_1(\omega) = \frac{2\rho\pi g cos(\beta)}{\omega^2 (m + m_{11})} \Big((-({R_{MC}}^2 (1 - e^{-kh_{MC}}) \tag{57}$$
$$+ \Big(R_{UC}^2 (1 - e^{-kh_{UC}})$$
$$+ R_{BC}^2 (e^{-kh_{UC}} - e^{-kh_D})) \Big(sin\big(kx'_{OC,1}\big) + sin\big(kx'_{OC,2}\big) + sin\big(kx'_{OC,3}\big) \Big) \Big)$$
$$+ i \Big(-({R_{MC}}^2 (1 - e^{-kh_{MC}})$$
$$+ \Big(R_{UC}^2 (1 - e^{-kh_{UC}})$$
$$+ R_{BC}^2 (e^{-kh_{UC}} - e^{-kh_D})) \big(cos\big(kx'_{OC,1}\big) + cos\big(kx'_{OC,2}\big) + cos\big(kx'_{OC,3}\big) \big) \Big) \Big)$$
$$= \frac{2\rho\pi g cos(\beta)}{\omega^2 (m + m_{11})} Re(H_1(\omega))^* + i \frac{2\rho\pi g cos(\beta)}{\omega^2 (m + m_{11})} Im(H_1(\omega))^*.$$

Thereby the absolute values and phases are

$$|H_1(\omega)| = \sqrt{\left(\frac{2\rho\pi g cos(\beta)}{-\omega^2 (m + m_{11})} \cdot Im(H_1(\omega))^* \right)^2 + \left(\frac{2\rho\pi g cos(\beta)}{-\omega^2 (m + m_{11})} \cdot Re(H_1(\omega))^* \right)^2} \tag{58}$$

$$\epsilon_1 = arctan\left(\frac{\frac{2\rho\pi g cos(\beta) Im\left(H_1(\omega)\right)^*}{-\omega^2(m+m_{11}))}}{\frac{2\rho\pi g cos(\beta) Re\left(H_1(\omega)\right)^*}{-\omega^2(m+m_{11})}}\right) = arctan\left(\frac{Im\left(H_1(\omega)\right)^*}{Re\left(H_1(\omega)\right)^*}\right) \quad (59)$$

For sway and heave motion, the absolute values and phases are displayed in table 4.

Table 6: Absolute values and phases for sway and heave motion

Absolute value	
Sway	$\lvert H_2(\omega)\rvert = \sqrt{\left(\frac{2\rho\pi g sin(\beta)}{\omega^2(m+m_{22})} Im(H_2(\omega)^*\right)^2 + \left(\frac{2\rho\pi g sin(\beta)}{\omega^2(m+m_{22})} Re(H_2(\omega)^*\right)^2}$
Heave	$\lvert H_3(\omega)\rvert = \sqrt{\left(\frac{\rho\pi g}{\omega^2(m+m_{33})-C_{33}} Im(H_3(\omega)^*\right)^2 + \left(\frac{\rho\pi g}{\omega^2(m+m_{33})-C_{33}} Re(H_3(\omega)^*\right)^2}$
Phase	
Sway	$\epsilon_2 = arctan\left(\frac{Im(H_2(\omega)^*}{Re(H_2(\omega)^*}\right)$
Heave	$\epsilon_3 = arctan\left(\frac{Im(H_3(\omega)^*}{Re(H_3(\omega)^*}\right)$

The graphic representation of absolute values and phases for different wave heading angles can be seen in figures 43 to 45.

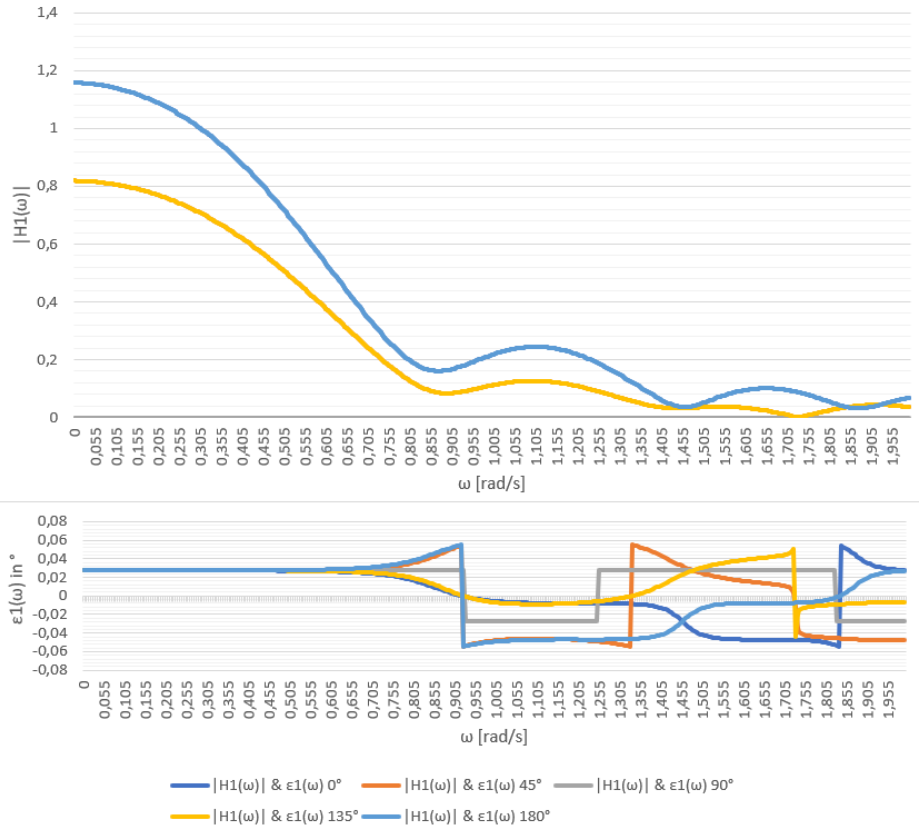

Figure 43: Absolute value and phase of surge RAO

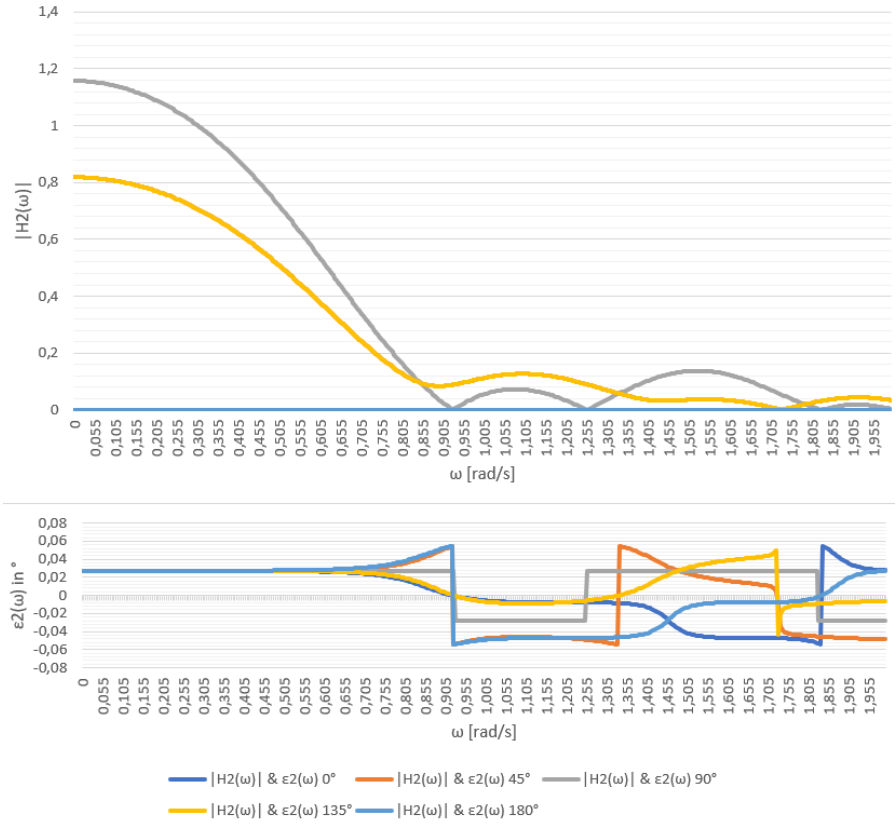

Figure 44: Absolute value and phase of sway RAO

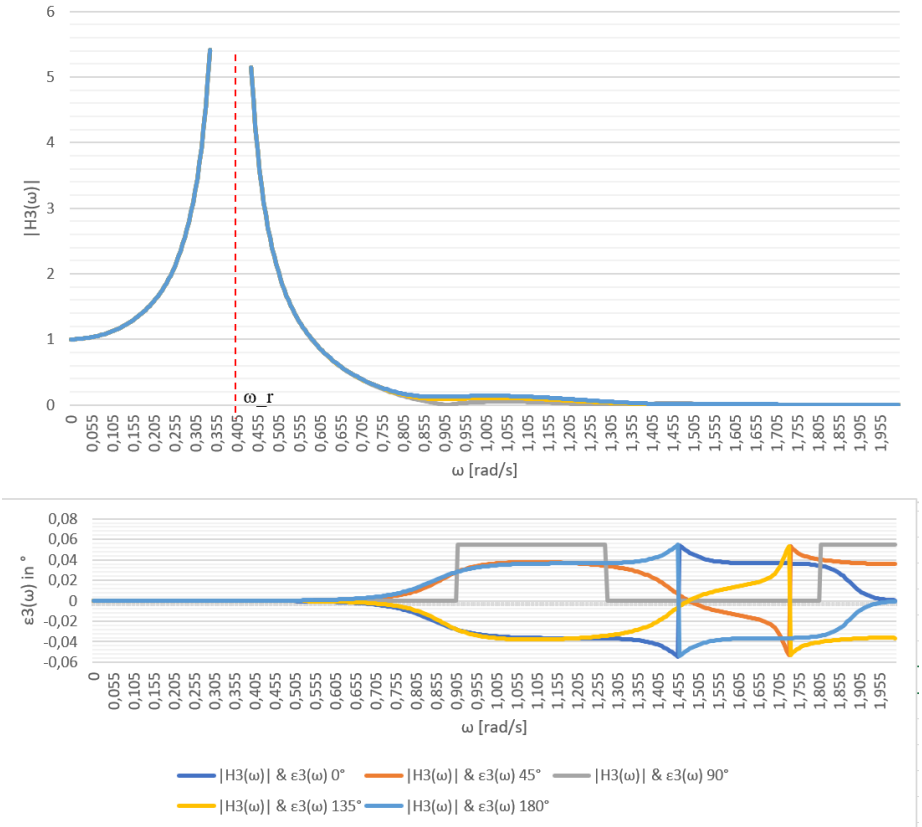

Figure 45: Absolute value and phase of heave RAO

For surge and sway motion, the absolute values of the RAOs for 45° and 135° and for 0° and 180° overlap each other. The RAOs for these two DOF fit fairly accurate to the sway RAO of a four-legged semisubmersible, displayed in figure 46. Like the horizontal force in figure 37, the zero crossings are again dependent on the sum of the real and imaginary part, whereby like the horizontal force 45°/135° have one zero crossing for surge and sway motion and the sway RAO for 90° has several zero crossings. The surge RAO for 90° and sway RAO for 0°/180° is zero as in those angles no horizontal force is occurring in the respective direction. Depending on the wave heading angle, for small frequencies the surge and sway motion is either slightly above or below one. However, the value is supposed to be exactly one as the structure follows the horizontal particle motion (Clauss et al. 1992, p. 271). With $\omega \rightarrow \infty$ the surge and sway RAO are declining towards zero as the denominator of the RAO increases with ω. The phases of both RAO, like the phases of all four other RAOs, are only effects of the phase and inversed phase as drag and resulting damping forces are neglected. They are opposite for 0°/180° and 45°/135° and shift at the minima, maxima and zero crossings. The maximum surge motion experienced the floater for 0°/180° and the maximum sway motion for 90°.

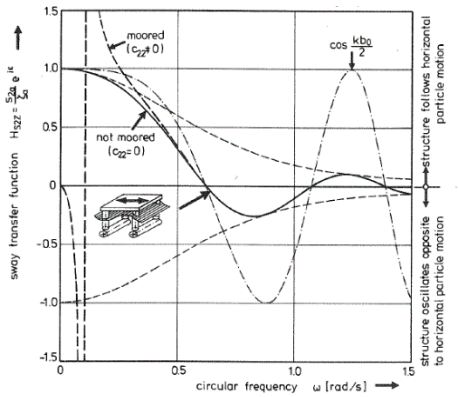

Figure 46: Sway RAO of a four-legged semisubmersible (Clauss et al. 1992, p. 274)

The heave RAO is for long waves independent of the wave heading angle 1, thereby follows the vertical particle motion while the phase angle is zero. With increasing frequency, the RAO comes closer to the heave resonance frequency, which is

$$\omega_R = \sqrt{\frac{C_{33}}{\rho \cdot \forall_{tot} + m_{33,tot}}} = 0.383 \ \frac{rad}{s} \tag{60}$$

and is also marked in figure 45. At this point, the RAO is theoretically infinity as damping is neglected. After the resonance frequency, the RAO is decreasing towards zero, but only reaching at 90°, as the forces on the offset columns are cancelling each other, but still, a small force is acting on the main column. To evaluate the influence of the main column, compare appendix E, where the heave RAO for the floater with caissons and with or without consideration of the main column is displayed. Before the heave RAO is zero for small waves, it experiences a local maximum after the cancellation frequency. As the floater is experiencing successively smaller heave oscillation amplitudes at higher frequencies, it is favourable to operate installation or maintenance operations in those conditions (Clauss et al. 1992, p. 275). Besides the cancellation frequency and the local maximum after it, the heave RAO is independent of the wave heading angles and overlaps for 45° and 135° as well as 0° and 180°, the overall highest heave motion experienced the floater at 0°/180° as the local minimum at the cancellation frequency was the smallest.

To validate the RAOs, they are now compared to published data comparisons on the loadings of the OC5 floater in figures 47 and 48. These studies were only referring to a wave heading angle of 0°,

where the sway RAO is zero and thereby wasn't reviewed, however, all comparison to the surge RAO is also applicable to the sway RAO for different wave heading angles.

As it can be seen in figure 47, the shape of the surge and heave RAO fit accurately to the calculated RAOs in figure 43 and 45. However, the size and frequency range of the validation data is significantly smaller than the calculated RAOs. For example, whereas the surge RAO has its second local maximum at around 1.155 Hz, the published RAO has its second local maximum at 0.16 Hz. Meanwhile, the resonance frequency in the data comparison is at around 0.05 Hz while it is 0.383 Hz for the calculated heave RAO.

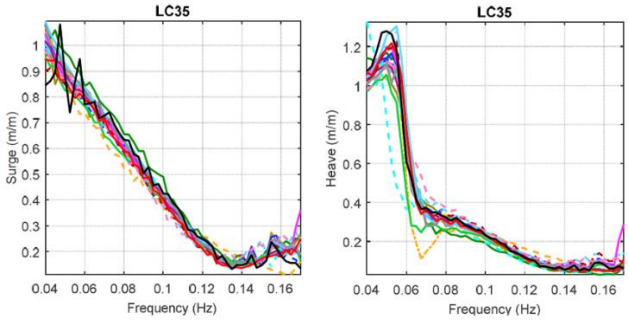

Figure 47: Comparison of RAOs for surge and heave motion for different models of the OC5 semisubmersible (Robertson et al. 2017, p. 52)

Those severe difference between the calculated surge and heave RAOs and the RAOs compared in (Robertson et al. 2017, p. 52) are based on the simplifications made. For this thesis, a simplified floater without cross bracings and pontoons was assumed, without consideration of turbine, tower and blade size and mass. Additionally, damping, drag, diffraction and coupled effects were neglected, whereby in total the denominator of the RAO becomes significantly smaller. When all factors are considered, the mass, added mass, damping and restoring force would have been significantly larger, and thereby also decrease the excitation force for small frequencies. To underline how different the RAOs are, the magnitude of the calculated RAOs is compared for a wave height of 9.4 m and a period of 14.3 s (ω = 0.4394 Hz) for surge and heave motion. While the RAO for surge motion in figure 43 would result at this point in a magnitude of 7.8176 m, the OC5 load comparison paper in figure 48 determined a magnitude of 0.7 m. Even more severe are the differences for heave motion: While the RAO in figure 45 is still declining from the resonance frequency at ω = 0.4394 Hz and has an undamped value of 5.1466 m/m and a resulting magnitude of 48.378 m, the comparison of the damped heave RAOs in figure 47 never exceeded 1.3 and has only a magnitude of 0.3 m at the looked at frequency.

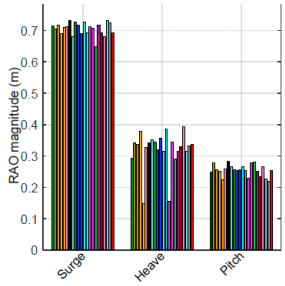

Figure 48: Comparison of RAOs at a wave height of 9.4 m and a period of 14.3 m (Robertson et al. 2017, p. 48)

In summary, it can be said, that the determined RAOs are similar in their form to the realistic models, however, to calculate accurate results of the transitional floater motion, significantly fewer simplifications have to be made. With reduced simplifications, also the rotational DOFs of the floater, which are important for the wind turbines performance, can be calculated accurately.

12.5 Wave loads for different drafts

In this final section, it is evaluated how the wave loads vary when the draft of the floater is varying. Therefore, the cases of +20% and -20% of the previous draft of 20 m are investigated. The new parameters of the drafts are displayed in table 11 and 12.

Table 7: Parameters for a 20% larger draft

+20%	
Symbol	Value
h_{D+}	$24\ m$
h_{MC+}	$24\ m$
h_{UC+}	$18\ m$
$m_{11+} = m_{22+}$	$1.1612 \cdot 10^7\ kg$

Table 8: Parameters for a draft decrease of 20%

-20%	
Symbol	Value
h_{D-}	$16\ m$
h_{MC-}	$16\ m$
h_{UC-}	$10\ m$
$m_{11-} = m_{22-}$	$1.0523 \cdot 10^7\ kg$

The forces and RAOs are determined for the wave heading angle, where the force/RAO exceeds its maximum. Therefore, the horizontal force is determined for 90°, the vertical force for 0°, the surge RAO for 0°, the sway RAO for 90° and the heave RAO for 0°.

The forces for the alternative drafts are displayed in figures 49 and 50, however in contrast to section 12.3 now depending on the wavelength $L = \frac{2 \cdot \pi}{k}$. As it can be seen in figures 41, 43, 44, 45, the largest forces and motions occur until a wave frequency of ω = 1,89 Hz ($L \approx 17\ m$). As the simplified velocity potential in (7) is only accountable for deep water $\frac{h}{L} \geq 0.5$ and the water depth is 200 m, the upper limit of the wavelength is set to 400 m (ω = 0,3925 Hz).

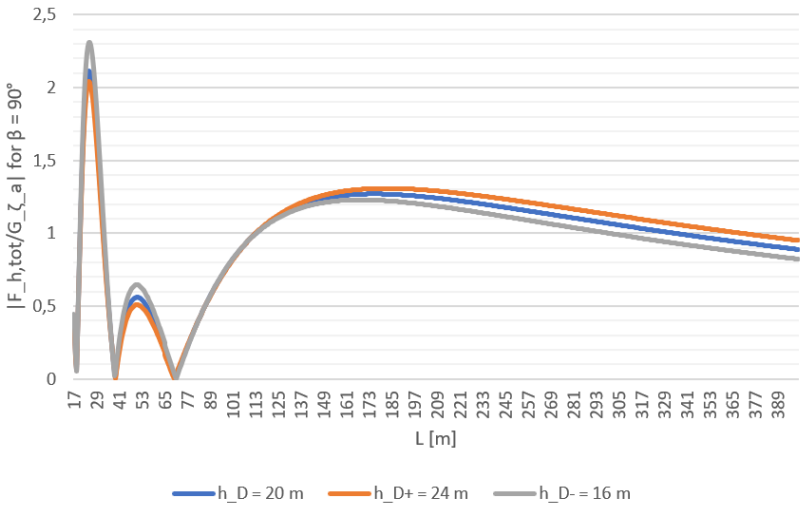

Figure 49: Comparison of the absolute values of the normalized horizontal force with different drafts for β=90°

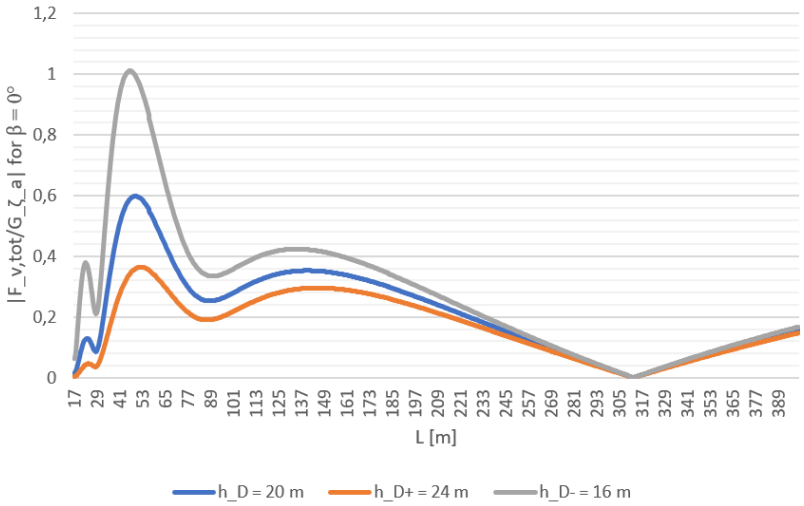

Figure 50: Comparison of the absolute values of the normalized vertical force with different drafts for β=0°

As it can be seen in figure 49, the horizontal force is independent for the draft for L=17 m, but then in the range up to 77 m, the decreased draft has significantly larger forces in the maximum, compared to the conventional draft of 20 m, while the increased draft leads to decreased maximum forces. In the zero crossings, the drafts overlap each other again with a slight shift in for the increased draft. Between the wavelength of 77 m and 137 m the forces overlap each other and after the horizontal force exceeds this value, it is larger for the increased draft and reduced for the decreased draft.

With rising wavelength, the vertical force is significantly larger for the decreased draft compared to the 20 m draft, especially at the maximum of the vertical force, while the increased draft is leading to a reduced vertical force. After the global maximum and a local maximum, the vertical force declines until it is the same for all drafts in the zero crossing at a wavelength of 310 m and then rises again with slightly higher vertical forces for the decreased draft and lower forces for the increased draft.

All differences in the horizontal and vertical forces for the different drafts h_{D-} and h_{D+} are based on the decay terms e^{-kh} (vertical) and $(1 - e^{-kh})$ (horizontal). With those decay terms, the magnitude of the corresponding force is changing depending on the draft.

As the Morison equation was applied to calculate the horizontal and vertical forces, the structure is considered as hydrodynamic transparent with $\frac{D}{L} \leq 0.2$. However, this is limiting the minimal wavelength to $L \geq \frac{D_{BC}}{0.2} = 120\,m$. For shorter wave lengths, the structure would be regarded as hydrodynamically compact and diffraction forces would play an important role for the wave loads, while drag forces can be neglected. Therefore, the forces for L < 120 m are inaccurate and would need additional calculation, which are not in the scope of this thesis.

The RAOs for surge, sway and heave motion in different drafts, are displayed in figures 51 to 53. They are also displayed in the range of 17 m to 400 m.

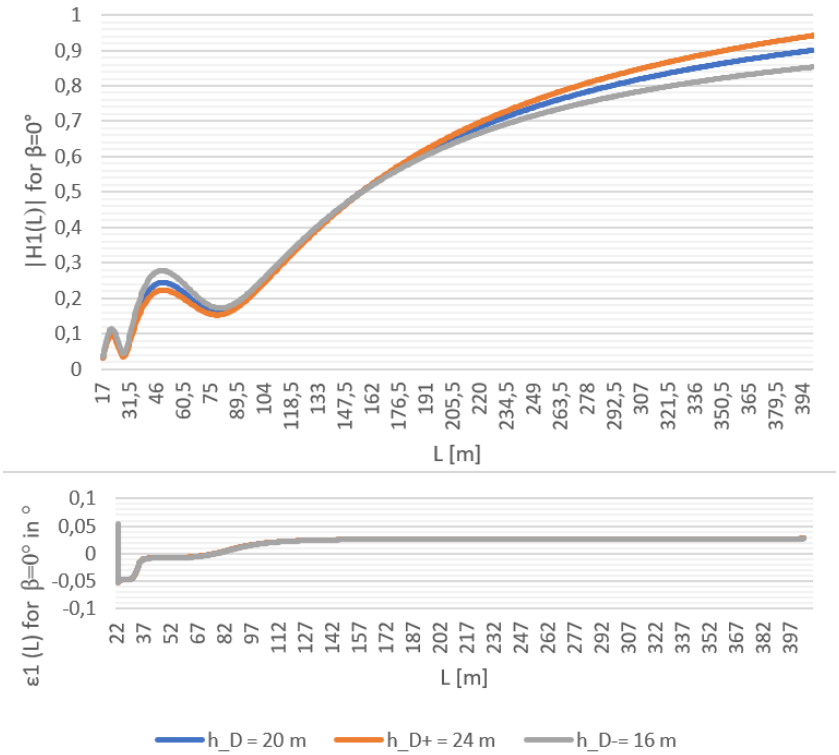

Figure 51: Comparison of the absolute values of the surge RAO with different drafts for β=0°

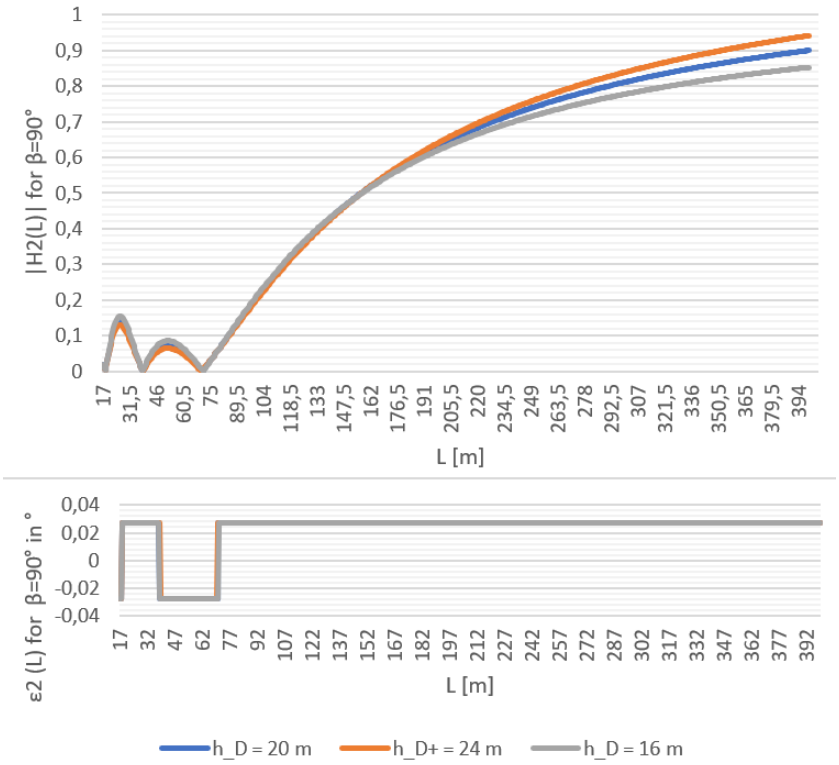

Figure 52: Comparison of the absolute values of the sway RAO with different drafts for β =90°

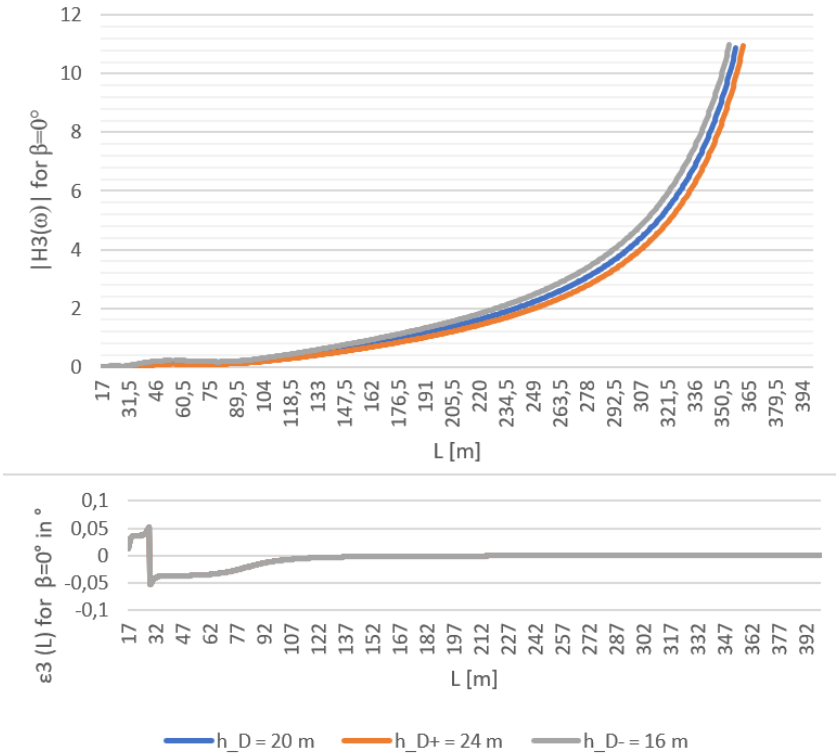

Figure 53: Comparison of the absolute values of the sway RAO with different drafts for β =0°

For surge motion, the structure is experiencing similar motions for small wavelengths up to 30 m. With increasing wavelength, the surge motion in the local maximum is larger for h_{D-} and smaller for h_{D+}. In the range between 90 and 191 m the surge motion its fairly equal for all drafts, but afterwards the increased draft has, corresponding to the horizontal force in figure 49, higher surge motions compared to h_D while the reduced draft is experiencing lower surge motion. The phase is the same for every draft.

The sway motion is hardly different for the different drafts until the wavelength of 191 m. Only in the local maxima, the absolute value of the RAO is slightly higher for the decreased draft and slightly lower for the increased draft. For long waves, ranging from 191 to 400 m, the floater is experiencing increased sway motions for h_{D+}, in contrast to h_{D-} which is slightly below h_D. The phase of the RAO only differentiates slightly in the range of 32 to 77 m, as the increased draft has minimal earlier zero crossings than the conventional and decreased draft.

With the selected range of wavelength, the resonance frequency of the heave motion, which for the normal draft lies at a wavelength of 420.1954 m, is not displayed, however the large increase to the undamped resonance frequency can already be seen in the range of 200 to 400 m (ω = 0.55 … 0.39 Hz). Like the vertical force, after overlapping for small wavelengths, the heave motion is constantly larger for the decreased draft and smaller for the increased draft. This characteristic can be used for offshore installation and maintenances activities: By temporarily increasing the draft of the floater with active ballasting systems, the motion of the floater can be reduced significantly, which eases any offshore activities. The phase of the heave RAO is independent of the drafts.

13 Conclusion

The goal of this thesis was to investigate in a literature review the different technological innovations for floating offshore wind turbines, which can enable the commercialisation of the technology by reducing its LCOE. Therefore, the different components of the floating offshore wind turbines, as well as the different project stages over its lifecycle, were examined in detail.

It was concluded that nearly all components of the floating offshore wind turbine could be further optimised, especially the FOWT specific parts like the substructure and dynamic cables. Those innovations regard the optimisation of existing technologies for the demand specific for floating wind, e.g. by improving moorings for shallow waters, or new innovative concepts like alternative turbine configurations and new substructure designs.

Especially the new concepts will require additional research by industry and universities and need to be proven in pilot or pre-commercial projects. However, once the demonstrated their feasibility, they can enable significant cost reductions of the floating wind technology potentially to a range of 50 – 70 $/MWh by 2030.

As the installed capacity of floating offshore wind is expected to ramp up significantly in the coming decade, several challenges need to be overcome. Those challenges mainly regard the large-scale deployment of FOWTs and the related logistical constraints. However, coming pilot and pre-commercial projects will prove methods for the serial production of the floater, the large-scale installation as well as operation and maintenance procedures. The knowledge gained from those projects must be shared in broad industry collaboration projects to enable the standardisation of the new technologies and processes.

Additionally, the floating wind industry will have to collaborate with policymakers to create regulatory frameworks, which are favourable for the broad deployment of the technology.

One potential constraint of the policymakers could be the intermittency of the wind turbines as well as their negative impact on the grid balance. As a solution to the problematic grid connection, floating offshore wind farms could be combined with the Power-to-X technology and thereby decouple from grid constraints. Additionally, this combination would enable new use cases for floating wind as it thereby can not only be used to produce carbon-free electricity but also could contribute to decarbonise other fossil-fuel dependent sectors.

In the second part of the thesis, the wave loads on an exemplary floater and resulting motions were determined by using the Morison equation. These loads and movements were examined for various wave heading angles as well as different drafts. While the calculated forces matched with other simplified models of semisubmersibles, the motions of the floater were severely larger than realistic models of the floater due to the simplifications made.

To accurately describe the motions of a floating offshore wind turbine, more precise models with less simplification need to be used. Those detailed models will be essential to understand the coupled behaviour of the FOWT. This knowledge then can be used to adjust the design of the turbine and floater accordingly and thereby optimise the performance of the wind turbine.

Bibliography

Achard J.-L., Maurice G., Balarac G., Barre S., 2017. Floating vertical axis wind turbine—OWLWIND project. In : 2017 International Conference on ENERGY and ENVIRONMENT (CIEM): IEEE, pp. 216–220.

Bard A., 2018. World's highest waves form west of Norway. Available online at https://sciencenorway.no/forskningno-norway-oceans/worlds-highest-waves-form-west-of-norway/1455407, checked on 11/15/2020.

Baring-Gould I., 2014. Offshore Wind Plant Electrical Systems. BOEM Offshore Renewable Energy Workshop, 2014. Available online at https://www.boem.gov/NREL-Offshore-Wind-Plant-Electrical-Systems/, checked on 10/19/2020.

Benitz M., 2015. Hydrodynamics of offshore structures with specific focus on wind energy applications. In *Engineering, Computing & Construction Management Faculty Publications*. Available online at https://www.sciencedirect.com/science/article/pii/S1364032115000313?via%3Dihub, checked on 11/15/2020.

Blaabjerg F., Liserre M., Ma K., 2011. Power electronics converters for wind turbine systems. In *IEEE Transactions on industry applications* 48 (2), pp. 708–719.

Buhagiar D., Sant T., Farrugia R. N., Aquilina L., Farrugia D., Strati F. M., 2019. Small-scale Experimental Testing of a Novel Marine Floating Platform with Integrated Hydro-pneumatic Energy Storage. In *Journal of Energy Storage* 24.

Bundesverband Windenergie. Maschinenhaus/ Antriebsstrang. Available online at https://www.wind-energie.de/themen/anlagentechnik/konstruktiver-aufbau/maschinenhaus/, checked on 9/16/2020.

Bundesverband Windenergie. Rotor. Available online at https://www.wind-energie.de/themen/anlagentechnik/konstruktiver-aufbau/rotor/, checked on 9/28/2020.

Caine D., Iliffe M., Kinsella K., Wahyuni W., Bond L., 2019. Dolphyn Hydrogen. Phase 1 - Final Report. Edited by Environmental Resources Management. Available online at https://assets.publishing.service.gov.uk/government/uploads/system/uploads/attachment_data/file/866375/Phase_1_-_ERM_-_Dolphyn.pdf, checked on 10/20/2020.

Carbon Trust, 2015. Floating Offshore Wind: Market and Technology Review. Prepared for the Scottish Government. Available online at https://prod-drupal-files.storage.googleapis.com/documents/resource/public/Floating%20Offshore%20Wind%20Market%20Technology%20Review%20-%20REPORT.pdf, checked on 10/25/2020.

Carbon Trust, 2018. Floating Wind Joint Industry Project - Phase I Summary Report. Key Findings from Electrical Systems, Mooring Systems, and Infrastructure & Logistic studies. Available online at https://www.carbontrust.com/resources/floating-wind-joint-industry-project-summary-report-phase-1, checked on 9/17/2020.

Carbon Trust, 2020. Floating Wind Joint Industry Project - Phase II summary report. Available online at https://www.carbontrust.com/resources/floating-wind-joint-industry-project-phase-2-summary-report, checked on 9/17/2020.

Clauss G., Lehmann E., Östergaard C., 1992. Offshore Structures. Volume I: Conceptual Design and Hydromechanics. London: Springer London.

Corewind, 2020. D2.1 Review of the state of the art of mooring and anchoring designs, technical challenges and identification of relevant DLCs. Available online at http://corewind.eu/publications/, checked on 9/17/2020.

DTU Wind Energy, 2019. PivotBuoy. Advanced Single Point Mooring System for lighter, cost-effective and reliable 10MW+ Floating Wind. Available online at https://www.vindenergi.dtu.dk/english/research/research-projects/pivotbuoy-advanced-single-point-mooring-system-for-lighter-cost-effective-and-reliable-10mw-floating, checked on 10/12/2020.

Equinor. Hywind Scotland. Available online at https://www.equinor.com/en/what-we-do/floating-wind/hywind-scotland.html, checked on 11/18/2020.

Equinor. Hywind Tampen: the world's first renewable power for offshore oil and gas. Available online at https://www.equinor.com/en/what-we-do/hywind-tampen.html, checked on 10/20/2020.

ETIP Wind, 2020. Floating Offshore Wind. Delivering Climate Neutrality. Available online at https://etipwind.eu/files/reports/ETIPWind-floating-offshore-wind-factsheet.pdf, checked on 10/25/2020.

Ferraro E., 2020. X1 Wind's PivotBuoy: Innovative floating platform to help scale offshore wind energy. Edited by Compasslist. Available online at https://www.compasslist.com/insights/x1-winds-pivotbuoy-innovative-floating-platform-to-help-scale-offshore-wind-energy, checked on 11/18/2020.

Ferri G., Marino E., Borri C., 2020. Optimal Dimensions of a Semisubmersible Floating Platform for a 10 MW Wind Turbine. In *Energies*, pp. 1–19.

Friends of Floating Offshore Wind, 2018. Offshore Energy - The Future's Floating. Available online at https://www.atkinsglobal.com/~/media/Files/A/Atkins-Corporate/group/sectors-documents/renewables/library-docs/brochures/Friends-of-floating-the-futures-floating-FINAL.pdf, checked on 10/25/2020.

Garcia A., 2019. This kite could harness more of the world's wind energy. Edited by CNN Business. Available online at https://edition.cnn.com/2019/10/01/tech/makani-wind-energy-kites-electricity-mission-ahead/index.html, checked on 11/18/2020.

GE Renewable Energy, 2020. GE's Haliade-X offshore wind turbine prototype operating at 13 MW. Available online at https://www.ge.com/news/press-releases/ge-haliade-x-offshore-wind-turbine-prototype-operating-at-13-mw, checked on 10/26/2020.

Global Wind Energy Council, 2020. Global Offshore Wind Report 2020. With assistance of Joyce Lee, Feng Zhao, Alastair Dutton, Ben Backwell, Liming Qiao, Shuxin Lim et al. Available online at https://gwec.net/global-offshore-wind-report-2020/, checked on 10/20/2020.

Greennovate Europe. Floatgen project. Available online at https://greenovate-europe.eu/floatgen-wind-power-going-further-offshore/, checked on 11/18/2020.

Guan Y., Zhu Z. Q., Li G.-J., Azar Z., Thomas A. S., Vedreno-Santos F., Odavic M., 2017. Influence of pole number and stator outer diameter on volume, weight, and cost of superconducting generators with iron-cored rotor topology for wind turbines. In *IEEE Transactions on Applied Superconductivity* 27 (6), pp. 1–9.

Hannon M., Topham E., Dixon J., McMillan D., Collu M., 2019. Offshore Wind, Ready to Float? Global and UK Trends in the Floating Offshore Wind Market.

Ideol. Ideol's first floater in operation. Available online at https://www.ideol-offshore.com/en/floatgen-demonstrator, checked on 11/18/2020.

InnoEnergy, 2018. Floating Offshore. 55 technology innovations that will have greater impact on reducing the cost of electricity from European floating offshore wind farms. With assistance of BVGassociates.

Ioannou A., Brennan F., 2019. A preliminary techno-economic comparison between a grid-connected and non-grid connected offshore floating wind farm. In : 2019 Offshore Energy and Storage Summit (OSES): IEEE, pp. 1–6.

IPCC, 2014. Climate Change 2014 Mitigation of Climate Change. Working Group III Contribution to the Fifth Assessment Report of the Intergovernmental Panel on Climate Change. Available online at https://www.ipcc.ch/site/assets/uploads/2018/02/ipcc_wg3_ar5_full.pdf, checked on 11/10/2020.

Jensen C., Kvarts T., Cavaleiro P., Casals L.-R., Dell'Anna G., Frelin W. et al., 2015. CIGRE TB 610 - Offshore generation cable connections.

Koh J. H., Ng E. Y., 2016. Downwind offshore wind turbines: Opportunities, trends and technical challenges. In *Renewable and Sustainable Energy Reviews* 54, pp. 797–808.

Larson A., 2020. Floating Platforms Are an Offshore Wind Gamechanger. Edited by POWER magazine. Available online at https://www.powermag.com/floating-platforms-are-an-offshore-wind-gamechanger/, checked on 11/18/2020.

Lewis, Edward V. (Ed.), 1989. Motions in waves and controllability. 2. revision, 1. print. Jersey City, NJ: Society of Naval Architects and Marine Engineers (Principles of naval architecture, / Edward V. Lewis, ed. ; 3).

Matha D., Brons-Illig C., Mitzlaff A., Scheffler R., 2017. Fabrication and installation constraints for floating wind and implications on current infrastructure and design. In *Energy Procedia* 137, pp. 299–306.

Mishnaevsky L., Branner K., Petersen H. N., Beauson J., McGugan M., Sørensen B. F., 2017. Materials for wind turbine blades: an overview. In *Materials* 10 (11).

Morris L., 2011. Direct Drive vs. Gearbox: Progress on Both Fronts. www.power-eng.com. Available online at https://www.power-eng.com/2011/03/01/direct-drive-vs-gearbox-progress-on-both-fronts/, checked on 9/16/2020.

National Offshore Wind Research & Development Consortium, 2019. Research and Development Roadmap 2.0. Available online at https://mk0pesafogiyof6m7hn7.kinstacdn.com/wp-content/uploads/2019/12/National-Offshore-Wind-Research-and-Development-Consortium-Roadmap-2.0.pdf, checked on 10/23/2020.

National Renewable Energy Laboratory, 2019. 2018 Cost of Wind Energy Review. With assistance of Tyler Stehly, Philipp Breiter. Available online at https://www.nrel.gov/docs/fy20osti/74598.pdf, checked on 10/26/2020.

Net Zero Guide. Direct Drive Wind Turbine. Available online at http://netzeroguide.com/direct-drive-wind-turbine/, checked on 9/16/2020.

Newman J. N., 2017. Marine hydrodynamics. With assistance of John Grue. 40th anniversary edition. Cambridge, Massachusetts: The MIT Press.

Offshore Renewable Energy Catapult, 2015. Floating wind: technology assessment. Interim findings. Available online at https://ore.catapult.org.uk/app/uploads/2018/01/Floating-wind-technology-assessment-June-2015.pdf, checked on 9/17/2020.

Offshore Wind Innovation Hub. Innovation Roadmaps. Available online at https://offshorewindinnovationhub.com/about-roadmaps/, checked on 9/16/2020.

Pecher, Arthur; Kofoed, Jens Peter (Eds.), 2017. Handbook of ocean wave energy: Springer Open (Ocean engineering & oceanography, volume 7).

Principle Power, 2020. Principle Power partners with an innovative Irish company Technology From Ideas (TfI) to develop novel mooring solutions for transitional waters. Available online at https://www.principlepowerinc.com/en/news-press/press-archive/2020/10/01/principle-power-partners-with-an-innovative-irish-company-technology-from-ideas-tfi-to-develop-novel-mooring-solutions-for-transitional-waters, checked on 10/11/2020.

Proskovics R., 2018. Floating Offshore Wind: A Situational Analysis. Edited by Offshore Renewable Energy Catapult. Available online at https://ore.catapult.org.uk/analysisinsight/floating-wind-situational-analysis/.

Quest Floating Wind Energy. Floater Concepts. Available online at https://questfwe.com/concepts/, checked on 9/30/2020.

Quest Floating Wind Energy, 2020. 2020 Global Floating Wind Energy Market and Forecast Report 2019 - 2034 Volume 2. Brochure of Report Highlights. Available online at https://questfwe.com/wp-content/uploads/2019/12/Global-Floating-Wind-Energy-Market-Forecast-Brochure-Volume-2-updated.pdf, checked on 10/25/2020.

Renewables Now. Final turbine arrives at Hywind Scotland floating wind farm. Available online at https://renewablesnow.com/news/final-turbine-arrives-at-hywind-scotland-floating-wind-farm-579966/, checked on 11/18/2020.

Reuters Events, 2019. Equinor cuts floating wind costs by 40% in design revamp. Available online at https://www.reutersevents.com/renewables/wind-energy-update/equinor-cuts-floating-wind-costs-40-design-revamp, checked on 11/18/2020.

Robertson A., Jonkman J., Wendt F., Goupee A., Dagher H., 2016. Definition of the OC5 DeepCwind Semisubmersible Floating System. Edited by National Renewable Energy Laboratory. Available online at https://www.google.com/url?sa=t&rct=j&q=&esrc=s&source=web&cd=&cad=rja&uact=8&ved=2ahUKEwiIwOTgroTtAhXH6aQKHfKGAoEQFjAAegQIBRAC&url=https%3A%2F%2Fcommunity.ieawind.org%2FHigherLogic%2FSystem%2FDownloadDocumentFile.ashx%3FDocumentFileKey%3D12510238-c40b-9597-a845-580276c1b88d&usg=AOvVaw0MYwMZwYRGDMUTZIj_3bFQ, checked on 11/15/2020.

Robertson A. N., Wendt F., Jonkman J. M., Popko W., Dagher H., Gueydon S. et al., 2017. OC5 Project Phase II: Validation of Global Loads of the DeepCwind Floating Semisubmersible Wind Turbine. In *Energy Procedia* 137, pp. 38–57.

Rodrigues S. F., Pinto R. T., Soleimanzadeh M., Bosman P. an, Bauer P., 2015. Wake losses optimization of offshore wind farms with moveable floating wind turbines. In *Energy Conversion and Management* 89, pp. 933–941.

Sant T., Buhagiar D., Farrugia R. N., 2017. Modelling the Dynamic Response and Loads of Floating Offshore Wind Turbine Structures With Integrated Compressed Air Energy Storage. In : International Conference on Offshore Mechanics and Arctic Engineering: American Society of Mechanical Engineers (57786), V010T09A049.

Schepers G., Pena A., Ely A., Palomares A., Attya A., Sieros G. et al., 2015. EERA-DTOC calculation of scenarios. In *Denmark: The European Energy Research Alliance*.

SeaTwirl, 2015. Lysekil prototype, S1, generates power for the first time! Available online at https://seatwirl.com/news/lysekil-prototype-s1-generates-power-for-the-first-time/, checked on 11/18/2020.

U. S. Department of Energy - Office of Energy Efficiency & Renewable Energy, 2018. 2018 Offshore Wind Technologies Market Report. Available online at https://www.energy.gov/sites/prod/files/2019/09/f66/2018%20Offshore%20Wind%20Technologies%20Market%20Report.pdf, checked on 10/25/2020.

U.S. Energy Information Administration, 2020a. Levelized Cost and Levelized Avoided Cost of New Generation Resources in the Annual Energy Outlook 2020. Available online at https://www.google.com/url?sa=t&rct=j&q=&esrc=s&source=web&cd=&cad=rja&uact=8&ved=2ahUKEwjbyIe1udLsAhVPM-wKHcehALMQFjABegQIAxAC&url=https%3A%2F%2Fwww.eia.gov%2Foutlooks%2Faeo%2Fpdf%2Felectricity_generation.pdf&usg=AOvVaw2oonu47uMw9UoZvYDV7pzJ, checked on 10/26/2020.

U.S. Energy Information Administration, 2020b. What is U.S. electricity generation by energy source? Available online at https://www.eia.gov/tools/faqs/faq.php?id=427&t=3, checked on 11/10/2020.

United Nations, 2015. PARIS AGREEMENT. Available online at https://unfccc.int/files/essential_background/convention/application/pdf/english_paris_agreement.pdf, checked on 11/10/2020.

van de Kaa G., van Ek M., Kamp L. M., Rezaei J., 2020. Wind turbine technology battles: Gearbox versus direct drive-opening up the black box of technology characteristics. In *Technological Forecasting and Social Change* 153.

van der Laan M. P., Andersen S. J., Ramos García N., Angelou N., Pirrung G. R., Ott S. et al., 2019. Power curve and wake analyses of the Vestas multi-rotor demonstrator. In *Wind Energ. Sci.* 4 (2), pp. 251–271.

Verschoof S., 2018. Technical Challenges and Benefits of Integrating Atlantic Salmon Production in Floating Offshore Wind Farms: A conceptual design study.

Wallmann J., 2016. Siliziumkarbid-Halbleiter auf der Überholspur. all-electronics.de. Available online at https://www.all-electronics.de/siliziumkarbid-halbleiter-auf-der-ueberholspur/, checked on 9/17/2020.

Watson S., Moro A., Reis V., Baniotopoulos C., Barth S., Bartoli G. et al., 2019. Future emerging technologies in the wind power sector: A European perspective. In *Renewable and Sustainable Energy Reviews* 113.

Weerheim R., 2018. Development of dynamic Development of dynamic power cables for commercial floating wind farms. Edited by TU Delft. Available online at http://resolver.tudelft.nl/uuid:487ba1e5-2764-4e96-808c-a9ee2772219d, checked on 9/17/2020.

Xiang X., Merlin M. M., Green T. C., 2016. Cost analysis and comparison of HVAC, LFAC and HVDC for offshore wind power connection.

Yin X., Zhang W., Zhao X., 2019. Current status and future prospects of continuously variable speed wind turbines: A systematic review. In *Mechanical Systems and Signal Processing* 120, pp. 326–340.

Zhengshun C., Helge A. M., Wei C., Zhen G., Torgeir M., 2017. A comparison of extreme structural responses and fatigue damage of semi-submersible type floating horizontal and vertical axis wind turbines. In *Renewable Energy* 108, pp. 207–219.

Appendix A

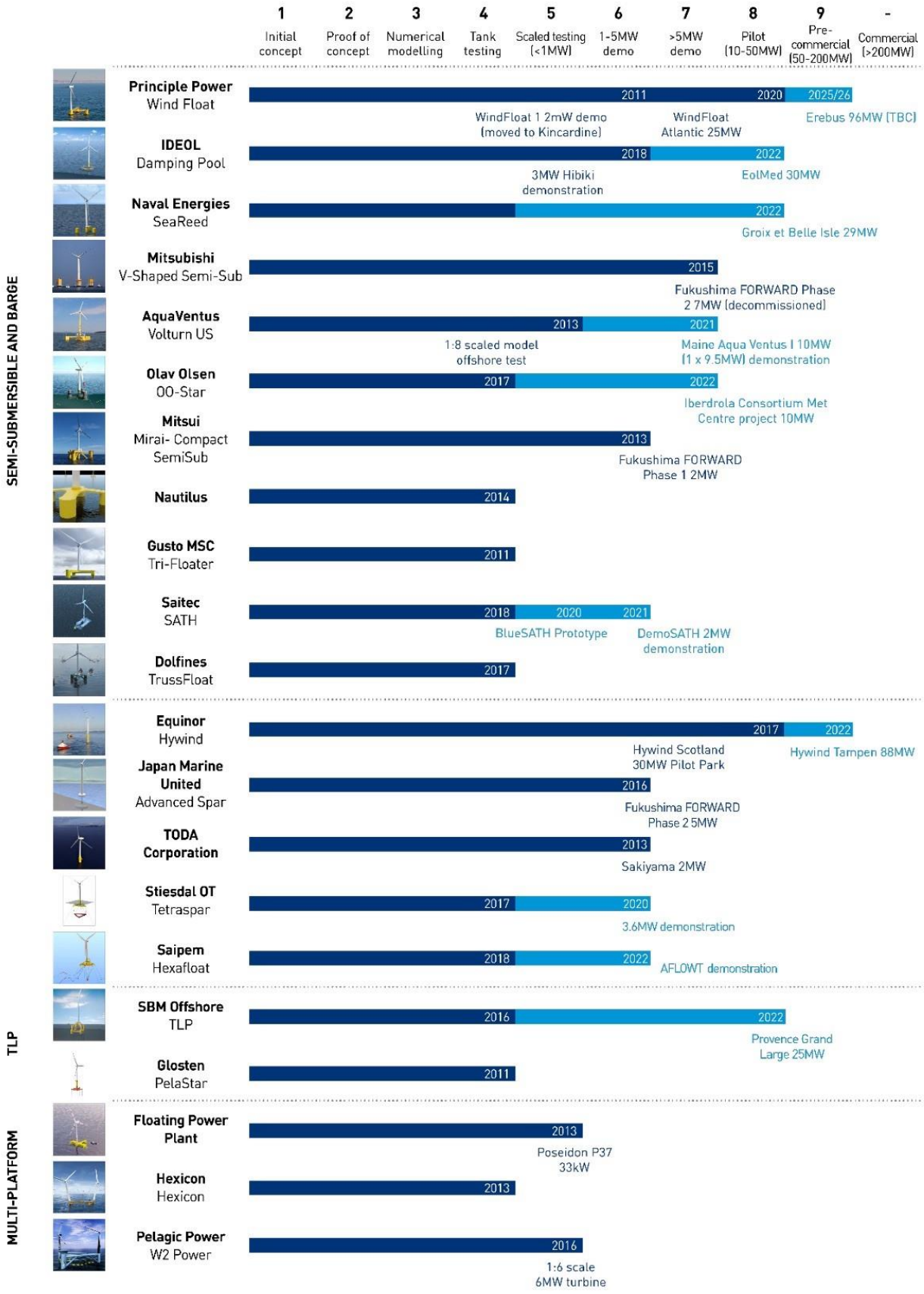

Appendix A: Technological Readiness Level (TRL) of different floater concepts with a forecast on planned upcoming projects (Carbon Trust 2020, p. 35)

Appendix B

Region	Project	Country	Pipeline Status	COD	Capacity (MW)	Water Depth (m)	Developer	Turbine Rating (MW)	Substructure
Asia	Fukushima Floating Offshore Wind Farm Demo Phase 1	Japan	Installed	2013	2	120	Marubeni Corporation	2	Semisubmersible
	Fukushima Floating Offshore Wind Farm Demo Phase 2	Japan	Installed	2015	5	120	Marubeni Corporation	5	Semisubmersible
	Sakiyama 2-MW Floating Wind Turbine	Japan	Installed	2016	2	100	TODA Corporation	2	Spar
	Kitakyushu – New Energy Development Organization (NEDO)	Japan	Under Construction	2019	3	70	NEDO/Ideol	3	Semisubmersible
	Hitachi Zosen	Japan	Permitting	2024	400	-	Equinor Hitachi	TBD	Semisubmersible
	Macquarie Japan	Japan	Planning	2025	500	100	Macquarie	TBD	TBD
	Ulsan 750-kilowatt Floating Demo	South Korea	Financial Close	2019	0.75	15	Consortium	0.75	Semisubmersible
	Donghae KNOC - Equinor	South Korea	Planning	2027	TBD	TBD	Equinor/KNOC	TBD	TBD
	Ulsan Shell, Coens, Hexicon	South Korea	Planning	2027	200	TBD	Shell/Coens/ Hexicon	TBD	Semisubmersible
	Ulsan Macquarie	South Korea	Planning	2027	200	TBD	Macquarie	TBD	TBD
	Ulsan SK E&S - CIP	South Korea	Planning	2027	200	TBD	SK E&S/CIP	TBD	TBD
	Ulsan KFWind – Principle Power – Wind Power Korea	South Korea	Planning	2027	200	TBD	KFWind/PPI/WPK	TBD	Semisubmersible
	Floating W1N	Taiwan	Planning	2025	500		Eolfi/Cobra	TBD	TBD
Europe	EOLINK 1/10-scale prototype	France	Installed	2018	0.2	10	EOLINK S.A.S.	0.2	Semisubmersible
	Floatgen Project	France	Installed	2018	2	33	Ideol	2	Barge
	Groix Belle Ille	France	Approved	2021	24	62	EOLFI	6	Semisubmersible
	Provence Grand Large	France	Approved	2021	24	30	EDF	8	Tension Leg Platform
	Eolmed	France	Approved	2021	24	62	Ideol	6.2	Barge
	Les Eoliennes Flotant du Golfe du Lion	France	Approved	2021	24	71	Engie, EDPR, Caisse de Depots	6	Semisubmersible
	GICON Schwimmendes Offshore Fundament SOF Pilot	Germany	Financial Close	2022	2.3	37	GICON	2.3	Tension Leg Platform
	Hywind - Demo	Norway	Installed	2009	2.3	220	UNITECH Offshore	2.3	Spar

Appendix B.1: Floating offshore wind projects in operation and in pipeline (U. S. Department of Energy - Office of Energy Efficiency & Renewable Energy 2018, p. 35)

Region	Project	Country	Pipeline Status	COD	Capacity (MW)	Water Depth (m)	Developer	Turbine Rating (MW)	Substructure
	TetraSpar Demonstrator	Norway	Financial Close	2019	3.6	200	Innogy, Shell, Stiesdal	3.6	Semisubmersible
	Hywind Tampen	Norway	Permitting	2022	88	110	Equinor	8	Spar
	NOAKA	Norway	Planning	2023	TBD	130	Equinor/Aker BP	TBD	TBD
	WindFloat Atlantic (WFA)	Portugal	Financial Close	2019	25	50	WindPlus S.A.	8	Semisubmersible
	DemoSATH - BIMEP	Spain	Approved	2020	2	68	Saitec Offshore Technologies	TBD	Semisubmersible
	X1 Wind prototype PLOCAN	Spain	Approved	2021	TBD	62	X1 Wind	TBD	Tension Leg Platform
	Floating Power Plant PLOCAN	Spain	Approved	2021	TBD	62	FPP	8 MW	Hybrid Wave Power Semisubmersible
	Hywind Scotland Pilot Park	United Kingdom	Installed	2017	30	100	Equinor	6	Spar
	Dounreay Tri	United Kingdom	Approved	2021	10	76	Hexicon	5	Semisubmersible
	Kinkardine Offshore Wind Farm Phase 1	United Kingdom	Installed	2018	2	62	Cobra	2 MW	Semisubmersible
	Kinkardine Offshore Wind Farm Phase 2	United Kingdom	Under Construction	2020	50	62	Cobra	9.5 MW	Semisubmersible
North America	**Castle Wind**	United States	Planning	2027	1,000	900	EnBW/Trident Winds	8+	Semisubmersible
	Redwood Coast Energy	United States	Planning	2025	150	550	EDPR/PPI	8+	Semisubmersible
	Aqua Ventus I	United States	Planning	2022	12	100	University of Maine	6+	Semisubmersible
	Oahu North	United States	Planning	2027	400	850	AW Wind	6+	Semisubmersible
	Oahu South	United States	Planning	2027	400	600	AW Wind	6+	Semisubmersible
	Progression Wind	United States	Planning	2027	400	650	Progression Wind	6+	Semisubmersible

Appendix B.2: Floating offshore wind projects in operation and in pipeline (U. S. Department of Energy - Office of Energy Efficiency & Renewable Energy 2018, p. 36)

Appendix C

Plant type	Capacity factor (percent)	Levelized capital cost	Levelized fixed O&M[1]	Levelized variable O&M	Levelized transmis-sion cost	Total system LCOE	Levelized tax credit[2]	Total LCOE including tax credit
Dispatchable technologies								
Ultra-supercritical coal	85	47.57	5.43	22.27	1.17	76.44	*NA*	76.44
Combined cycle	87	8.40	1.59	26.88	1.20	38.07	*NA*	38.07
Combustion turbine	30	16.17	2.65	44.33	3.47	66.62	*NA*	66.62
Advanced nuclear	90	56.12	15.36	9.06	1.10	81.65	-6.76	74.88
Geothermal	90	20.38	14.48	1.16	1.45	37.47	-2.04	35.43
Biomass	83	39.92	17.22	36.44	1.25	94.83	*NA*	94.83
Non-dispatchable technologies								
Wind, onshore	40	29.63	7.52	0.00	2.80	39.95	*NA*	39.95
Wind, offshore	44	90.95	28.65	0.00	2.65	122.25	*NA*	122.25
Solar photovoltaic[3]	29	26.14	6.00	0.00	3.59	35.74	-2.61	33.12
Hydroelectric[4,5]	59	37.28	10.57	3.07	1.87	52.79	*NA*	52.79

[1]O&M = operations and maintenance.

[2]The tax credit component is based on targeted federal tax credits such as the production tax credit (PTC) or investment tax credit (ITC) available for some technologies. It reflects tax credits available only for plants entering service in 2025 and the substantial phaseout of both the PTC and ITC as scheduled under current law. Technologies not eligible for PTC or ITC are indicated as *NA,* or not available. The results are based on a regional model, and state or local incentives are not included in LCOE calculations. See text box on page 2 for details on how the tax credits are represented in the model.

[3]Costs are expressed in terms of net AC (alternating current) power available to the grid for the installed capacity.

[4]As modeled, EIA assumes that hydroelectric generation has seasonal storage so that it can be dispatched within a season, but overall operation is limited by resources available by site and season.

[5]Costs are for 2023 online year. See page 6 for details on the exception.

Appendix C: Estimated LCOE for new generation energy sources deployed in 2025 (U.S. Energy Information Administration 2020a, p. 7)

Appendix D

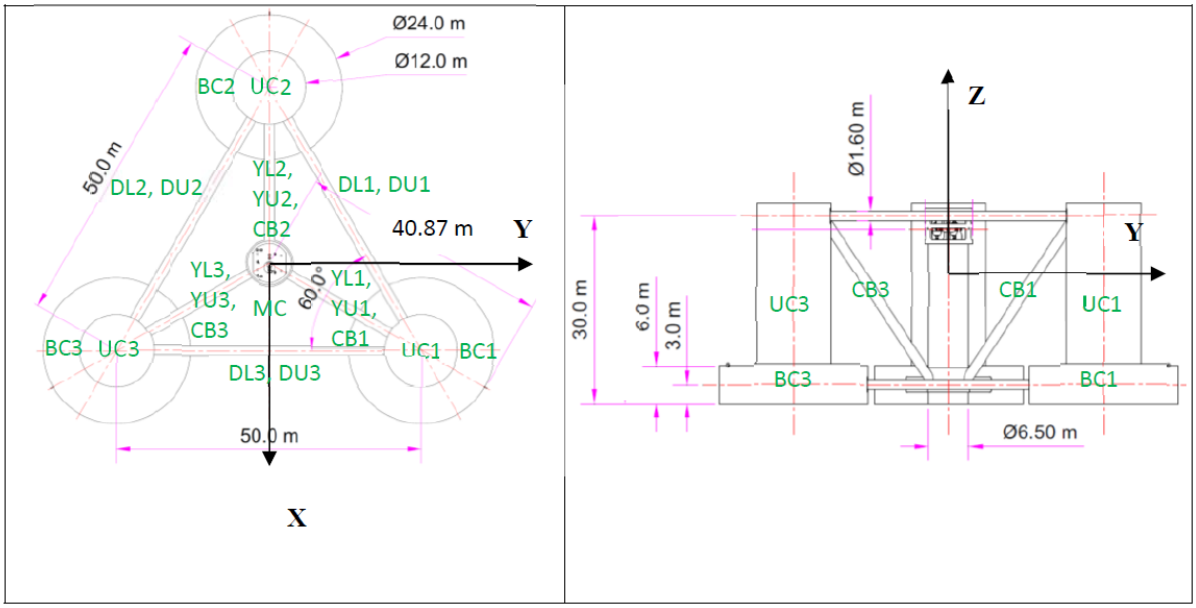

Appendix D: Numbering of the floater columns (Robertson et al. 2016, p. 24)

Note that the displayed coordinate system is the opposite to the used coordinate system in the thesis, as the displayed coordinate system was used for the model tests whereas the coordinate system of the thesis was used for simulations (Robertson et al. 2016, p. 14).

Appendix E

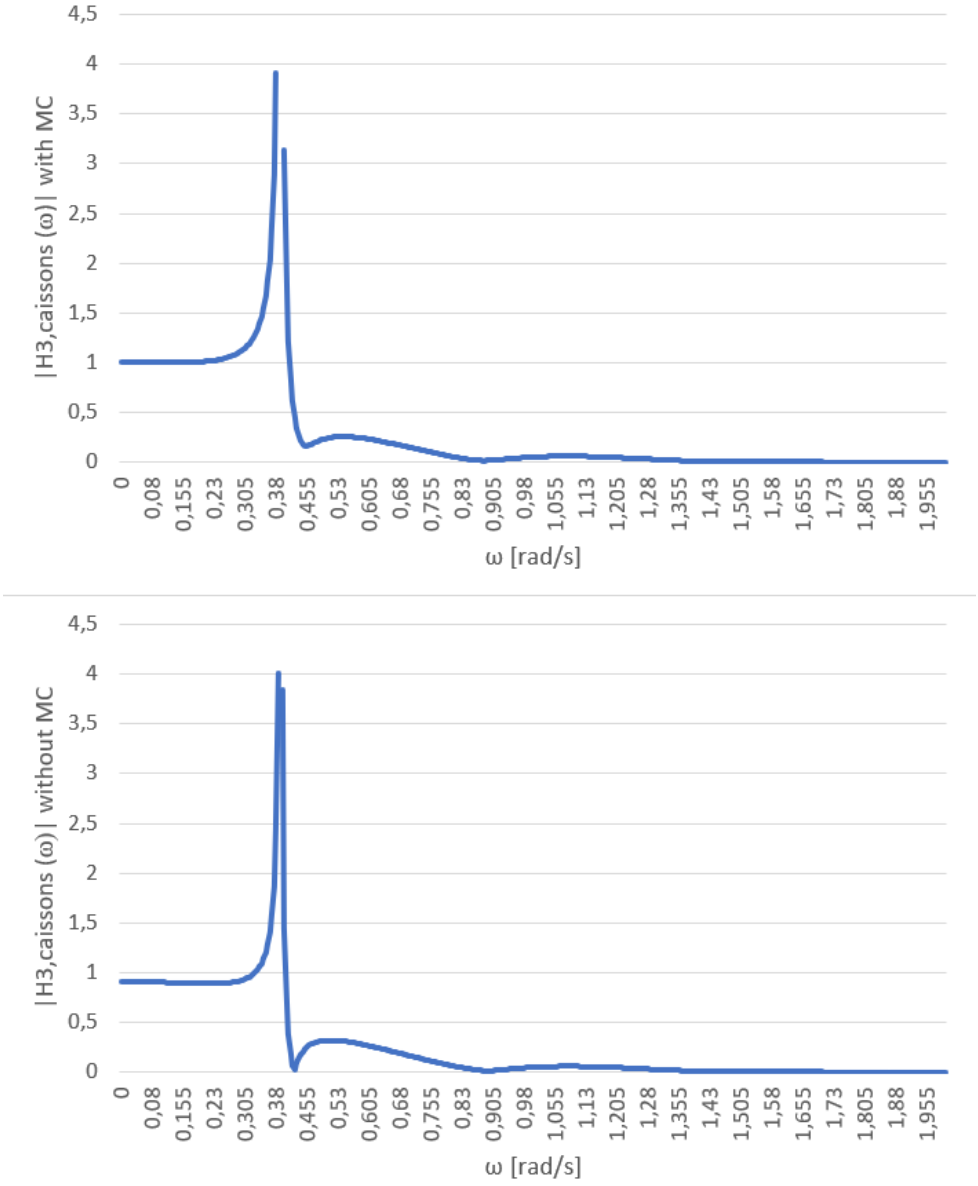

Appendix E: Heave RAO of the floater with base caissons with and without consideration of the main column